DEVELOPMENT OF BIOMIMETIC, HYBRID PROTEIN-SYNTHETIC MEMBRANES: DETERMINING PROTEIN INSERTION EFFICIENCY, MEMBRANE MATERIAL SUITABILITY AND RELEVANCE OF AQUAPORIN Z

BY

MICHELLE K. MARINCEL PAYNE

DISSERTATION

Submitted in partial fulfillment of the requirements
for the degree of Doctor of Philosophy of Environmental Engineering in Civil Engineering
in the Graduate College of the
University of Illinois at Urbana-Champaign, 2017

Urbana, Illinois

Doctoral Committee:

Research Assistant Professor Julie L. Zilles, Chair and Director of Research
Emeritus Professor Mark M. Clark
Associate Professor Mark W. Fitch, Missouri University of Science and Technology
Professor Charles J. Werth

ABSTRACT

Biomimetic membranes are designed to mimic the selective permeability of cell membranes, and can be engineered for a multitude of environmental applications including water purification, remediation, and sensing. Biomimetic membranes consist of membrane proteins, such as the bacterial water channel protein aquaporin Z (AqpZ), embedded in a lipid bilayer or a polymer that mimics a cell's natural lipid bilayer. Permeability and stability pose critical barriers to implementation of biomimetic AqpZ-based membranes. To achieve maximum permeability, it is essential to understand the relationship between protein insertion and membrane permeability. This work introduces a method using fluorescence correlation spectroscopy to quantify the number of AqpZ embedded in the membrane. This work demonstrates that membrane permeability is a function of protein insertion and that detergent inhibits protein insertion. Substantial variation was observed in protein insertion and permeability between protein batches, perhaps due to differences in the multimeric state of the protein.

For many applications, biomimetic technologies will only be pursued if they can be formed into planar sheets and if they remain stable under environmental or membrane cleaning stress conditions. This work provides proof of concept for the synthesis of solid-supported, planar mixed lipid-polymer membranes. While lipid and polymer membranes both insert proteins, lipids are more readily available and more closely mimic natural cell membranes. However, polymer improves vesicle toughness and stability. The mixed lipid-polymer membranes I created exhibited the desirable characteristics of both lipid and polymer membranes. I also demonstrated that in *Escherichia coli*, the presence of AqpZ increased permeability at neutral pH, and reduced survival under acid shock conditions. These findings may suggest possible physiological relevance for AqpZ.

Highly permeable and selective biomimetic membranes are a promising technology for water purification, and understanding their formation and properties are crucial for development and implementation. Development of hybrid protein-synthetic membranes for water treatment will allow for small energy savings. More importantly, these membranes will make it more feasible to treat challenging water sources and encourage water reuse.

DEDICATION

To my family,
without whom all of this work, and all that I have worked towards, would not be possible.

ACKNOWLEDGMENTS

For any student, the PhD journey cannot be completed without tremendous support from those around her. Many individuals have helped me achieve my goal, and I am eternally grateful. My advisor, Dr. Julie Zilles, guided me through a very challenging project and her coaching in developing my writing and critical thinking were particularly helpful. I also thank my committee for their time and constructive feedback. All CEE faculty at Illinois have helped me; I used equipment in almost all labs on the fourth floor, and elsewhere on campus. I additionally thank Dr. Julie Zilles and Dr. Jeremy Guest for their teaching and career mentoring that allowed me to pursue my academic career goals.

My research group members were also critical to my success. Dr. Manish Kumar initiated hybrid protein-synthetic membrane research at Illinois. Working with Manish, I learned to never let a day go by without trying something new or attempting to explain data from new viewpoints. I admire his creativity and dedication to his craft. My work at the University of Basel in Switzerland summer 2009 with Dr. Wolfgang Meier and his research group launched my graduate research career and allowed me to expand my cultural understandings. Dr. Sean and Gail Poust and Justin and Katie Hutchison were crucial friends during my graduate studies, and Sean and Justin's lab experiences proved extremely helpful. I also enjoyed working with Dr. Sania Bäckström, Dr. Sabine Fiedler, Courtney Flores and Sarah Hathaway. Sabine has been a wonderful friend and confidant. My fondest memories of my time at Illinois involve sharing lab space, time, housing, family and friends with her.

Many additional friends beyond my immediate research group have helped me achieve my goals. I thank Dr. Andrea Zimmer for providing support as my friend and roommate, and Melinda and Aaron Higley for offering me and baby Aaron with not only a place to live, but companionship in the summers of 2014 and 2015. To all of my friends at Illinois and beyond, thank you! I would not have achieved my goals nor enjoyed the experience if it were not for you.

I also thank my friends and colleagues at Rose-Hulman Institute of Technology. I received immense support in terms of encouragement, help with service duties, and review of my writing. I look forward to many fruitful years ahead.

Ultimately, my success would not be possible without the help and support of my family. My selfless parents, Dr. Jack and Mary Ann Marincel, made my success a priority by being wonderful grandparents to Aaron Payne while allowing me to work. My brother and my sister-in-law, Dr. Dan Marincel and Dr. Jordan Trachtenberg, provided desperately needed support by helping with Aaron, reviewing my writing, and providing just-in-time encouragement. Most importantly, I cannot thank my loving husband, Brian Payne, enough for his commitment to seeing me through. Brian's endless sacrifices to allow me to work and his never-ending encouragement were crucial to my success. Lastly, I thank my son, Aaron Payne, and my growing baby, for the motivation to model hard work and focus. Thank you.

Lastly, I acknowledge the University of Illinois SURGE, Graduate Assistance in Areas of National Need (GAANN), and the joint National Water Research Institute (NWRI) and the American Membrane Technology Association (AMTA) fellowship programs for financially supporting my graduate studies.

TABLE OF CONTENTS

LIST OF TABLES

LIST OF FIGURES

LIST OF EQUATIONS

CHAPTER 1: INTRODUCTION AND OBJECTIVES

1.1 Introduction

Available sources of freshwater are becoming increasingly stressed due to population growth, economic growth and climate change (1). Currently, the number of people suffering from lack of freshwater is in the billions and is expected to quadruple by 2050 (2, 3). Membrane desalination technologies, such as reverse osmosis (RO) and forward osmosis (FO), have come to the forefront as important means to develop new water sources from seawater (4), brackish water (5), recycled wastewaters for reuse (6-8), and waters impaired with persistent emerging contaminants (9, 10). Membranes are a promising technology for addressing emerging water treatment concerns including saltwater intrusion issues, wastewater recycling, and increasingly stringent drinking water standards. First, intrusion of saline and other pollutants into freshwater aquifers continues to contaminant previously usable waters (11). Second, recycling of wastewaters is becoming more common practice for a variety of uses (12). Third, drinking water standards are beginning to include emerging contaminants such as endocrine disruptors and other difficult-to-treat contaminants (13). Development of impaired and recycled waters will lessen current stress on scarce freshwater sources and the environmental burden of once-through water practices. Predictions suggest that water reuse will grow 14% annually (12) and desalination will expand globally (14) through 2020. As a result, higher quality water may also become available for consumers. In addition, while reverse osmosis plants operate near the thermodynamic equilibrium, there may be small energy savings of up to 10-20% (15) by increasing membrane permeability without sacrificing selectivity. To attend to water quality needs, we must meet the clear need for both highly permeable and selective membranes.

Biomimetic membranes are designed to mimic the selective permeability and enhanced efficiencies of cell membranes, and can be engineered for a multitude of environmental applications including water purification, remediation, and sensing, as depicted in Figure 1.1. Biomimetic membranes consist of membrane proteins embedded in a lipid bilayer or polymer that mimics cells' natural lipid bilayer. In this simplified form, the engineer can control the functions of biologically-derived materials, without competing with a cell's goal of reproduction.

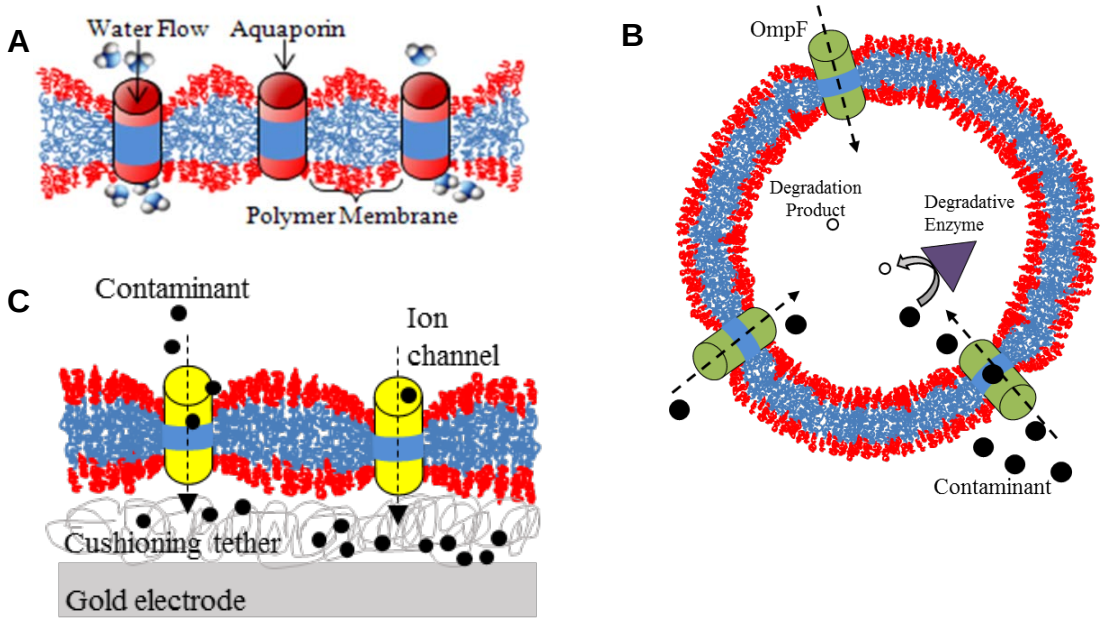

Figure 1.1. Schematics of hybrid, biomimetic protein-synthetic membrane-based technology applications
In all of the schematics, a protein is embedded in a membrane for the following applications: (A) water purification membranes, (B) remediation nanoreactors, and (C) membrane-based biosensors.

Application: Water purification membranes

Additionally, due to the highly specialized machinery developed through millions of evolutionary years, biological materials have the potential to significantly outperform existing synthetic technologies. For example, for water purification (Figure 1.1A), the bacterial water channel protein aquaporin Z (AqpZ) embedded in a polymer membrane has been shown to transport water rapidly and selectively, with a productivity of up to an order of magnitude greater than commercially

available membranes (16, 17). These highly permeable, yet selective, membranes have the potential to allow for careful control of contaminant separation.

Application: Remediation nanoreactors

Membrane-based remediation nanoreactors are also being developed for water remediation purposes. Remediation nanoreactors are simplified synthetic "cells" that concentrate and treat trace or hard-to-treat contaminants. They include proteins in a membrane enclosing enzymes to degrade environmental contaminants from surface or ground water (Figure 1.1B) (18-21). A prime example is a nanoreactor designed to treat perchlorate, an environmental contaminant found in drinking water of 16 million Americans (13, 22). Hypothetical perchlorate-reducing nanoreactors are composed of outer membrane porin (OmpF) embedded in a hollow, spherical lipid or polymer vesicle membrane with the encapsulated perchlorate biocatalysts perchlorate reductase and chlorite dismutase. The OmpF transports perchlorate across the membrane to the interior of the vesicle where the enzymes systematically reduce perchlorate to innocuous chloride and oxygen in the protected environment (23). To this end, increasing the OmpF incorporation and vesicle stability will increase performance of these remediation nanoreactors.

A different example describes the treatment of polycyclic aromatic hydrocarbons (PAH), which also provide remediation challenges (24). In this situation, gold nanoparticle catalysts embedded in the outside of the polymer membrane amended with naphthalene groups would allow for high local concentration and chemical degradation of 4-nitrophenol with the addition of sodium borohydride (25). In this situation, increasing gold nanoparticle incorporation and vesicle stability would be critical for implementation.

Application: Membrane-based biosensors

Membrane protein-based biosensor applications are also emerging as important environmental tools for detection of molecules ranging from metal ions to macromolecules and microorganisms (26-29). These biosensors consist of either a membrane-embedded receptor protein that senses and transfers a signal, or a channel that transports molecules directly as the signal (26, 27, 29) (Figure 1.1C). Maximizing signal and sensor stability will advance development of biosensors. Key

advantages of membrane protein-based sensors are low detection limits and high signal-to-noise ratios. For example, a detection limit of 30 nM was demonstrated for a sensor consisting of glutamate receptor ion channel protein embedded in planar lipid bilayer (30). For potential environmental applications, a gramicidin A-based gated ion channel biosensor device is being developed that could detect heavy metals. The gramicidin A channels transport ions and detection is initiated by receptors including metal chelates (31). An alpha-hemolysin-based ion channel biosensor is also being developed to detect divalent metal ions using the membrane protein itself. The protein was amended to contain histidine residues making it sensitive to submicromolar concentrations of zinc and cobalt ions (26). As with all hybrid protein-synthetic membrane applications, increasing the concentration of proteins in the membrane would increase permeability, or signal, of the sensor. To be useful, the sensor must also be stable under environmental conditions.

1.2 Proposed directions to improve biomimetic applications

Understanding the relationship between membrane permeability and protein insertion

In all of these applications, protein insertion and membrane assembly are key. To optimize these biomimetic materials, the relationship between the amount of protein added during membrane formation and the final membrane permeability needs to be determined. Many studies have investigated the functional insertion of membrane proteins into lipid and polymer membranes by measuring the permeability of small molecules. The literature review chapter (Chapter 2) describes previous studies on AqpZ insertion into lipid and polymer membranes, and discusses OmpF reconstitution as well. However, in most protein-membrane studies, insertion was not measured, even though unexpected decreases in or leveling off of permeability were sometimes observed. I hypothesize that membrane permeability is related to protein insertion, and that these effects are due to presence of polymer (88), high detergent concentrations (13, 20), and/or the synthesis methods (75, 87). Due to the recent interest in developing hybrid protein-synthetic membrane systems and the potential impact on water treatment and sensing if permeability is optimized, the investigation of the relationship between vesicle permeability and membrane protein insertion is critical.

Developing planar membranes

Other important hurdles for developing biomimetic membrane technology are membrane stability and configuration. To improve membrane stability, the formation of hybrid lipid-polymer membranes should be investigated. Lipids and polymer membranes both have advantages and disadvantages. Briefly, lipid membranes may be better suited for membrane protein insertion, but are less stable. Copolymer membranes, synthetic analogs of lipid membranes, are more stable (32, 33) and water impermeable, but are less similar to the natural membrane environment. The literature review chapter (Chapter 2) describes the advantages and disadvantages of these materials in more detail. Studies have examined the membrane integrity or half-life of lipid vesicles for fundamental study and drug delivery applications and report that membrane integrity is mainly a function of membrane composition (34). I hypothesize that a membrane comprised of both lipid and polymer would be advantageous because it would exhibit the desired attributes of both membrane materials: good membrane protein insertion in a stable membrane environment.

In addition to controlling the insertion capability and stability of membranes, it is also of interest to control the configuration of membranes. Specifically, while the vesicular form may be preferable for remediation nanoreactors, planar membranes would be advantageous for many applications to mirror existing technologies and provide flexibility in application. While planar membranes have been demonstrated for both lipid (35, 36) and polymer (37-40) materials, to our knowledge, neither hybrid lipid-polymer vesicles, nor hybrid lipid-polymer planar membranes, have been previously reported. Further discussion on planar membrane development is presented in the literature review chapter (Chapter 2). I hypothesize that hybrid lipid-polymer vesicles can form planar membranes when the material ratios and the solution and solid surface chemistry are optimized. Development of planar hybrid lipid-polymer membranes would offer tremendous opportunity for future development and application of biomimetic membranes.

Understanding protein response to stress conditions

For a membrane to be useful, it must be able to withstand chemical, physical, and biological stresses. Specifically, water purification membranes need to be able to withstand acid cleaning to remove foulants such as mineral scale. Membrane-based nanoreactors may also be exposed to a

variety of environmental stresses. Fortunately, AqpZ-polymer membranes have demonstrated reduced and reversible permeability under acid shock conditions due to potential AqpZ gating activity (41). This behavior would be advantageous for the cleaning processes necessary for efficient membrane operation. Additionally, as described in the literature review chapter (Chapter 2), the physiological relevance of bacterial aquaporins is unknown. I hypothesize that investigating the behavior of *E. coli* under shock conditions may demonstrate the physiological relevance of AqpZ in *E. coli*. For these reasons, determining the permeability and survival of *E. coli* with and without *aqpZ* under acid conditions is warranted. Highly permeable biomimetic membranes are a promising technology for a variety of environmental applications. Understanding the behavior of their components under stress conditions is necessary for their development.

Overall, my findings will serve as a platform from which insertion, permeability, and stability information can be translated to emerging environmental applications. The results of my work will greatly advance hybrid protein-synthetic technologies for water treatment.

1.3 Research goals and objectives

The overarching goal of this thesis is to further development of hybrid protein-synthetic membranes for environmental applications. In this work, I demonstrated that membrane permeability is related to protein insertion, mixed lipid-polymer membranes can be fabricated, and *aqpZ* increases permeability and survival in *E. coli* under acid shock conditions. Below are the specific objectives and brief descriptions of the work completed to achieve them.

Objective 1: Quantify membrane protein insertion efficiency in polymer and lipid membrane (Chapter 3)

This chapter elucidates the relationship between membrane permeability and protein insertion. Using the novel method I developed to count the number of membrane proteins in vesicles using fluorescence correlation spectroscopy (FCS), I show quantitatively and directly that vesicle permeability is a function of protein insertion. I also demonstrate that high detergent concentrations (above 0.3% (w/v) DDM) inhibit protein insertion, and thus, membrane

permeability. I also discovered that protein preparation matters, as the insertion and permeability behavior for AqpZ in lipid membranes, varied with the protein batch.

Objective 2: Develop planar, mixed lipid and polymer membranes (Chapter 4)

This chapter demonstrates formation of mixed lipid and polymer membranes. I demonstrate that mixed material membranes exhibit characteristic attributes of both lipid and polymer vesicles. Depending on the ratio of the polymer to lipid of the depositing vesicles, supported planar mixed membranes are formed on negatively-charged quartz and mica surfaces. I found that the percentage of lipid to polymer in the mixed membranes determined if they acted more like lipid (permeable, more readily formed planar membranes), or polymer (water-tight, more resistant to forming planar membranes). As such, these mixed membranes could be tailored for a variety of biomimetic applications.

Objective 3: Examine the behavior of AqpZ in E. coli under acid and osmotic stress conditions (Chapter 5)

In this chapter, my findings confirm that *aqpZ* increased permeability of *E. coli* at neutral pH conditions. I also demonstrated that *aqpZ* reduced cell survival under acid shock and combined acid and osmotic shock conditions. These findings verify the benefit of AqpZ to *E. coli*.

1.4 Dissertation organization

This dissertation begins with introduction (Chapter 1) and literature review (Chapter 2) chapters, followed by chapters describing my experimental work to achieve the objectives defined above (Chapters 3-5). Chapter 6 provides an overall summary of my work, focusing on its significance and proposed future work for development of hybrid protein-synthetic membranes.

CHAPTER 2: LITERATURE REVIEW ON KEY ELEMENTS OF HYBRID PROTEIN-SYNTHETIC MEMBRANES

2.1 Introduction

This literature review chapter examines the existing literature on topics pertinent to my work on developing hybrid protein-synthetic membranes for environmental applications. Specifically, this review first looks at reconstitution of AqpZ and OmpF in membranes, discrepancies in the resulting permeability trends obtained from those attempts, and the possible factors affecting insertion. Second, this review discusses the types of membranes used for reconstitution in vesicle and planar form and the methods for forming those membranes. Third, this review describes the roles of AqpZ and OmpF in natural membranes.

2.2 Reconstitution of AqpZ and OmpF in lipid and polymer membranes

Many transmembrane proteins have been functionally reconstituted in both lipids and polymer membranes. Proteins important to this work include the bacterial water channel protein, AqpZ, and outer membrane porin, OmpF. AqpZ specifically and passively transports water across bacterial cell membranes and was first discovered in *E. coli* (42). AqpZ functional reconstitution was initially demonstrated in *E. coli* lipid extract (43) and subsequently in synthetic triblock copolymer poly(2-methuloxazoline)-poly(dimethylsiloxane)-poly(2-methuloxazoline) ($PMOXA_{15}$-$PDMS_{110}$-$PMOXA_{15}$) (16). The AqpZ-polymer membranes were found to be 80 times more permeable than commercially available water treatment membranes (16). Existing studies describing incorporation of AqpZ in lipid and polymer membranes are detailed in Table 2.1. Recent research efforts have focused on developing planar AqpZ polymer membranes (44, 45) and hydrated polymer-cushioned lipid membranes (46). Additionally, a water channel protein from a

purple photosynthetic bacteria, *Rhodobacter sphaeroides*, was reconstituted in lipid and polymer membranes. The *R. sphaeroides* AqpZ polymer membrane exhibited greater water permeability than membranes with *E. coli* AqpZ (47).

Because OmpF is a well-characterized, slightly cation-specific porin, it has been used extensively to study lipids, protein reconstitution, and proof of concept for biomimetic technologies. OmpF was first purified and reconstituted into lipid membranes in 1976 (48); since then OmpF has been used extensively in reconstitution studies in lipids (49, 50). Given the well-studied nature of OmpF, it was natural for researchers to test its reconstitution and design applications in block copolymer materials as well (18, 19, 51-55). OmpF was reconstituted in lipid and polymer vesicles to control the enzymatic activity of encapsulated enzymes for drug delivery (21) and environmental remediation (23) purposes. OmpF has also been crystallized in polymer to form a planar membrane (56).

The development of artificial water channels that mimic the high permeability and selectivity of aquaporins provides another potential route to stable and reproducible biomimetic materials for membrane applications. While in early development, the current approaches are to either functionalize carbon nanotubes or construct nanochannels from organic building blocks such as amino acids or DNA (57). An artificial water channel comprised of alkylureido-ethylimidazole that forms imidazole-quartet channels transported water at approximately 10^6 water molecules/s (within 2 orders of magnitude of some aquaporins). While these channels were able to reject most ions, they were still permeated by protons (58). For these artificial water channels, the challenge lies in the ability to achieve the selectivity of aquaporins, while maintaining high water permeation.

Table 2.1. Summary of previously reported AqpZ insertion in lipid and polymer membranes

Membrane material	Study focus	AqpZ/ membrane molar ratio range	Permeability behavior at high molar ratio ratio [a]	molar ratio ratio at decrease or level-off	Permeability at peak (μm/s) [a]	Permeability at decrease or level-off (μm/s)	Ref
E. coli total lipid extract	Functional reconstitution in vesicles	1/7467-1/467	Decreased	1/467	53.9	38.8	(43)
$PMOXA_{15}$-$PDMS_{110}$-$PMOXA_{15}$	Functional reconstitution in polymer vesicles	1/500-1/25	Decreased	1/25	3032.2	220.5	(16)
E. coli total lipid extract	Determine ion conductivity	3/56-30/56	Increased	---	41.4	---	(59)
DOPC	Form planar membrane on nanofiltration membrane support	1/800 & 1/200	Increased	---	279.0	---	(60)
DOPC	Form stable, immobilized vesicles on microporous membrane support	1/3562-1/356	Increased	---	459.3	---	(61)
DMPC	Form planar, polymer cushioned membrane	1/6000-1/1000	Decreased	1/1000	368.8	73.8	(46)
$PMOXA_{12}$-$PDMS_{54}$-$PMOXA_{12}$	Form planar membrane on polycarbonate support	1/400-1/50	Decreased	1/50	2180.9	1222.0	(62)
DOPC	Form planar, thin film composite membrane	1/200	---	---	60 [b]	---	(63)
$PMOXA_{1000}$-b-$PDMS_{4000}$-$PMOXA_{1000}$	Form planar membranes on cellulose acetate substrate	1/200-1/50	Increased	---	1733	---	(44)
$PMOXA_{8}$-$PDMS_{55}$-$PMOXA_{8}$	Functional reconstitution of EcAqpZ and insertion efficiency in vesicles	1/1031-1/516	Decreased	1/516	617.7	287.9	(47)
$PMOXA_{8}$-$PDMS_{55}$-$PMOXA_{8}$	Functional reconstitution of RsAqpZ and insertion efficiency in vesicles	1/1878-1/939	Decreased	---	1500.7	---	(47)
PC_4-PS	Functional reconstitution of EcAqpZ and insertion efficiency in vesicles	1/35723-1/893	Leveled-off	1/3572	623.9	623.9	(47)
PC_4-PS	Functional reconstitution of RsAqpZ and insertion efficiency in vesicles	1/65065-1/1627	Leveled-off	1/2169	2057.5	1966.7	(47)

Abbreviations are defined as follows: poly(methyloxazoline)–poly(dimethylsiloxane)–poly(methyloxazoline) (PMOXA–PDMS–PMOXA); 1,2-dioleoyl-sn-glycero-3-phosphocholine (DOPC), 1,2-dimyristoyl-sn-glycero-3-phosphocholine (DMPC) , and 75% L-α-phosphatidylcholine (egg PC) with 25% L-α-lysophosphatidylserine (porcine PS), reference (Ref), *E. coli* AqpZ (EcAqpZ), *R. sphaeroides* AqpZ (RsAqpZ).

[a] Permeability values were corrected to 10^0C using an activation energy of 3.4 kcal/mol (16) for EcAqpZ and 2.93 kcal/mol for RsAqpZ (34).

[b] No temperature was reported.

Membrane permeability behavior and factors inhibiting protein insertion

For the studies listed in Table 2.1, protein insertion was not measured, with one exception (47) However, unexpected decreases in or leveling-off of permeability were sometimes observed. When observing permeability behavior at high protein reconstitution ratios, reports have hypothesized that use of polymers (64, 65), high detergent concentrations (16, 43), and/or synthesis methods (66) might impact protein insertion, and thus membrane permeability.

i. Presence and properties of polymer

Generally, theoretical models describe that protein insertion should cause an energetic penalty in lipid and polymer membranes as a function of hydrophobic mismatch and vesicle curvature (67). When there is mismatch between the length of the hydrophobic residue band of a membrane protein and the hydrophobic membrane thickness, the membrane will stretch or compress to accommodate the protein. This can cause perturbations in the membrane, characterized as the coherence length, or perturbation decay length. The perturbation decay length is the length along the membrane where the influence of the protein is observed (membrane stretches or compresses to accommodate protein) and has been studied quite extensively in lipid models (67-71).

In polymer, it has been proposed that protein insertion would decrease as a function of the mismatch in hydrophobic thickness between the hydrophobic portions of the protein and the polymer (64). While polymer vesicles are stiffer than lipid vesicles, the perturbation decay length was estimated to still be large. Using a mean field analysis modeling approach, the energetic penalty from protein insertion into the polymer membrane was estimated to increase slowly as a function of polymer length such that membrane proteins could still insert into polymer membranes that were thick and exhibited a large hydrophobic mismatch (64). Polymer membranes can be up to several times thicker than the 4 to 5 nm thickness of lipid membranes. Molecular dynamic simulations demonstrate that thicker polymer membranes may even close around the opening of the protein even when proteins do insert (72).

Experimentally, shorter polymer chains were found to better mimic natural lipid membranes and allow proteins to functionally insert (28, 65). Two studies experimentally demonstrated that the thickness of the polymer might inhibit protein insertion. These studies tested protein incorporation into polymer membranes with different hydrophobic band thicknesses. One study tested $PMOXA_{15}$-$PDMS_{68}$-$PMOXA_{15}$ which was 10.2 nm in length, and $PMOXA_{13}$-$PDMS_{33}$-$PMOXA_{13}$ which was 6.1 nm in length. In this study, alpha-haemolysin was unable to insert in the longer polymer, and alamethicin took much longer to insert even in the shorter chain polymer than it did in lipid membranes (28). Another study tested two methacrylated PMOXA-PDMS-PMOXA polymers that were 4 and 8 nm in thickness. In this study, the shorter polymer was able to incorporate more OmpF than the longer polymer (65). These observations were attributed to the ability of the shorter polymer to better mimic the natural membrane environment (28, 65).

ii. High detergent concentrations

Detergent is necessary for purification of all membrane proteins, including AqpZ, and is thus inevitably present during AqpZ reconstitution in lipid or polymer. Detergent concentration has been hypothesized to cause reduced permeability of membranes by decreasing AqpZ insertion efficiency during vesicle formation (16, 43). Vesicle formation method could affect the detergent concentration. In some cases, vesicles were formed by film rehydration where a thin film of membrane material is mechanically dispersed in the presence of the protein-detergent buffer solution (16, 73). In previous studies using this method, detergent concentration was invariably increased as more AqpZ was added. Sometimes, detergent was removed by adding detergent-absorptive biobeads SM-2 after vesicle formation (44, 46, 62). In other studies, the vesicles were formed by dialysis (43, 47) and enough detergent was removed from the lipid-protein mixture to form vesicles. In studies utilizing dialysis or biobeads, it is possible that detergent removal could have been less complete at higher concentrations of AqpZ added, especially when the detergent n-Dodecyl β-D-maltoside (DDM) was used because it has a low critical micelle concentration (CMC) and is gentle. Octyl β-D-glucopyranoside (OG) has a CMC two orders of magnitude larger than DDM and while it is harsher than DDM, it is more readily removed from solution (74). OG was used in some studies as an alternative detergent for AqpZ purification, and for vesicle formation via dialysis. In all these studies, the initial amount of detergent was not held constant,

and the final amount of detergent was not quantified. Collectively, these studies report a large range of detergent concentrations used during vesicle formation. A summary of the estimated detergent characteristics in previous work is presented in Table 2.2. Estimated detergent concentrations at peak vesicle permeability ranged from 0.01-0.3%. It should be noted, however, that it is impossible to know actual detergent concentrations because they were not measured in the previous work, and size exclusion chromatography was also often employed to separate unreacted, small molecules from vesicles during vesicle preparation, with unknown effects on detergent concentrations.

Table 2.2. Summary of estimated detergent characteristics of AqpZ-containing vesicles in previous work

Membrane material	Detergent for AqpZ purification	AqpZ stock [Det] (%)	Vesicle formation method	Detergent removal after reconstitution?	AqpZ/mem molar ratio range	Vesicle [Det] range (%)	[Det] at peak permeability (%)	[Det] at decrease or level-off (%)	Ref
E. coli total lipid extract	DDM	1.5	Dialysis with OG	N/A	1/400-1/25	0.075-1.2	?	?	(43)
$PMOXA_{15}$-$PDMS_{11}$-$PMOXA_{15}$	DDM	1.5	Film rehydration	None	1/500-1/25	0.03-0.6	0.3	0.6	(16)
DMPC	DDM	0.5	Film rehydration	Bio-beads	1/6000-1/1000	0.003-0.02	0.01	0.02	(46)
$PMOXA_{12}$-$PDMS_{54}$-$PMOXA_{12}$	DDM	1	Film rehydration	Bio-beads	1/400-1/50	0.06-0.5	0.23	0.47	(62)
$PMOXA_{1000}$-b-$PDMS_{4000}$-$PMOXA_{1000}$	DDM	1	Film rehydration	Bio-beads	1/200-1/50*	0.008-0.03	0.033	---	(44)
$PMOXA_{8}$-$PDMS_{55}$-$PMOXA_{8}$	OG	1	Dialysis with OG	N/A	1/1031-1/516 (EcAqpZ), 1/1878-1/939 (RsAqpZ)	?	?	?	(47)
PC_4-PS	OG	1	Dialysis with OG	N/A	1/35723-1/893 (EcAqpZ), 1/65065-1/1627 (RsAqpZ)	?	?	?	(47)

? denotes values that could not be estimated because dialysis was used as the vesicle formation method.
* denotes that the AqpZ/polymer ratios were not defined as molar or weight; for calculations in this table, they were assumed to be molar ratios.
Abbreviations are defined as in Table 2.1 with the addition of detergent (Det).

iii. Synthesis methods

In addition to detergent and the use of polymers, synthesis methods are hypothesized to impact the insertion of membrane proteins. It has been previously hypothesized that film rehydration reduced protein insertion compared to dialysis based on comparing vesicle permeability values for vesicles formed both with film rehydration and dialysis (66). While film rehydration was used successfully to create vesicles in this study and others (16), slow detergent removal via dialysis is also used to form vesicles with reconstituted proteins (47, 66) and 2D protein crystallization (66, 75-79). Using dialysis for vesicle formation, incorporation of the mammalian lens-specific aquaporin-0 (Aqp0) into polymer membrane depended on the detergent removal rate (66). Comparing studies, greater vesicle water permeability was achieved with Aqp0/polymer vesicles formed via dialysis (66) compared to AqpZ/polymer vesicles formed via film rehydration (16). Since Aqp0 is less permeable than AqpZ, it was speculated that dialysis was the most efficient method for membrane protein insertion (66). However, in these studies, the impact of synthesis method was not specifically tested, nor was protein insertion measured.

2.3 Synthetic membrane materials suitable for protein incorporation

There are two general classes of membrane materials suitable for membrane protein incorporation: lipids and block copolymers. Lipid bilayers are a key component of cell membranes, separating and maintaining osmotic, charge and pH differentials (80), and housing membrane proteins that transport small molecules into and out of cells. For use in a hybrid protein-synthetic membrane, lipids have the advantages of being better studied and more similar to the native environment for incorporation of membrane protein. Copolymer membranes are synthetic analogs of lipid membranes, and are composed of hydrophilic and hydrophobic blocks that mimic the properties of lipid membranes. Polymer membranes typically possess greater stability (32, 33) and mechanical strength (32), and are less leaky to water and small molecules (81). In addition, polymer membranes offer more options for the engineer to specify the desired properties of the membrane (37). However, they are less understood and may be less suited for protein insertion due to their larger thickness and reduced fluidity compared to lipid membranes (28, 82).

The functional insertion of some membrane proteins have been demonstrated in both lipid and block copolymers membranes. For lipids, a large number of membrane proteins have been inserted into a variety of lipids. For example, Table 2.1 above presents only literature reporting insertion of AqpZ in various lipid and polymer membranes. Insertion of OmpF in lipids has been studied even more extensively, and it was one of the first membrane proteins studied in block copolymer membranes (21, 83).

Vesicles

For inserting membrane proteins, lipid or polymer dispersions can self-assemble into vesicles through mechanically dispersion, solvent dispersion, dilution, or removal of detergent (84). The formation method can impact the size of the vesicle. For forming large unilamellar vesicles (100-1000 nm (84)) capable of entrapping small molecules and allowing insertion of transmembrane proteins for a variety of applications, mechanical dispersion or slow detergent removal via dialysis is typically used (73, 75, 85). For film rehydration, a thin film of lipid or polymer is dried from a solvent, followed by rehydration in aqueous buffer with the protein solution. For dialysis, powdered or solvent dispersed lipid is dissolved in a high concentration of detergent with the protein solution followed by buffer exchanges with lower concentrations of detergent (85). In yet another approach, protein can also be inserted after vesicle formation where already formed vesicles are destabilized by detergent followed by addition of the protein solution. It has been suggested that this method is not as reproducible (41, 86).

Planar membrane configuration

While many membrane protein reconstitution and other studies have been performed in vesicles, substantial recent effort has been spent to form planar membranes that functionally reconstitute membrane proteins, especially AqpZ (44-46, 60, 63, 66). In the absence of protein, a planar membrane configuration has been achieved for both lipid (35, 36) and polymer (37-40) materials. Formed at the air-water interface, Langmuir films have been long used as ideal membrane models as they allow for study of the organization of lipid and other molecules introduced to the membrane in a monolayer. For preparing supported lipid planar films, the Langmuir-Blodgett vertical transfer or the Langmuir-Schaefer horizontal transfer modes were first demonstrated and are still common

(87). Other methods include introducing lipid membranes to a small (< 1 mm) hydrophobic aperture (80, 88) or a hydrophobic scaffold with apertures on the order of 300 μm for free-standing membranes (89, 90). Formation of lipid membranes on a solid support with a polymer-cushion has also been useful, especially for studying protein behavior because there is separation between the bilayer and the solid support (91). Hydrogels have also been shown to encapsulate and support planar lipid membranes (92, 93). A simple and reproducible method to form supported lipid bilayers is vesicle collapse on hydrophilic surfaces (35, 94, 95). Along with the Langmuir-Blodgett transfer method, vesicle collapse is most common at present for forming supported lipid membranes (91). Examining vesicle collapse for forming planar lipid membranes, Table 2.3 summarizes various affecting factors.

Table 2.3. Summary of factors that can affect the deposition and adsorbing behavior of lipid vesicles to form lipid bilayer

Factor	Effect	Reference
Vesicle properties		
Vesicle size (diameter)	Larger size increases deformation of adsorbed vesicles	(36, 96, 97)
Lipid composition	Greater ratio of positively charged lipids promotes rupture on negatively charged supports	(35, 96)
Surface charge	Greater net positive charge promotes rupture on negatively charged supports	(35, 36, 97)
Support surface properties		
Surface chemistry	Hydrophilic such as fused silica, borosilicate glass, mica, oxidized silicon work best	(91, 98)
Cleanliness	Clean yields best adsorption of vesicles	(91)
Roughness	Smooth yields best adsorption of vesicles and defect-free bilayer formation	(91, 99)
Charge	Negatively charged supports (mica, SiO_2) promote rupture	(100)
Solution chemistry		
pH	Slightly basic pH promotes vesicle fusion	(91, 99)
Concentration of vesicles	Greater concentrations means less time to rupture	(100, 101)
Ionic strength	Higher ionic strength promotes vesicle adherence	(91, 98)
Presence of Ca^{2+}	Increases rupture and time to rupture for moderately positively- and neutrally-charged vesicles.	(35, 91, 96)
Temperature	Higher temperature promotes bilayer formation	(91, 98)
Osmotic pressure	Higher osmotic pressure promotes bilayer formation	(98)

2.4 Aquaporins and OmpF

Nature provides a great variety of specific channels that allow passage of small molecules across biological membranes. Transmembrane proteins span the entire lipid bilayer membrane and have important functions in cells.

Aquaporins

Aquaporins are a type of membrane protein that form water-specific channels, are found across all domains of life, and are essential for satisfying water transport needs in mammalian and plant cells (102, 103). Aquaporins have a narrow, hour-glass shaped hydrophobic pore with a constriction zone diameter of approximately 3 Å and a length of 5 Å through which frictionless, single-file water transport can occur (104). Aquaporins are made up of alpha helices that configure into three-dimensional monomers. They typically exist as a group of four monomers, or tetramers. Agre et al. (103) discovered the first aquaporin, aquaporin-1 (105). Since their discovery, aquaporins have been studied in a variety of capacities to reveal physiological relevance. The physiological relevance in bacteria, however, is unknown. The large surface area to volume ratio of bacteria is sufficient to meet water transport needs by diffusive water transport (106). Additionally, aquaporins do not exist in some types of microorganisms, suggesting that they are not essential (106, 107). Some studies have disrupted AqpZ and found subtle detectable changes in cellular growth or function, if any (106, 108, 109). Studies suggest that AqpZ may help alleviate cellular dehydration or osmotic stress conditions by providing rapid water transport (106, 109-111).

Initial work using AqpZ-polymer vesicles and *E. coli* demonstrated that AqpZ-polymer vesicles exhibited reduced and reversible permeability under acid shock conditions (41). It was also shown that whole *E. coli* cells have reduced permeability and survival under acid shock conditions, suggesting that the presence of AqpZ and its gating behavior at low pH may be advantageous, especially under combined acid and osmotic shock (41).

OmpF

The outer membrane of Gram-negative bacteria contains many porins grouped into 6 families. Like other outer membrane porins, OmpF is made of beta barrels that configure into monomers. OmpF typically exists as a group of three monomers, or trimers. They have an elliptical constriction zone that is approximately 9 Å long with dimensions of 11 x 7 Å (112). OmpF is of the general, or non-specific, porin family, and passively transports ions and other small hydrophilic molecules across the outer membrane (113). OmpF has a slight preference for cation molecules. In *E. coli*, for uncharged molecules, size has been reported to impact diffusion rate through the

OmpF pore (114). In addition, environmental conditions have been shown to determine the expression of OmpF. The expression of another general porin, OmpC, appears linked with the expression of OmpF (115, 116). Higher concentrations of OmpF exist when a cell is exposed to low osmotic, poor carbon source or low temperature conditions (115). It has also been reported that bacterial strains with lower than average concentrations of OmpF had slight increases in antibiotic resistance (115). In general, in conditions where nutrients and salinity are more dilute, OmpF is expressed in greater amounts (115), however, loss of OmpF did not lead to cell sensitivity to changes in the osmolarity of media.

CHAPTER 3: INSERTION EFFICIENCY OF AQPZ MEMBRANE PROTEINS IN LIPID AND POLYMER VESICLES[1]

3.1 Abstract

Recent research has attempted to mimic the biological separation properties of cell membranes, typically by incorporating membrane proteins into synthetic lipid or polymer membranes. This work quantified protein insertion and compared insertion to vesicle permeability using two *Escherichia coli* membrane proteins: aquaporin Z (AqpZ) and an outer membrane porin (OmpF), and two membrane materials: block co-polymer and lipids. A fluorescence correlation spectroscopy method was developed to measure protein insertion. The detergent dodecyl-maltoside substantially inhibited AqpZ insertion into and the permeability of 1/100 molar ratio AqpZ/lipid vesicles at concentrations beyond 0.3%. Vesicle permeability was found to be a function of protein insertion. At high amounts of AqpZ added, decreases or leveling-off in AqpZ insertion and vesicle permeability were sometimes observed. This variability was found to be affected by protein preparation. For lipid and polymer membranes made with AqpZ, protein insertion and maximum water permeability occurred between 1/100-1/25 molar ratio. For OmpF/lipid vesicles, protein insertion and permeability was optimal at 1/25 molar ratio. By quantifying protein insertion and determining the relationship between protein insertion and membrane permeability, these findings benefit future development of biomimetic membranes for many environmental applications including water purification, remediation, and biosensors.

[1] Author contributions: I performed all of the experiments described in this chapter and analyzed and interpreted the data. A couple of liters of AqpZ were grown by Kenny Long, an undergraduate research assistant whom I mentored.

3.2 Introduction

Biological membranes evolved to efficiently separate, organize and protect biological molecules in compartments such as cells. Transmembrane proteins found in the bilayers of cellular membranes can efficiently transport small molecules across the cell membrane. Biomimetic membranes are designed to mimic the highly efficient and selectively permeable nature of biological cell membranes. Biomimetic membranes consist of membrane proteins embedded in a lipid bilayer or polymer that mimics cells' natural lipid bilayer. For example, for water purification, the bacterial water channel protein aquaporin Z (AqpZ) has been shown to transport water rapidly and selectively when reconstituted in lipid and polymer membranes, with a productivity of up to 80 times that of commercially available reverse osmosis membranes (16). Potential uses for biomimetic membrane technology span a wide range and could benefit any process that currently employs a membrane for separation or protection, including drug delivery vesicles (20, 117), environmental remediation nanoreactors (23, 118), membrane-based biosensors (29-31, 119), and desalination membranes (16).

As membrane-based biomimetic technologies have emerged as promising systems for separation and sensing, many transmembrane proteins have been functionally reconstituted in lipids and polymers. Important proteins to this study are AqpZ, and the bacterial outer membrane porin (OmpF). AqpZ specifically and passively transports water across bacterial cell membranes. Functional reconstitution has been demonstrated as described in Chapter 2. To reconstitute membrane proteins in lipid or polymer vesicles, the detergent-protected protein is typically mixed with lipid or polymer. Typically through mechanical dispersion or slow detergent removal via dialysis, these mixed micelles, or aggregates of the various molecules, self-assemble into vesicles (73, 75, 85). Vesicles on the order of 100-1000 nm are capable of entrapping small molecules and allowing insertion of transmembrane proteins for a variety of applications (84). For engineering applications, lipids and polymers each have advantages and disadvantages as described in chapter 2. Lipid vesicles are more understood and biocompatible, but they can have a short half-life, and allow leakage of small molecules (73, 85). In contrast, polymer vesicles generally possess greater stability and mechanical strength and are less leaky to water and small molecules (33, 73, 81, 120).

The more robust behavior of polymer vesicles is attributed to its thicker membrane. However, polymer is less understood and may be less suited for protein insertion.

To optimize biomimetic materials, high membrane permeability is desired. Many studies have investigated the functional insertion of membrane proteins into lipid and polymer membrane by measuring the permeability of small molecules. However, in most of these studies protein insertion was not measured, even though unexpected decreases in membrane permeability were sometimes observed. For example, in comparing the six studies that examined the permeability of AqpZ-membranes (16, 43, 44, 46, 47, 121), differing trends were reported. In five of these studies, a decrease in water permeability was found to occur when AqpZ was reconstituted at high concentrations (16, 43, 46, 47, 121). In another study, water permeability leveled off at high concentrations (44). While permeability is expected to be a function of insertion, only one study has addressed this question (44). Using insertion measurements, *Rhodobacter sphaeroides* AqpZ incorporation efficiency was calculated as 80% for 1/2348-1/722 AqpZ/lipid molar ratio after which it decreased for 1/470-1/235 AqpZ/lipid molar ratio (44). However, the direct relationship between permeability and insertion has not been reported, and it is prudent to examine this relationship with different protein and membrane materials. When observing previous permeability behavior at high reconstitution ratios, it was hypothesized that use of polymers (64), high detergent concentrations (16, 43), and/or synthesis methods (66, 122) might impact protein insertion, and thus, permeability. Supporting the hypothesis that polymer could reduce protein insertion, theoretical models describe an energetic penalty due to protein insertion in both polymer and lipid (67). Models and some experiments suggest that shorter polymer chains better mimic natural membranes in allowing proteins to functionally insert (28, 64, 65), as described in Chapter 2. The remaining hypotheses, however, have not yet been verified experimentally.

To study the relationship between membrane permeability and protein insertion, protein insertion needs to be quantified. Fluorescence correlation spectroscopy (FCS) is a
single-molecule-sensitive technique that has been used for a variety of cellular and biomaterial applications including determination of diffusion coefficients, concentrations, aggregation, rate constant and surface interaction kinetics (123-129). The advantage of FCS is that the detection volume is sufficiently small (~1 femtoliter) so that it is possible to monitor fluctuations in

fluorophore brightness one at a time (123, 124). FCS was used to quantify the number of encapsulated soluble fluorescently-labeled protein in polymer vesicles (52, 130-134). In this approach, the brightness of vesicles with encapsulated fluorescently-labeled protein were compared to the brightness of freely diffusing fluorescently-labeled protein micelles (130). FCS was also used to estimate the abundance of fluorescently-labeled human aquaporin 5 proteins in a cell membrane (135). In other studies, the insertion of reconstituted membrane proteins in lipid and polymer was determined using FCS where the brightness of vesicles were compared to the brightness of resolubilized vesicles (protein micelles) (47, 136, 137). These studies assume complete dispersion of vesicle components after resolubilization. Theoretically, it may be more accurate to compare the brightness of vesicles to the brightness of freely diffusing protein micelles before reconstitution.

In this work, my objectives were to quantify the insertion of membrane proteins in lipid and polymer membranes, determine the relationship between membrane permeability and membrane protein insertion, and investigate the effects of detergent, membrane material, and membrane protein on the insertion and permeability behavior of hybrid protein-synthetic vesicles. To accomplish these tasks, I developed an FCS method to quantify membrane protein insertion by modifying the method for quantifying encapsulated soluble protein (130). I additionally quantified protein using the resolubilization approach previously reported (47).

3.3 Materials and Methods

Nanopure water (18 MΩ cm) was purified from deionized water in a Barnstead NANOpure system (Pittsburgh, PA) and was used to prepare all solutions. Poly(2-methuloxazoline)-poly(dimethylsiloxane)-poly(2-methuloxazoline) ($PMOXA_{15}$-$PDMS_{110}$-$PMOXA_{15}$) polymer was obtained from Drs. Wolfgang Meier and Mariusz Grezwalski (University of Basel, Switzerland). Lipids 1-palmitoyl-2-oleoyl-sn-glycero-3-phosphocholine (POPC), 1-palmitoyl-2-oleoyl-sn-glycero-3-phosphoethanolamine (POPE), and 1,2-dioleoyl-sn-glycero-3-phosphate (DOPA) were purchased from Avanti Polar Lipids (Alabaster, AL). Superdex 200 size exclusion chromatographic media and high pressure column were purchased from GE Healthcare (Piscataway, NJ). Lennox Luria broth was purchased from Becton, Dickinson, and Co. (Sparks,

MD) and n-Dodecyl-β-D-Maltopyranoside, sol-grade detergent was purchased from Anatrace (Santa Clara, CA, USA). Uranyl acetate was purchased from SPI (West Chester, PA, USA) and sodium azide was purchased Sigma Aldrich (St. Louis, MO).

AqpZ purification

AqpZ was purified according to Borgnia et al. (43) and Kumar et al. (16) except that cells were disrupted using sonication instead of a French press, and to prevent precipitation, isopropyl β-D-1-thiogalactopyranoside (IPTG) was immediately removed from purified protein using dialysis or a desalting column.

i. Growth

Ten ml of Lennox Luria broth (LB) (Becton, Dickinson and Co., Franklin Lake, NJ) containing 50 µg/ml Ampicillin (Amp) was inoculated with a single colony of an ampicillin-resistant *Escherichia coli* AqpZ overexpression strain JM109 pTrc10HisAqpZ (16) and incubated at 37°C with agitation at 250 rpm for 18 h. The culture was diluted 1:100 into 1 L LB and incubated at 37°C with agitation at 250 rpm for 24 h or until optical density (O.D.) reaches 1.5 (λ=600). At O.D. 1.5, the culture was induced with 1 mM IPTG for overexpression of AqpZ for 7 h before centrifugation (20 min, 4°C at 5,000 × g).

ii. Extraction and solubilization of membrane fraction

Pellets were resuspended in 4°C lysis buffer (0.1 M K_2HPO_4, 1 mM $MgSO_4$, 1 mM phenylmethylsulfonyl fluoride (PMSF), 1 mg/ml deoxyribonuclease I (DNAse I), pH 7.0) and cell membranes were disrupted by sonication (Branson S-450D, 37% amplitude for 10 min at 5 sec on and off rotations) three times with equal periods of rest on ice in between cycles. Disrupted cells were centrifuged (20 min, 4°C at 5,000 × g) and the supernatant ultracentrifuged (60 min, 4°C at 140,000 × g) to extract the membrane fraction. The membrane fraction pellets were homogenized, resuspended in solubilization buffer (1.5% (w/v) dodecyl maltoside (DDM) sol grade, 0.1 M K_2HPO_4, 135 mM NaCl, 10 mM imidazole, 0.1% (v/v) glycerol, 5 mM 2-mercaptoethanol (BME), pH 8.0) and incubated with shaking overnight on ice to solubilize the membrane proteins.

iii. AqpZ purification utilizing His-tag

Pre-washed nickel nitrilotriacetic acid (Ni-NTA)-agarose beads (Qiagen) were incubated with the solubilized membrane proteins at 0.08% (v/v) for 2 h before packing a 2 cm diameter gravity column. The column was washed with 10 bed volumes of wash buffer 1 (0.03% (w/v) DDM, 0.1 M K_2HPO_4, 0.2 M NaCl, 100 mM imidazole, 0.1% (v/v) glycerol, 5 mM BME, pH 7.0) and 50 bed volumes of wash buffer 2 (0.03% (w/v) DDM, 0.1 M K_2HPO_4, 0.2 M NaCl, 100 mM imidazole, 0.1% (v/v) glycerol, 5 mM BME, pH 7.0). The column was incubated at room temperature for 15 minutes midway through washing with wash buffer 2 (0.03% (w/v) DDM, 0.1 M K_2HPO_4, 0.2 M NaCl, 20 mM imidazole, 5 mM BME, pH 7.0). AqpZ was eluted with 1 bed volume of elution buffer (0.15% (w/v) DDM, 0.1 M K_2HPO_4, 0.2 M NaCl, 1 M imidazole, 0.1% (v/v) glycerol, 5 mM BME, pH 7.0) with 3 passes. Beads were eluted 3-4 times for maximum recovery. To prevent precipitation following elution, AqpZ was immediately dialyzed against elution buffer without imidazole and with 0.03% (w/v) DDM for at least 48 h and four buffer exchanges, or was desalted using PD-10 Desalting Columns with G-25 Sephadex media (GE Healthcare, Piscataway, NJ) and subsequently dialyzed. Purity was verified by sodium dodecyl sulfate (SDS)-acrylamide gel electrophoresis (10% acrylamide gel, unless noted). Purifed AqpZ was incubated in cracking buffer for approximately 15 min (33 mM Tris, 1.3% SDS, 0.67% glyucerol, 97 mM ß-mercaptoethanol) at room temperature. Combined elutions yielded concentrations between 1-2 mg/ml measured using the 660 Assay kit (Pierce Protein Products, Pittsburgh, PA). Multiple batches of AqpZ that were purified at one time were pooled for future use. AqpZ was concentrated using 30 kDa MW cut-off Amicon Ultra-4 centrifugal filters (Millipore, Billerica, MA) to concentrations suitable for fluorescent labeling (>2 mg/ml).

OmpF purification

OmpF was purified according to (55) with modifications as previously reported (23).

i. Growth

Ten ml starter cultures of LB containing 50 µg/ml Amp were inoculated with a single colony of an ampicillin-resistant *E. coli* OmpF overexpression recombinant strain BL21(DE3) omp8, picked

from a fresh plate. Cultures were incubated at 37°C on a shaker at 250 rpm for 18 h before 1:100 dilution into 1 L LB. At O.D. 0.5-0.8 (λ=600; after approximately 3-7 h) the cultures were induced with 1 mM IPTG for overexpression of OmpF and subsequently grown until O.D. 1.8 was reached (λ=600; after approximately 6 h). Cells were harvested by centrifugation (15 min at 6000 x g, 4°C).

ii. Extraction and solubilization of membrane fraction

Cell pellets were resuspended in 10 ml per g cell pellet ice cold lysis buffer (20 mM Tric-Cl, pH 8) and 10 µL DNase I (1 U/µL) per g cell pellet. Cell membranes were disrupted by sonication (Branson S-450D, 25% amplitude, 3 sec on and 2 sec off for 5 min). Cells rested 5 min on ice between sonication cycles for 3 cycles. One ml per ml of cell suspension of fresh 20% SDS was added to the cell suspension, and it was incubated for 1 h at 60°C with gentle mixing. If addition of SDS did not turn the cell suspension clear, samples were sonicated for additional time until a clear solution was achieved. The cell membrane fractions were removed by centrifugation (60 min. at 40,000 x g, 4°C) and subsequently washed with ice cold 20 mM phosphate buffer (pH 7.4) to remove residual SDS. Protein pre-extraction was achieved by adding 5 mg/g cell pellet 0.125% n-Octyl-oligo-oxyethylene (octyl-POE; Enzo Life Sciences) in 20 mM phosphate buffer (pH 7.4) and homogenizing the pellet (Wheaton Homogenizer, 7 ml). The suspension was incubated for 1 h at 37°C and the cell membrane fractions were removed by ultracentrifugation (45 min. at 145,000 x g, 4°C).

iii. OmpF extraction

For OmpF extraction, the fractions were treated with 3% Octyl-POE in 20 mM phosphate buffer (pH 7.4), homogenized (Wheaton Homogenizer, 7 ml), and incubated for another 1 h at 37°C before the solubilized OmpF was separated from the membrane fraction via centrifugation (45 min at 145,000 g, 4°C). Purity was verified by SDS-acrylamide gel electrophoresis (12% acrylamide gel). OmpF yields ranged between 1.6-4.4 mg per L of culture. To reduce the detergent concentration, OmpF was dialyzed against 20 mM phosphate buffer (PB) with 1% octyl-POE for at least 48 h and four buffer exchanges. OmpF was quantified using a BCA assay (Pierce Protein Products), and concentrated using 30 kDa MW cut-off Amicon Ultra-4 centrifugal filters (Millipore, Billerica, MA) to concentrations suitable for fluoresce labeling (>2 mg/ml).

Fluorescent labeling

AqpZ and OmpF were labeled with Alexa Fluor 488 based on the Amine-Reactive Probes Protocol from Invitrogen (138) with modifications. A step-by-step protocol is provided in APPENDIX A. Ten mg/ml Alexa Fluor 488 carboxylic acid, succinimidyl ester, amine-reactive dye (Thermo-Fisher Scientific, Pittsburgh, PA) stock was prepared by adding DMSO directly to the Alexa Fluor 488 powder. Concentrated (>2 mg/ml) AqpZ or OmpF was incubated with 0.2 M NaHCO3, pH 8.3 and excess Alexa Fluor 488 (protein:dye molar ratio $8.6x10^{-2}$ to $4.3x10^{-2}$) for 4 h with agitation in the dark at room temperature. The labeling reaction was stopped and excess dye separated from AqpZ by size exclusion chromatography with a Superdex 200 pressurized Tricorn 50 ml column using an Äkta prime plus instrument (GE Healthcare, Chicago, IL). An SDS-PAGE gel (10% acrylamide) with BSA standards and stained with Coomasie Brilliant Blue (Sigma-Aldrich, St. Louis, MO) was used to quantify labeled protein by analysis with ImageJ Analysis Software (v.1.34S; National Institutes of Health, Bethesda, MD). The degree of labeling (DOL) was calculated by Equation 3.1 (138).

$$DOL = \frac{A_{max} * MW}{[protein] * \varepsilon_{dye}}$$

Equation 3.1. Degree of labeling

where A_{max} is the absorbance measured at the known maximum wavelength of 495 nm for Alexa Fluor 488 using a UV spectrometer (UV-2450, Shimadzu, Kyoto, Japan), MW is the known molecular weight of the protein monomer (AqpZ: 28 kDa, OmpF: 38 kDa), [protein] is the concentration of protein in mg/ml determined from a quantification gel as described above, and ε_{dye} is the known extinction coefficient of 71,000 $cm^{-1}M^{-1}$ for Alexa Fluor 488 at its absorbance maximum (139). DOL values ranging between 1.15-2.62 per AqpZ tetramer and 0.34-2.25 per OmpF trimer were achieved. DOL values were included in FCS calculations.

Vesicle preparation

Vesicles were prepared by film rehydration (16) by dissolving 12 mg (poly-(2-methyloxazoline)-polydimethylsiloxane-poly-(2-methyloxazoline) $PMOXA_{15}$-$PDMS_{55}$-$PMOXA_{15}$ triblock copolymer in 2 ml chloroform or combining 1-palmitoyl-2-oleoyl-*sn*-glycero-3-phosphocholine (POPC), 1-palmitoyl-2-oleoyl-sn-glycero-3-phosphoethanolamine (POPE) and 1,2-dioleoyl-sn-glycero-3-phosphate (DOPA) (each 10 mg/ml in chloroform) at a 70:15:15 molar ratio in a 100-ml round-bottom flask. A thin polymer or lipid film was formed by removing chloroform with rotary vacuum evaporation (vacuum <400 mbar) at room temperature. Trace chloroform was removed under a high vacuum (<0.3 mbar) for at least 2 h. For AqpZ-containing vesicles, the films were rehydrated with varying amounts of fluorescently labeled AqpZ in phosphate-buffered sodium (PBS) and DDM sol grade (final concentrations 0.06% (w/v) AqpZ/polymer, 0.08-0.09% (w/v) AqpZ/lipid) pH 7.2 for a final polymer or lipid concentration of 6 mg/ml. For OmpF-containing vesicles, the films were rehydrated with varying amounts of fluorescently labeled OmpF, 20 mM PB, octyl-POE (final concentration 0.3% (w/v)), pH 7.2 for a final lipid concentration of 6 mg/ml. Films were rehydrated at 4°C with a magnetic stir bar for 36 h and extruded using a pneumatic thermobarrel extruder (Northern Lipids, Burnaby, Canada) through a 1.0 μm track-etched membrane (Millipore, Billerica, MA) at least 5 times. Subsequently, vesicles were sequentially extruded through 0.6, 4.0 and 0.2 μm track-etched membranes, at least 5 times each. Vesicles were size excluded from any excess materials with a Superdex 200 pressurized Tricorn 50 ml column using an Äkta prime plus instrument (GE Healthcare, Chicago, IL). Monitoring column flow through (UV-Vis λ=600 nm), care was taken to collect small fractions during size exclusion to include only vesicles.

Cleaving the Alexa Fluor label post-reconstitution

The protocol by New England Biolabs, Inc. (140) was followed with slight modifications for cleaving the Alexa Fluor 488 fluorescent probe from AqpZ. AqpZ/lipid vesicles were incubated with Factor Xa (1:50 (w/w) Factor Xa:AqpZ), 2 mM $CaCl_2$, pH 8 overnight at room temperature with agitation. To remove cleaved fluorescent label, treated vesicles were size excluded with a Superdex 200 pressurized Tricorn 50 ml column using an Äkta prime plus instrument (GE Healthcare, Chicago, IL).

Vesicle characterization

Vesicle size was measured by dynamic light scattering (DLS) using a 4W Zetasizer nanoseries instrument with a He-Ne standard laser with a wavelength of 632.8 nm at 90º scattering angle at room temperature (Zetasizer nano-ZS90, Malvern Instruments, Malvern, UK). An autocorrelation function was used to determine vesicle size, and diameter and polydispersivity index (PDI) values from three sets of measurements were averaged. Vesicles were also imaged with transmission electron microscopy (TEM) (2100 Cryo, JEOL, Tokyo, Japan) at 200 kV using thin film holey carbon grids (Ted Pella, Redding, CA, USA) glow-discharged on Denton DPG-1 (Denton Vacuum Inc., Moorestown, NJ, USA) at 20 V for 45-60 seconds. Samples were incubated on the grid surface for 60 seconds and stained with 0.1% uranylacetate for 60 seconds. The contact angles of prepared vesicle solutions were measured as previously described (141). Using a CAM200 optical goniometer (Biolin Scientific, Paramus, NJ), 20 µl of sample were deposited on parafilm M (Bemis, Neenah, WI), allowed to equilibrate for 30 s, and imaged by a high speed camera. Images formed by the droplet with respect to the parafilm substrate were fitted using a Young-Laplace drop profile fitting method.

FCS method developed to quantify membrane protein insertion

FCS was used to determine the number of molecules of both vesicles with fluorescently labeled protein and freely diffusing fluorescently labeled protein. A discussion of the theory and protocol used is provided in APPENDIX B. Fluorescence intensity was measured using single-photon FCS with an Alba fluorescence correlation spectrometer (ISS, Champaign, IL) with a wavelength of 467 nm. The instrument was calibrated using nanomolar aqueous solutions of Alexa Fluor 488 with a pinhole of 50. Three aliquots of each sample were measured for 100 seconds at 30 or 50% power three times in fluorescence fluctuation spectroscopy (FFS) mode. Measurements at 50% power were corrected to 30% power during fitting by measuring labeled AqpZ at both powers. Measurements yielded smooth autocorrelation curves. No decrease in signal intensity was observed during these measurements, indicating that bleaching was not a problem.

Autocorrelation data for 10 ten-second measurements were averaged and fit by a single species 3D Gaussian diffusion model described by Equation 3.2:

$$G(\tau) = \frac{1}{N} \cdot \frac{1}{1+\tau/\tau_D} \cdot \frac{1}{\left[1+\left(w_o/z_o\right)^2\left(\tau/\tau_D\right)\right]^{1/2}}$$

Equation 3.2. 3D Gaussian diffusion model

where N is the average particle number in the focal volume, w_o and z_o are half-height dimensions, τ is the measurement time, and τ_D is the 2D lateral diffusion time in the focal volume or the characteristic decay time of the correlation function. N can be calculated by the amplitude of the of the autocorrelation curve knowing the radius and dimensions w_o and z_o from calibration measurements. When $\tau = 0$, 1/G(0) is the average number of particles, N. The diffusion time, τ_D, is related to the particle's diffusion coefficient, D, as shown in Equation 3.3. The diffusion coefficient for a given particle is based on its size (123, 142).

$$\tau_D = \frac{w_o^{\,2}}{4D}$$

Equation 3.3. Diffusion time

Data was analyzed using the confocal spectroscopy and imaging application, VistaVision (version 4.0 build 00144; ISS, Champaign, IL, USA). Data was separated into 10, 10-second measurements and the correlation curves were averaged into one correlation curve per measurement per aliquot. Correlation curves for all measurements were fit using the single species 3D Gaussian autocorrelation function (Equation 3.2) and the range of each correlation curve fit was at least 0-0.2 seconds. For Alexa Fluor 488, the diffusion coefficient was fixed to the known value at 20°C of 380 $\mu m^2 s^{-1}$ (143), concentrations were fixed, and the excitation volume parameters, ω_o and z_o, were linked to determine the ω_o and z_o values for each measurement session. For labeled AqpZ and OmpF, the excitation volume parameters, ω_o and z_o, were fixed as obtained from fitting the Alexa Fluor 488, and initial values for diffusion coefficients and concentrations were set to 30 $\mu m^2 s^{-1}$ and 1 nM, respectively. For vesicles, ω_o and z_o were also fixed and initial values for vesicle diffusion coefficients and concentrations were set to 5 $\mu m^2 s^{-1}$ and 1 nM, respectively. Distinct diffusion coefficients were obtained for three diffusing species ranging from the known 380 $\mu m^2/s$

(143) for Alexa Fluor 488, 34±8.8 $\mu m^2/s$ for AqpZ micelles, 19.8±6.0 $\mu m^2/s$ for OmpF micelles, and 2.5±1.9 $\mu m^2/s$ for vesicles. These findings are discussed in Section 3.4.

The number of protein inserted in an average vesicle was subsequently determined by comparing the counts (brightness) per molecule per second (CPMS) of the vesicle to that of the labeled protein micelles (130). The CPMS for vesicles was calculated by Equation 3.4.

$$CPMS = CPS/[1/G(0)]$$

Equation 3.4. CPMS for vesicles

where CPS is the counts per second and 1/G(0) is the number of fluorescent molecules. The CPMS for protein was calculated by Equation 3.5.

$$CPMS = CPS/[1/G(0)\times DOL]$$

Equation 3.5. CPMS for protein

where DOL is the degree of labeling. The degree of labeling ranged from 1.2-2.6 mol dye/mol AqpZ monomer and 0.3-0.7 mol dye/mol OmpF monomer. As first described to quantify the number of encapsulated soluble proteins in polymer vesicles (130), the number of protein present in an average vesicle was determined by the ratio of the counts per molecule of the vesicle to the counts per molecule of the labeled protein, as shown in Equation 3.6.

$$\#\ \text{protein per vesicle} = CPMS_{vesicle}/CPMS_{protein}$$

Equation 3.6. Number protein/vesicle

Due to the high photo stability of Alexa Fluor 488 (144), differences in fluoresce intensity in buffer and in the vesicle membrane were not expected nor identified by data collected. Insertion data is tabulated in APPENDIX C.

Resolubilization method to quantify membrane protein insertion

Following previous studies (47, 136, 137), vesicles with fluorescently-labeled AqpZ and OmpF were measured on FCS and then resolubilized and measured again on FCS. Vesicles were agitated

with 2.5-3% octyl-glucoside (OG) for 24-86 h. Vesicles and resolubilized vesicles were measured using the same FCS procedure and data fitting techniques already described for vesicles and freely-diffusing fluorescently-labeled protein micelles. The number of fluorescently labeled species, 1/G(0), was determined from the 3-D Gaussian diffusion model when $\tau = 0$. The number of protein inserted in an average vesicle was determined by comparing the number of vesicles to that of the labeled protein (47), as shown in Equation 3.7.

$$\#\ \text{protein per vesicle} = [1/G(0)]_{vesicle}/[1/G(0)]_{protein}$$

Equation 3.7. Number protein/vesicle (resolubilization)

Vesicle permeability measurements

Vesicle permeability was determined using an SX.18MV-R stopped-flow spectrometer (Applied Photophysics, Surrey, UK) with light scattering according to Borgnia et al (43). Vesicles were mixed with equal volumes of a 1 M NaCl (AqpZ-containing vesicles) or 1 M glucose (OmpF-containing vesicles) osmotic agent at 10°C. Change in vesicle size due to water efflux was monitored by light scattering at 600 nm emission wavelength. The light scattering curves (at least 7) were averaged and fitted using an exponential rise equation in Origin software (Origin v.8.1) and permeability (P_f) calculated using Equation 3.8 as previously described (43).

$$P_f = k/[(S/V_o)\times V_w\times \Delta_{osm}]$$

Equation 3.8. Vesicle permeability

where k is the exponential rise rate constant, S/V_o the initial vesicle surface area to volume ratio, V_w the known molar volume of water (18 cm^3/mol), and Δ_{osm} the imposed osmolar gradient. Vesicle permeability data is tabulated in APPENDIX C.

3.4 Results and Discussion

Vesicle characterization

To ensure that vesicles were formed, each preparation was examined with DLS, and representative preparations were examined with TEM. For AqpZ/polymer vesicles, the average diameter was 234.9±37.1 nm (Figure 3.2). These values were within the range expected for PMOXA-PDMS-based co-polymer vesicles (145), albeit larger than values reported for polymer vesicles with AqpZ inserted (16). For AqpZ/lipid vesicles, the average diameter was 176.4±37.9 nm, (Figure 3.2), consistent with previously reported values for phospatidylcholine (PC)-based lipid vesicles (146), but approximately 40-50 nm larger than previously reported values for AqpZ/lipid vesicles (43, 147). For OmpF/lipid vesicles, the average diameter was 124.3±37.2 nm (Figure 3.2), again consistent with PC-based lipid vesicles (146). Overall, for AqpZ/polymer and OmpF/lipid vesicles, as more protein was added during vesicle reconstitution, I observed a slight increase in vesicle diameter. The diameters of AqpZ/lipid vesicles did not appear to change with changing molar ratios.

A PDI value of 0.2 is considered low and below which monodisperse vesicles are assumed to exist (148, 149). AqpZ/polymer and AqpZ/lipid vesicles had an average PDI value of 0.22±0.08. For AqpZ/polymer vesicles, the average PDI value did increase beyond 0.2 for 1/250 to 1/25 molar ratio (ranged from 0.21±0.05 to 0.28±0.08). Although these PDI values were not ideal, I included these vesicles in the study due to limited polymer availability. AqpZ/lipid and OmpF/lipid vesicles had ideal average PDI values of 0.15±0.05 and 0.17±0.06, respectively, with most values falling below the 0.2 threshold. As more protein was added during vesicle reconstitution, I observed a slight increase in vesicle diameter and PDI value, especially for AqpZ/polymer and OmpF/lipid vesicles (Figure 3.1).

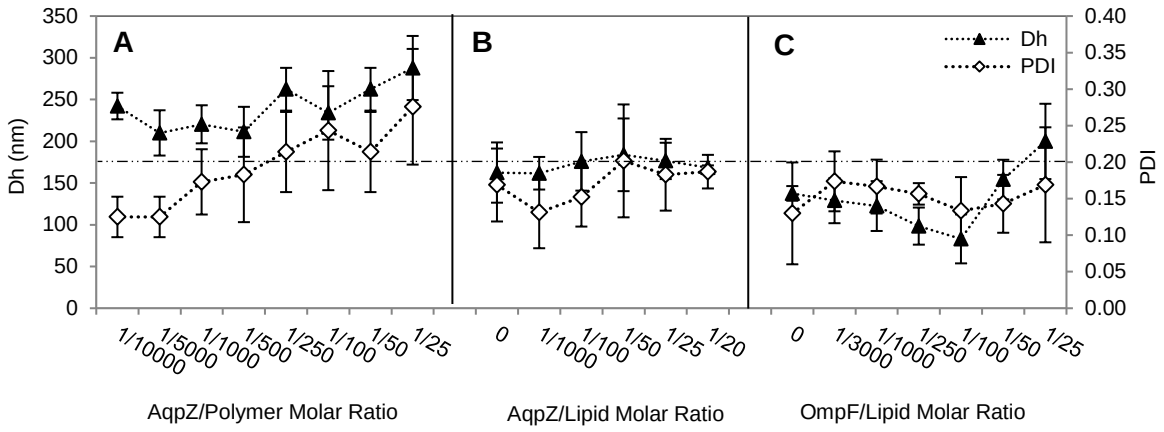

Figure 3.1. Hydrodynamic diameter (D_h) and polydispersivity index (PDI) of vesicles
Dh indicates vesicle size and PDI indicates vesicle uniformity. (A) AqpZ/polymer, (B) AqpZ/lipid, and (C) OmpF/lipid vesicles. The horizontal dashed line indicates a PDI value of 0.2, below which fairly uniform vesicles are assumed to exist (148, 149); most lipid vesicle samples fell within this range. Error bars represent standard deviations of replicates across all vesicle samples at a particular ratio and composition.

TEM images showed formation of polymer and lipid vesicles (Figure 3.2). Polymer vesicles exhibited the spherical, vesicle-like aggregates expected of polymer vesicles (16, 52, 132, 150). Lipid vesicles also exhibited spherical shapes but appeared more translucent, distorted and collapsed or folded compared to polymer vesicles (146, 148), due to the negative staining procedure and drying techniques employed in TEM sample preparation which can alter the shape of the vesicles (148). Since polymer vesicles have been shown to exhibit much higher resistance to rupture than lipid vesicles (144), it is not surprising that they were less affected by the stresses of the TEM sample preparation. The images were not visibly affected when AqpZ was reconstituted into the membranes.

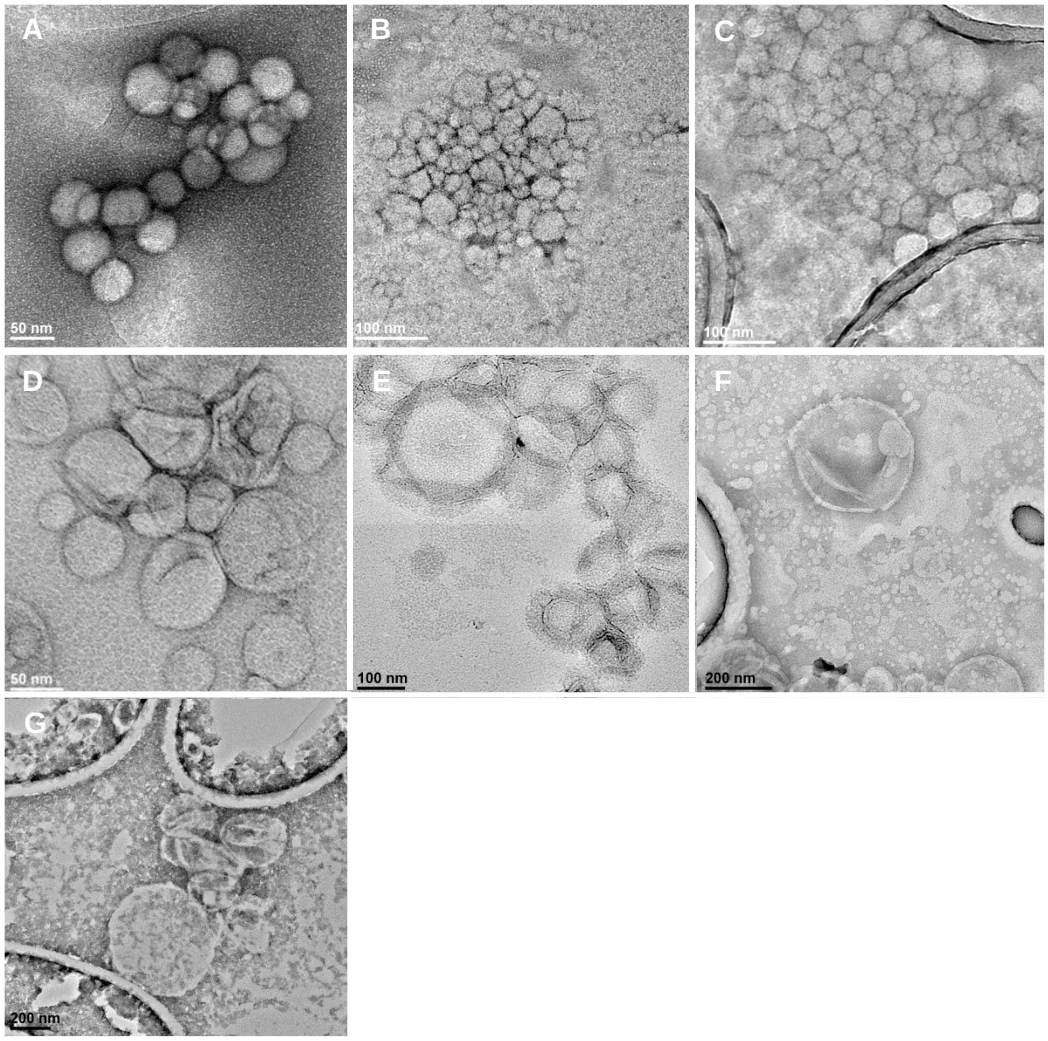

Figure 3.2. TEM images of lipid and polymer vesicles with and without AqpZ
(A) 0 molar ratio AqpZ/polymer vesicles, (B) 1/100 molar ratio AqpZ/polymer vesicles, (C) 1/50 molar ratio AqpZ/polymer vesicles, (D) 0 molar ratio AqpZ/lipid vesicles, (E) 1/1000 molar ratio AqpZ/lipid vesicles, (F) 1/50 molar ratio AqpZ/lipid vesicles, and (G) 1/25 molar ratio AqpZ/lipid vesicles. Vesicles were loaded onto ultrathin film holey carbon TEM grids and negatively stained with 1% uranyl acetate.

Development of an FCS method to quantify membrane protein insertion in vesicles

To measure the amount of membrane protein inserted in vesicle membranes, I developed an FCS method building on previous work for quantifying the number of encapsulated soluble proteins in polymer vesicles (130). Free Alexa Fluor 488 (AF488) was used to calibrate the FCS instrument for each use and to calculate the geometric parameters needed to fit data (Figure 3.3A).

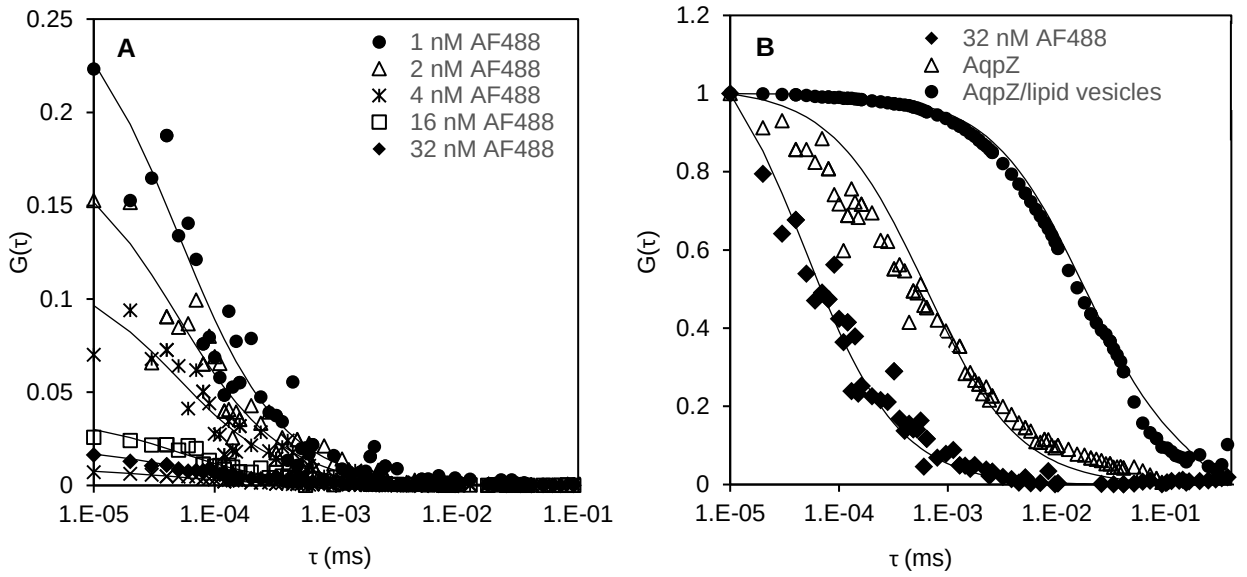

Figure 3.3. FCS standards and calibration
(A) Autocorrelation curves for free label (AF488) used for calibration of the Alba FCS instrument and to obtain the confocal dimensions, w_o and z_o, needed for fitting of the data measured for labeled-protein micelles and labeled-protein in vesicles. (B) Representative normalized and fitted FCS single species 3D Gaussian autocorrelation curves of free fluorescent label, AqpZ, and AqpZ/lipid vesicle data show distinctly different diffusion coefficients and diffusion times.

Free fluorescent label, labeled protein (micelles), and labeled protein in vesicles were measured separately to obtain their diffusion coefficients (Figure 3.3B). They ranged from 380 $\mu m^2/s$ (143) for free fluorescent label, 34±8.8 $\mu m^2/s$ for AqpZ micelles, 19.8±6.0 $\mu m^2/s$ for OmpF micelles, and 2.5±1.9 $\mu m^2/s$ for vesicles. The single species 3D Gaussian diffusion model fit each well, suggesting that size exclusion chromatography was effective at removing excess label from the protein and unincorporated, labeled protein from vesicles. The number of labeled proteins present in an average vesicle was then determined based on the ratio of the counts per molecule of the vesicle to the counts per molecule of the labeled protein, allowing quantification of protein insertion.

Quantification of AqpZ insertion and vesicle permeability with varying detergent concentrations during reconstitution

To test the influence of detergent on membrane protein insertion, I quantified the number of AqpZ inserted and the permeability of 1/100 molar ratio AqpZ/lipid vesicles when the vesicles were reconstituted with varying concentrations (up to 1% (w/v)) of the detergent dodecyl maltoside (DDM). Vesicle permeability decreased at 0.6% DDM (Figure 3.4). AqpZ insertion appeared to decrease with increasing DDM concentration, but was substantially inhibited at 0.3%. These results suggest that detergent does inhibit AqpZ insertion into, and thus the permeability of, 1/100 molar ratio AqpZ/lipid vesicles at high detergent concentrations.

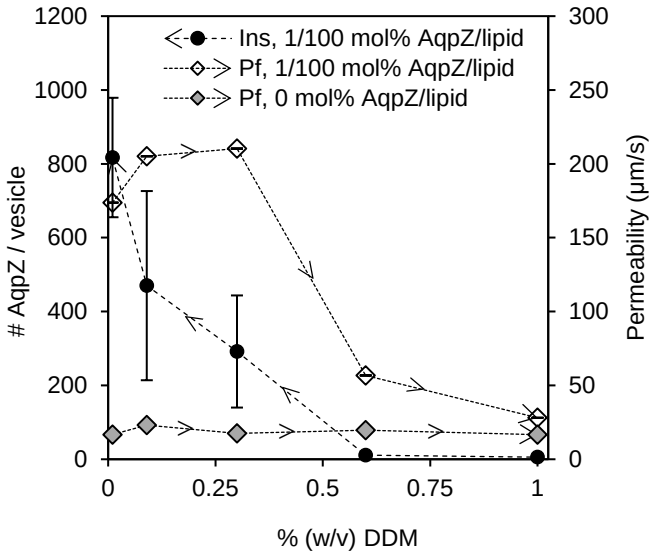

Figure 3.4. Effect of DDM detergent on AqpZ insertion and vesicle permeability
DDM inhibited AqpZ insertion into and permeability of 1/100 molar ratio AqpZ/lipid vesicles beyond 0.3%. Insertion was inhibited even with 0.1% DDM. For no protein vesicles, no change in permeability was observed. Error bars represent the propagated standard error from fitting light scattering data and of the multiple FCS measurements of each vesicle preparation. Abbreviations are as follows: insertion (ins), permeability (P_f).

In previous work, as the amount of AqpZ added increased, so did the detergent concentration during reconstitution into membrane materials, up to 1% (w/v) (16, 43), and decreases in vesicle permeability were observed. For the rest of the data presented herein, I kept the DDM concentrations in vesicles relatively constant and below 0.3% (w/v), the point at which AqpZ

insertion was substantially inhibited. Specifically, AqpZ/polymer and AqpZ/lipid vesicles were prepared at 0.06% and 0.08-0.09% (w/v) DDM, respectively. However, difficulty in removing detergent via dialysis for low critical micelle concentration (CMC) detergents like DDM have been described (151, 152), so it is possible that DDM concentrations were higher than anticipated during AqpZ/lipid vesicle formation. Even if no DDM was removed following AqpZ purification, vesicles would have no more than 0.12% (w/v) DDM during reconstitution. OmpF/lipid vesicles were prepared with a different detergent, n-Octyl-oligo-oxyethylene (Octyl-POE), at 0.3% (w/v).

Additionally, to test if the detergent concentrations during reconstitution reflected an increase in bulk detergent concentrations of the vesicle suspensions, contact angles between the solution and parafilm were measured (Figure 3.5A). Surprisingly, the contact angles were very similar across the range of DDM concentrations tested (exception: 1/100 molar ratio AqpZ/lipid vesicles reconstituted at 0.6% DDM), and were similar between the 0 and 1/100 molar ratio AqpZ/lipid vesicle preparations. This similarity may be explained by the fact that after the film rehydration phase, vesicles were separated from unreacted molecules by size exclusion chromatography in detergent-free buffer, further reducing detergent concentrations of the vesicle suspensions. It is possible that detergent molecules still resided inside vesicles, or in the membrane itself, which contact angle measurements of the vesicle suspensions would not capture.

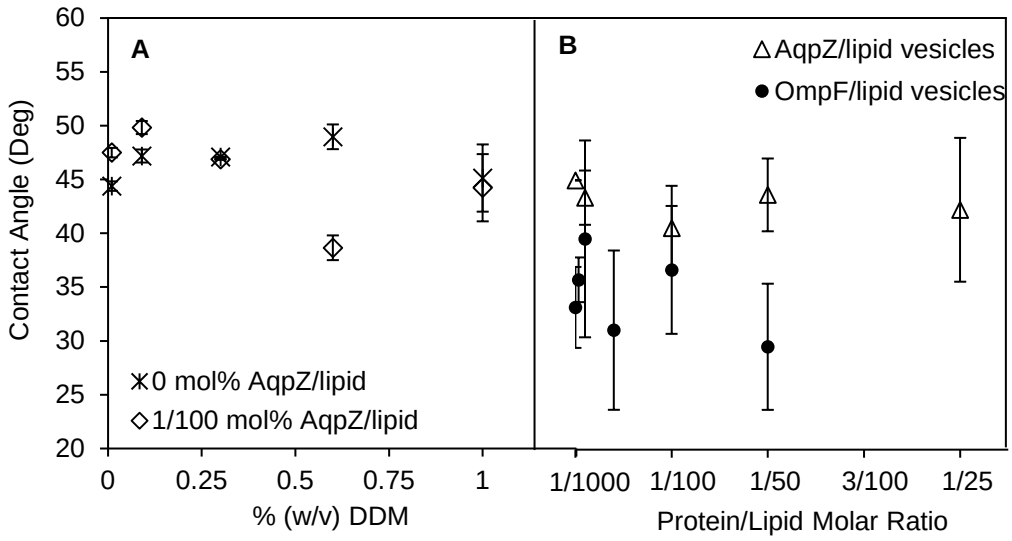

Figure 3.5. Contact angle measurements to measure amount of DDM detergent
(A) 0 and 100 molar ratio AqpZ/lipid vesicles reconstituted at varying DDM concentrations. (B) AqpZ/lipid (four replicates, representing two protein preps) and OmpF/lipid (duplicates of single protein prep) vesicles.

To determine if there were differences in bulk vesicle detergent concentrations when vesicles were prepared with fairly constant detergent concentrations (AqpZ/lipid vesicles: 0.08-0.09% (w/v) DDM; OmpF/lipid vesicles: 0.3% (w/v) Octyl-POE), contact angles were measured for AqpZ/lipid and OmpF/lipid vesicles made with varying amounts of protein added (Figure 3.5B). Similar bulk vesicle detergent concentrations were found across molar ratios, especially for AqpZ/lipid vesicles.

Quantification of protein insertion and vesicle permeability with varying concentrations of protein added

To determine the influence of the amount of protein added during reconstitution on protein insertion and vesicle permeability, I measured insertion and permeability for OmpF/lipid, AqpZ/lipid and AqpZ/polymer vesicles with varying amounts of protein added. Generally, I found that protein insertion affected vesicle permeability. For OmpF/lipid vesicles, as more protein was added, more protein inserted and vesicle permeability increased for 0-1/25 molar ratio (Figure 3.6). In addition, two independent OmpF protein preparations produced similar insertion and vesicle permeability behavior.

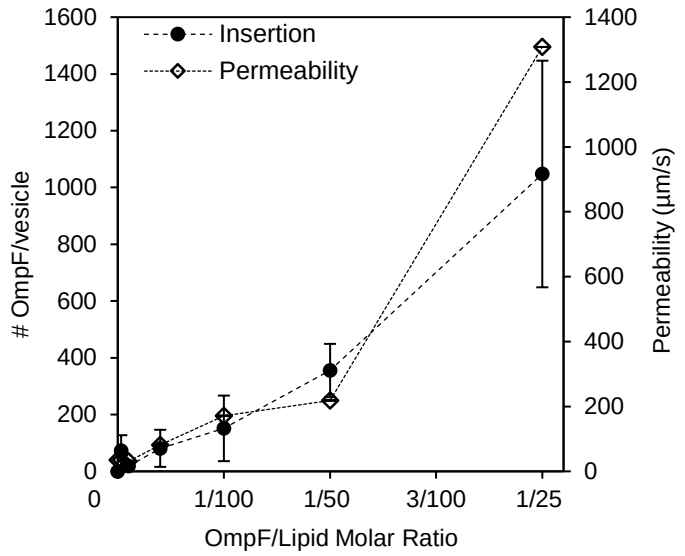

Figure 3.6. Insertion and permeability measurements of OmpF trimer in lipid vesicles
Measurements from duplicate vesicle preparations for two protein preparations were averaged. Error bars represent propagated standard error of the permeability measurements from fitting light scattering data and of the multiple FCS measurements of each vesicle preparation.

For AqpZ/lipid vesicles, I found that vesicle permeability was linearly related to AqpZ insertion (Figure 3.7). Linear regression of AqpZ/lipid vesicle permeability and insertion data yielded a good fit ($R^2 = 0.89$). Using a Z-score test, one outlier was not included in the fit. Experimental conditions do not suggest an explanation for the existence of the outlier. The linear relationship verifies my hypothesis that vesicle permeability increases with AqpZ insertion across the range tested.

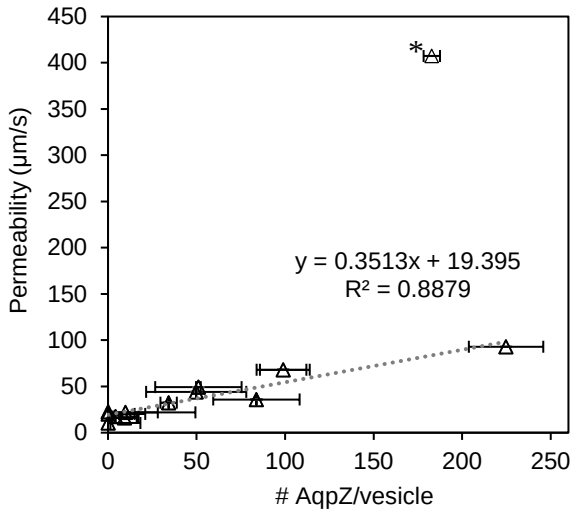

Figure 3.7. Permeability versus insertion of AqpZ/lipid vesicles
All data except for an outlier identified using the Z-score (threshold > 3) were included in the linear trendline fit. * denotes the outlier. Vertical error bars represent propagated standard error of the permeability measurements from fitting light scattering data and are too small to appear. Horizontal error bars represent propagated standard error of the multiple FCS measurements of each vesicle preparation. For the insertion analysis, AqpZ was assumed to be in tetramers.

Interestingly, insertion and permeability behavior for AqpZ/lipid and polymer vesicles was consistent among replicate vesicle preparations for a single protein preparation (Figure 3.8). However, I found variability in permeability behavior between protein preparations for AqpZ/lipid vesicles. For AqpZ/lipid vesicles, insertion and permeability data for each protein preparation are therefore presented in separate panels of Figure 3.8. For AqpZ/lipid replicates, the decrease in permeability beyond the maximum observed at 1/100 or 1/50 molar ratio AqpZ/lipid can be explained by a decrease in AqpZ insertion (Figure 3.8A and B). Similarly, the continued increase in permeability in Figure 3.8C was a result of increasing AqpZ insertion. AqpZ/lipid vesicles that exhibited maximum permeability at 1/50 molar ratio were consistent with previously reported optimal permeability (16, 43, 46, 121). For AqpZ/polymer vesicles, the increase in permeability through 1/100 molar ratio followed by a decrease at 1/50 molar ratio and again an increase at 1/25 molar ratio was a result of varying protein insertion (Figure 3.8D). Note that only one protein preparation was tested in polymer.

The decreases or leveling off of insertion and permeability at high molar ratios of AqpZ added for some replicates of AqpZ/lipid vesicles (Figure 3.8A and B) was similar to previous reports (16,

43, 46, 47, 121). However, in this work, detergent concentrations were kept relatively constant and well below where I saw severe insertion inhibition (0.3% DDM). As such, detergent concentrations cannot be the only factor influencing protein insertion, and thus, the water permeability, of vesicles. Due to the high photo stability of Alexa Fluor 488 (144), differences in fluorescence intensity in buffer and in the vesicle membrane were not identified by the data collected. Additionally, for AqpZ/lipid vesicles, I found the insertion and permeability trends and absolute values to depend on protein preparation. It appears that differences in protein concentration or AqpZ/lipid vesicles, I found the insertion and permeability trends and aggregation between the protein preparations might explain the different insertion behaviors.

Comparing AqpZ multimer state between protein preparations, suggests the possibility that AqpZ insertion behavior at high AqpZ reconstitution ratios may be explained by the degree of AqpZ aggregation. The AqpZ insertion and vesicle permeability behavior appeared to correlate with the AqpZ multimer state observed on SDS-PAGE gels (Figure 3.9). While these gels are not native (non-denaturing), AqpZ has been reported as unusually stable under SDS-PAGE conditions (1% SDS, 143 mM ß-mercaptoethanol, 1 hr incubation at room temperature) (43). Vesicles where insertion and permeability increased overall from 0-1/25 molar ratio AqpZ/membrane material had more higher order (octomer or more) AqpZ complexes quantified using pixel analysis and summarized in Table 3.1. Conversely, vesicles where insertion and permeability either remained constant or decreased beyond the peak at 1/100 or 1/50 had greater amounts of monomer and tetramer present. This observation suggests that at high AqpZ concentrations, AqpZ monomers were not inserting as expected, whereas the higher order AqpZ were still inserting and active. To our knowledge, this phenomenon has not been reported previously.

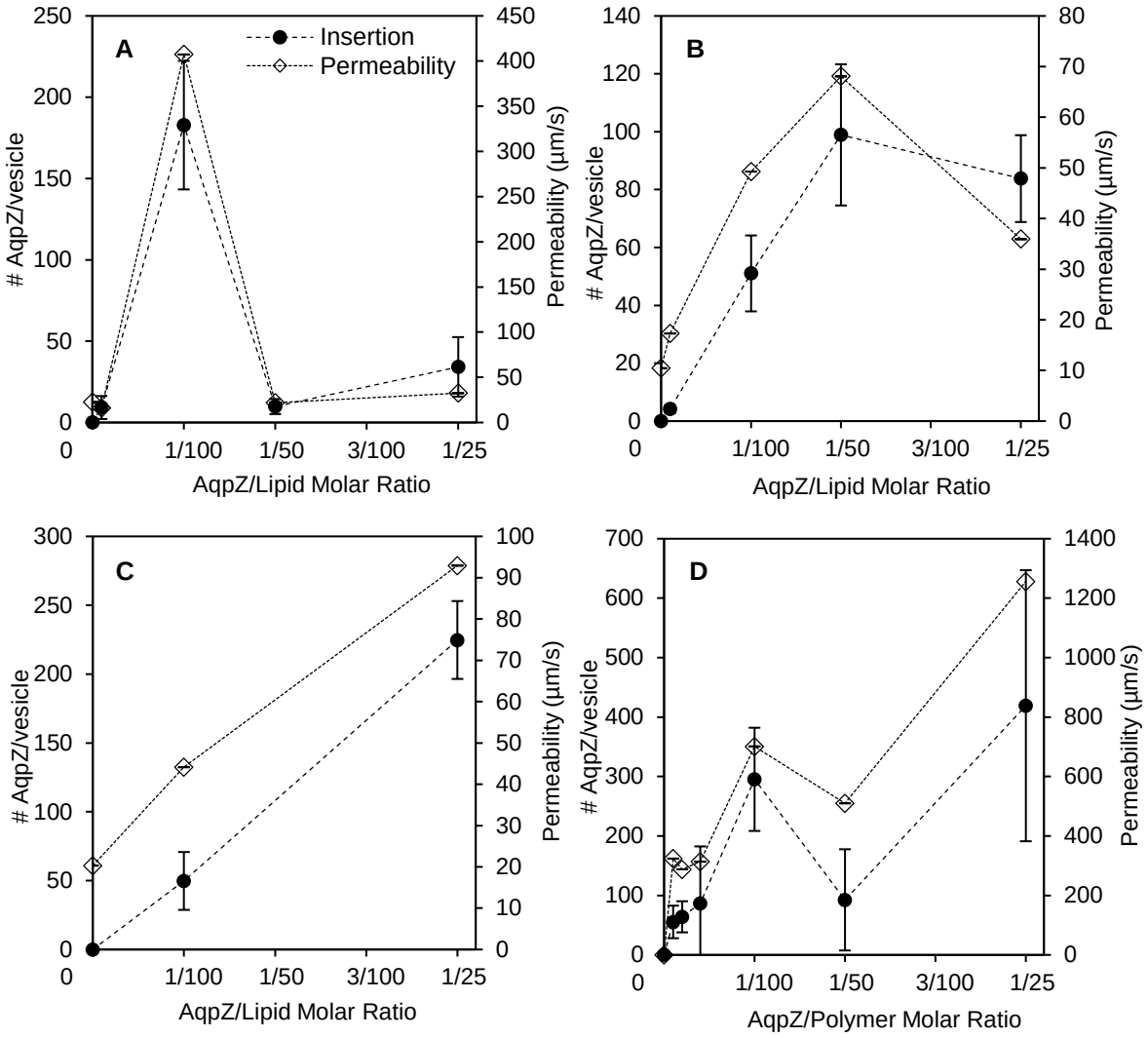

Figure 3.8. Insertion and permeability measurements of AqpZ in polymer and lipid vesicles at varying molar ratios of protein added
(A-C) AqpZ/lipid vesicles, replicates (at least duplicates) from independent protein preparations. (D) AqpZ/polymer vesicles. Error bars represent propagated standard error of the permeability measurements from fitting light scattering data and of the multiple FCS measurements of each vesicle preparation. Note that scales vary among the panels. For the insertion analysis, AqpZ was assumed to be in tetramers.

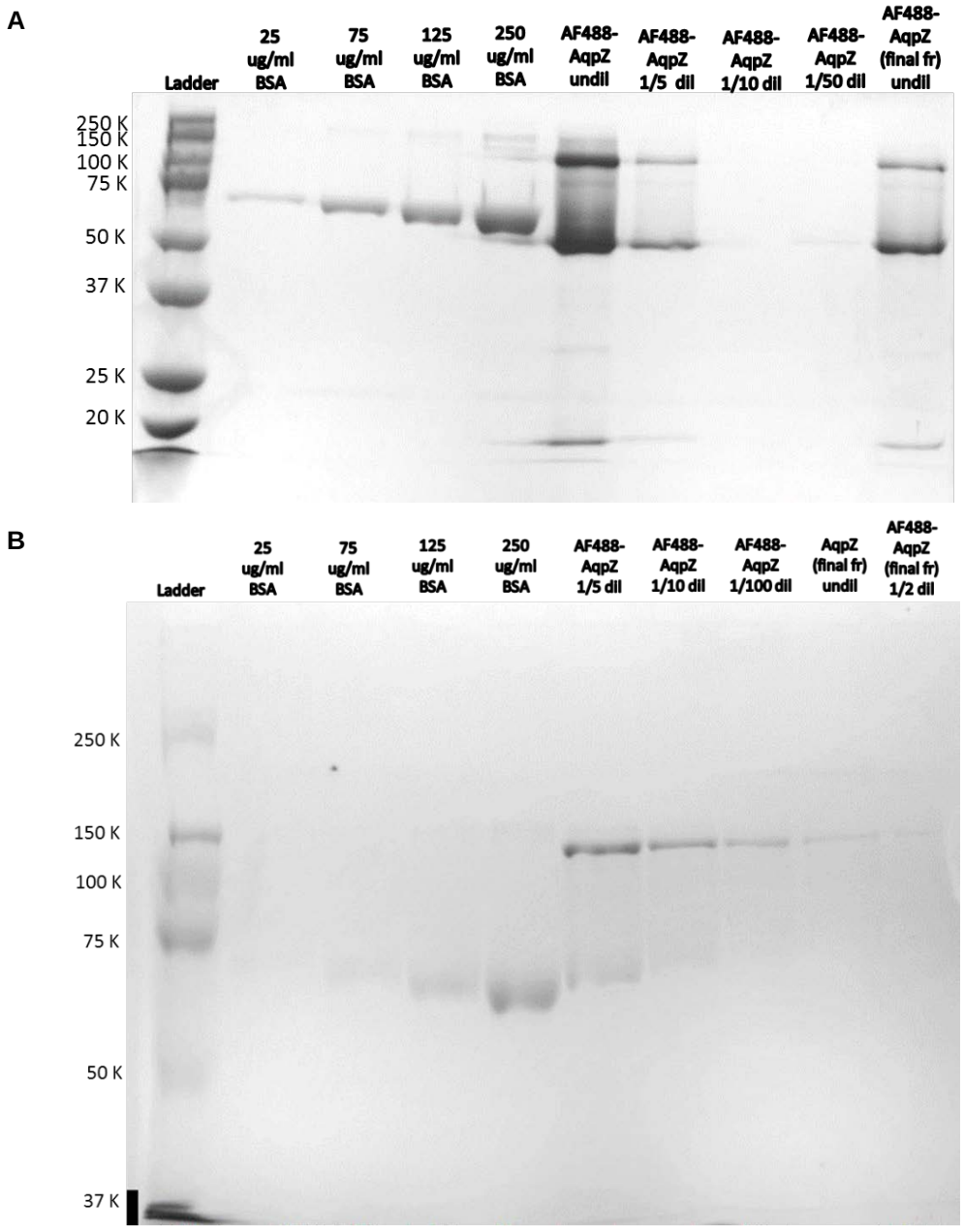

Figure 3.9. SDS-PAGE gels to quantify labeled AqpZ
AqpZ tetramer has an apparent molecular weight of 53 KDa on 10% (w/v) acrylamide (43). All gels were handcast 10% (w/v) acrylamide except as noted. Dilutions are noted and initial or final fractions are size exclusion fractions checked separately from the pooled fractions. (A) AqpZ corresponding to Figure 3.7A. (B) AqpZ corresponding to Figure 3.7B. The gel shown includes both labeled AqpZ (AF488-AqpZ) and unlabeled AqpZ as noted. (C) AqpZ corresponding to Figure 3.7C. The gel shown includes both labeled and unlabeled AqpZ as noted. (D) AqpZ corresponding to Figure 3.7D, 4-20% acrylamide (w/v) pre-cast gel. The gel shown includes both labeled and unlabeled AqpZ as noted. Abbreviations are as follows: Bovine serum albumin (BSA), AF488 labeled AqpZ (AF488-AqpZ), diluted (dil), undiluted (undil), fraction (fr).

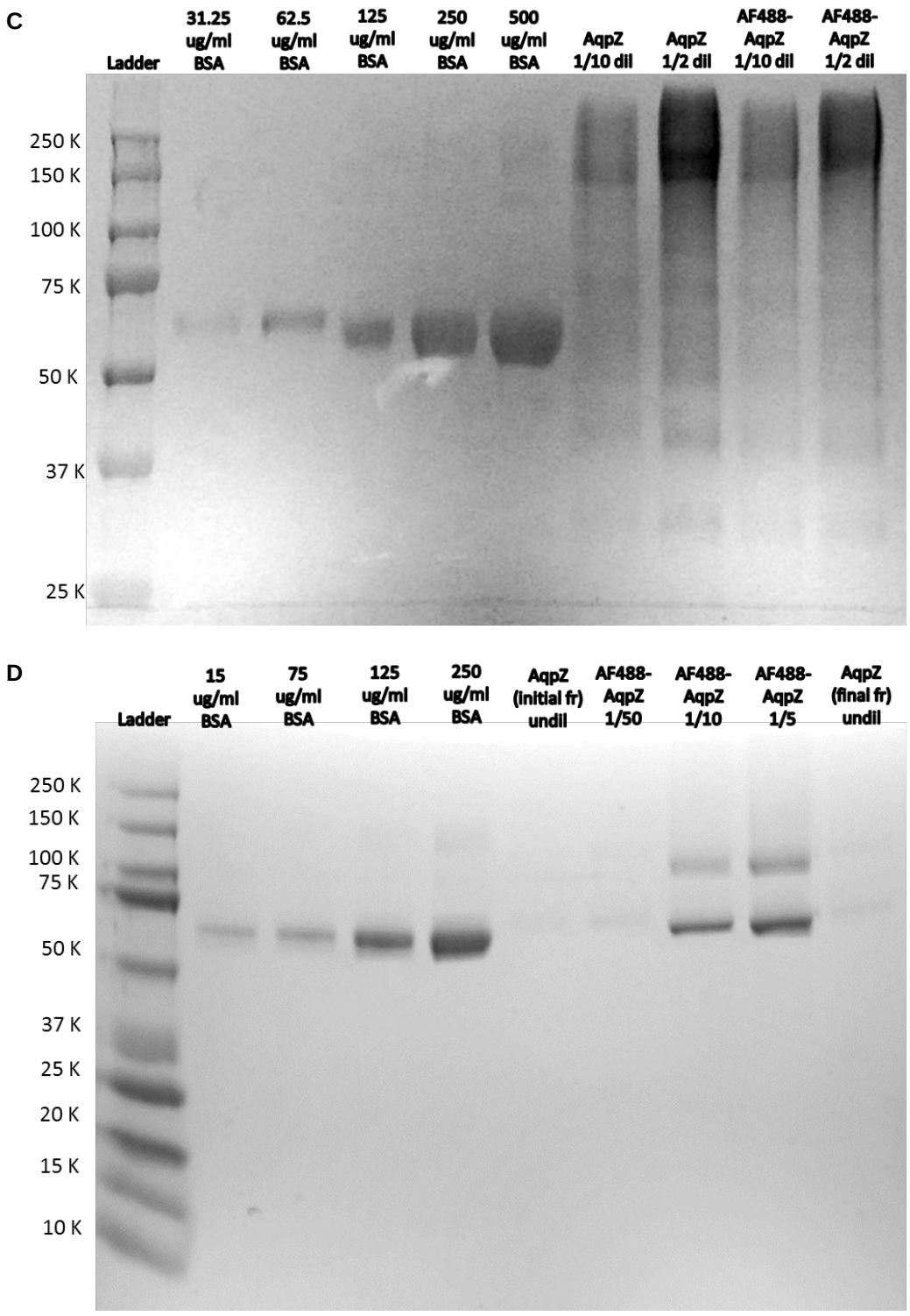

Figure 3.9 cont'd

Table 3.1. Summary of AqpZ multimer state calculated from SDS-PAGE gels used in this study

Vesicle materials make-up	Summary of AqpZ multimer state estimated from gel (%)	Permeability & insertion behavior (behavior and protein/membrane molar ratio)	Max insertion (#AqpZ tetramer/ vesicle)	Max permeability (μm/s)
AqpZ/lipid (Figure 3.7A)	20% monomer, 50% tetramer, 30% high order	Increase through 1/100, decrease beyond 1/50	183	407
AqpZ/lipid (Figure 3.7B)	50% tetramer, 50% high order	Increase through 1/50, decrease slightly beyond	99	68
AqpZ/lipid (Figure 3.7C)	5% monomer, 5% tetramer, 90% high order	Increase through 1/25	225	90
AqpZ/polymer (Figure 3.7A)	60% tetramer, 40% high order	Increase through 1/100, decrease at 1/50, increase again to 1/25	813	1256

This work was motivated in part by a decrease or leveling-off of vesicle permeability at high AqpZ/membrane material molar ratios in previous studies (16, 43, 44, 46, 47, 121). Some of these studies reported the calculated permeability per monomer of AqpZ. I found that the water permeability of AqpZ monomers was between $1.1x10^{-14}$ to $2.9x10^{-13}$ with an average of $1.0\pm0.9x10^{-13}$ cm/s. Previous experimental studies reported water permeability of *E. coli* AqpZ monomers between $2x10^{-14}$ to $1x10^{-13}$ cm/s (43, 59, 153, 154). Molecular dynamics simulations reported a value of $1.6x10^{-13}$ (155, 156). The majority of the water permeability values calculated in this work fell within the range of previously reported values, and some values were nearly three times greater than the largest reported values. Thus, previous reports that assumed 100% insertion efficiency may have been underestimating the water permeability per AqpZ monomer. This observation was also consistent with the previous AqpZ insertion study (47).

Testing the possibility of encapsulation of AqpZ inside vesicles

A potential issue with the FCS insertion method described in this study is that the number of protein measured per vesicle would be artificially high if membrane proteins were encapsulated inside of the vesicle (instead of embedded in the membrane). Encapsulation would be of greatest concern at high protein to membrane reconstitution rations. To test the possibility of encapsulation, several approaches were undertaken. Insertion was measured before and after these treatments: using a chemical to cleave the fluorescent probe and labeling the membrane protein post-reconstitution. The basis for these two approaches is that AqpZ insertion is assumed to not be directionally specific and the membrane is assumed to be protective against labeling. Thus, if encapsulation was occurring, vesicle brightness should be more than half of the original brightness after treatment. If encapsulation was not occurring, vesicle brightness should be one-half of the original brightness after treatment.

i. Approach 1: Cleaving the fluorescent probe

Trypsin is a protease shown to cleave between the Arg and His residues of the N-terminal domain of solubilized 10-His-AqpZ. In initial tests, however, Borgnia et al. reported that no cleavage was observed when AqpZ was reconstituted in *E. coli* total lipid extract (43). They hypothesized that the cleavage site was protected by the lipid membrane, but no details were given on conditions of their test. Factor Xa is another protease known to cleave after the Arg residue in the recognition sequence Ile-(Glu or Asp)-Gly-Arg, which matches exactly the Ile-Glu-Gly-Arg sequence on the N-terminal domain of 10-His-AqpZ. However, FCS measurements before and after treatment with Factor Xa did not reveal any decrease in vesicle brightness. This finding further supports the hypothesis that the protein is well protected by the lipid membrane, including the N-terminal domain of 10-His-AqpZ.

ii. Approach 2: Labeling the protein post-reconstitution

1/100 and 1/25 molar ratio AqpZ/lipid vesicles were prepared with unlabeled and labeled AqpZ. Subsequently, vesicles were labeled with AF488 (pre-labeled vesicles were dummy-labeled). If AqpZ were encapsulated, greater than 50% reduction in brightness was expected for post-labeled

vesicles. However, no difference in insertion was observed at 1/100 molar ratio, and only 30% reduction (not significant) was observed for post-labeled 1/25 molar ratio vesicles (Figure 3.10). I cannot rule out the possibility that the reduction in AqpZ insertion was based on differences in vesicle prep. Additionally, based on the knowledge that small molecules can cross the lipid membrane, AF488 may have been able to cross the membrane. Depending on the diffusion rates of the labeling buffers and AF488, conditions may or may not have remained favorable for it to react inside the vesicle. However, with consistent insertion and permeability results, I did not observe evidence of encapsulation.

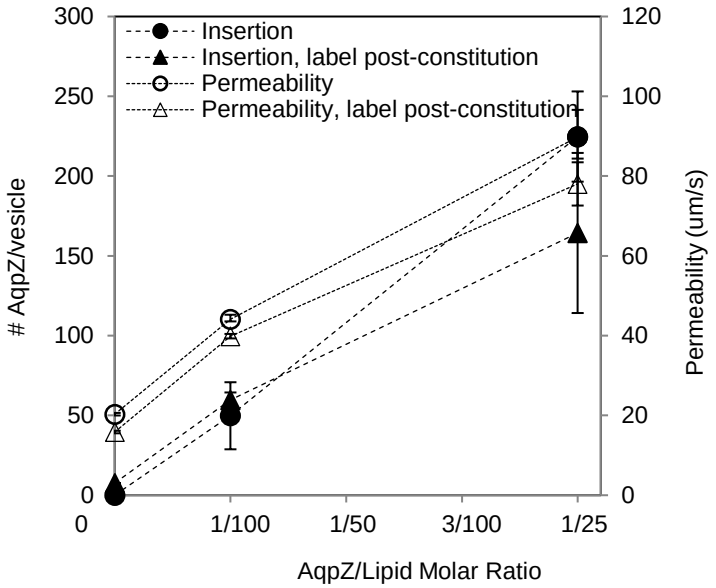

Figure 3.10. Insertion and permeability measurements of AqpZ/lipid vesicles where AqpZ was labeled before and, separately, after vesicle formation
Error bars represent propagated error of the permeability measurements from fitting light scattering data and of the multiple FCS measurements of each vesicle preparation.

Quantification of AqpZ in lipid vesicles after resolubilizing fully-formed vesicles

For comparison to prior work (47), I also attempted to quantify insertion by resolubilizing vesicles and quantifying the labeled protein that was released. I found vesicles to be highly stable and had to expose them to detergent significantly longer than reported to observe resolubilization. After resolubilization of AqpZ/lipid vesicles, I found micellar diffusion coefficients between 9-17 $\mu m^2/s$, approximately 3 times greater (meaning smaller particles) than vesicular diffusion coefficients.

Resolubilitzation of OmpF/lipid vesicles yielded diffusion coefficients between 7-25 $\mu m^2/s$, approximately 4 times greater than vesicular diffusion coefficients. In contrast, previous findings reported micellar diffusion coefficients between 1-2 orders of magnitude greater (47, 136, 137) than vesicular ones. In those findings, the diffusion coefficients of the AqpZ micelles were reported as slightly smaller than for the original AqpZ micelles. I found the diffusion coefficients to be 2-4 times smaller. I hypothesize that this difference between the free and resolubilized AqpZ micelles can be attributed to phospholipids remaining with the AqpZ in the resolubilized form and/or high detergent concentrations that could affect the diffusion of micelles. After resolubilization, detergent concentrations in the samples were almost two orders of magnitude greater than beforehand.

For AqpZ vesicles, I observed 3 times (1/100 molar ratio vesicles) to 7 times (1/25 molar ratio vesicles) less insertion using the resolubilization approach compared to our FCS approach (Figure 3.11A). For OmpF/lipid vesicles, insertion measured via resolubilization yielded similar values to the number of OmpF measured in vesicle form for 0-1/50 molar ratio (Figure 3.11B). At 1/25 molar ratio, I observed 2 times less insertion using the resolubilization approach compared to our FCS approach. These differences in insertion could be due to incomplete resolubilization of vesicles which would lead to artificially low insertion values from the resolubilization method. Complete dissolution of vesicles was assumed previously (47). However, if resolubilization was not complete, there could be more than one protein (AqpZ or OmpF) per micelle. This situation would underestimate protein insertion and could explain the mismatch that I observed between the number of free protein and protein measured after resolubilization, especially at high AqpZ/lipid ratios. My original FCS approach would underestimate insertion if there were differences in molecular brightness of Alexa Fluor 488 in the aqueous and membrane environments. The resolubilization approach attempts to measure vesicles and protein micelles in the same lipid environment. If there were differences in molecular brightness of Alexa Fluor 488 based on its environment, the resolubilization approach would result in a greater estimated insertion than my original FCS approach. Since my original FCS approach estimates greater insertion, a potential decrease in brightness does not explain this discrepancy. Overall, using the resolubilization approach, I observed similar trends as found using my original FCS approach: increased protein insertion was a function of increased protein added (Figure 3.6 and Figure 3.7).

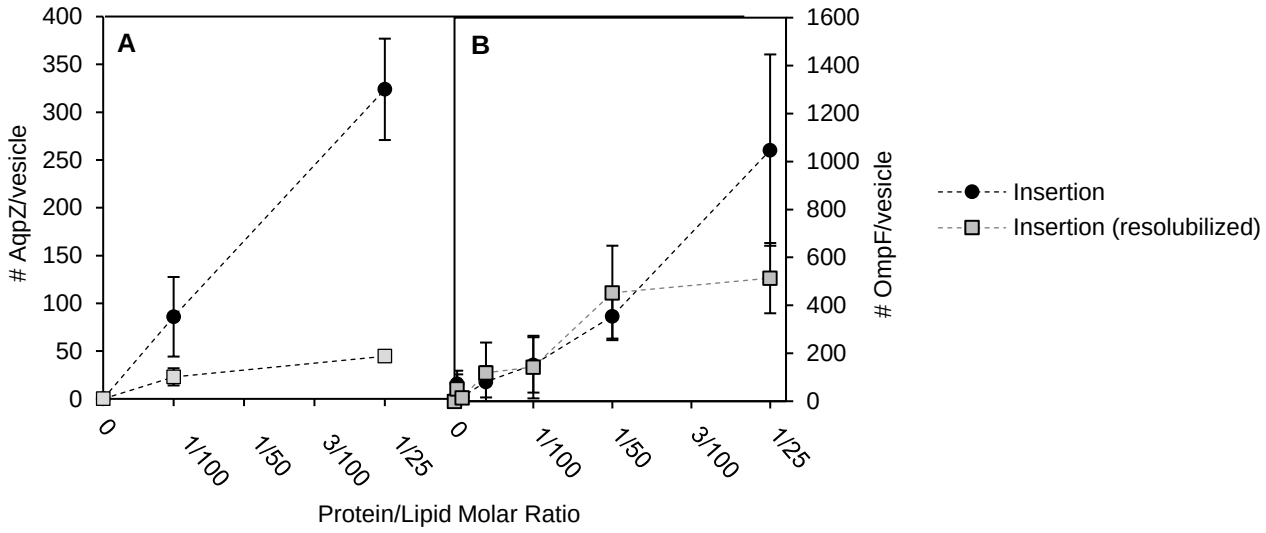

Figure 3.11. Comparison of our FCS method and the resolubilization method
(A) AqpZ/lipid vesicles. (B) OmpF/lipid vesicles. For resolubilization, vesicles were incubated with 2.5-3% OG. Error bars represent propagated error of the multiple FCS measurements of duplicate vesicle preparations (single protein preparation).

3.5 Conclusions

To further development of hybrid protein-synthetic membranes, this work has provided the following conclusions:

- Comparing vesicle brightness to protein brightness using FCS is a viable method for measuring the number of membrane proteins in vesicles. This work contributes another tool to investigate protein insertion.

- DDM concentrations greater than 0.3% (w/v) substantially inhibit AqpZ insertion into lipid vesicles, resulting in lower permeability. Lowering the detergent concentration can increase protein insertion and thereby improve the functional capacity of biomimetic membranes.

- Vesicle permeability of AqpZ and OmpF in lipid and polymer vesicles correlate to the insertion of AqpZ and OmpF into the membrane material. Vesicle permeability that decreases at high resconstitution ratios, is likely due a decreases in protein insertion.

- AqpZ insertion and permeability behavior appeared to depend on the AqpZ preparation. Greater insertion, and thus permeability, may be observed when AqpZ exists in higher order multimer states.

3.6 Acknowledgements

Support for this work was provided by the US National Science Foundation (CBET 08-28512 and CBET-1336620); and the Graduate Assistance in Areas of National Need (GAANN), the University of Illinois SURGE, and the joint National Water Research Institute (NWRI)-American Membrane Technology Association (AMTA) fellowships. I thank Dr. Wolfgang Meier (University of Basel, Switzerland) for the strain BL21(DE3) omp8, Dr. Dianwen Wang (Beckman Institute for Advanced Science and Technology, University of Illinois) and Dr. Shih-Chu Liao (ISS Inc.) for helpful discussions about FCS measurements and data analysis, Dr. Robert Gennis (Department of Biochemistry, University of Illionios) and Dr. Benito Marinas (Department of Civil and Environmental Engineering, University of Illinois) for use of stopped flow instruments, Dr. Irene MaCallister (Construction Engineering Research Lab) for use of an Äkta prime plus instrument, and Dr. Eric Reyes (Department of Mathematics, Rose-Hulman Institute of Technology) for helpful discussions about error propagation. TEM experiments were carried out in the Frederick Seitz Materials Research Laboratory Central Facilities, University of Illinois. FCS experiments were carried out at the Microscopy Suite in the Beckman Institute, University of Illinois. Glow-discharging of copper grids for TEM was carried out at the Microscopy Suite in the Beckman Institute, University of Illinois.

CHAPTER 4: BIOMIMETIC MEMBRANES FORMED BY DEPOSITION AND RUPTURE OF MIXED POLYMER-LIPID VESICLES ON SOLID SUPPORTS[2]

4.1 Abstract

Biomimetic triblock copolymers were combined with lipids to test whether hybrid planar membranes could be formed through vesicle deposition. Poly-(2-methyloxazoline)-polydimethylsiloxane-poly-(2-methyloxazoline) ($PMOXA_{15}$-$PDMS_{110}$-$PMOXA_{15}$) polymer was mixed with either zwitterionic 1-palmitoyl-2-oleoyl-sn-glycero-3-phosphocholine (POPC) or positively charged 1,2-dioleoyl-3-trimethylammonium-propane (DOTAP) lipids at varying ratios. Hybrid vesicles were produced containing both polymers and lipids. Depending on the vesicle composition, deposition behavior on quartz followed one of three scenarios: I) rupturing spontaneously to form planar membranes (pure lipids and 89molar ratio DOTAP), II) rupturing with calcium (67molar ratio and 89molar ratio POPC), or III) depositing as intact vesicles (pure polymer and high polymer content). Increased rupture was observed for hybrid vesicles as compared to pure polymer vesicles and on mica as compared to quartz. Hybrid polymer-lipid vesicles with as little as 11molar ratio polymer had 1.4 – 3 times lower water permeability than

[2] Author contributions: The data in this chapter was collected during a joint project with Sania Bäckström, a visiting PhD student from the Technical University of Denmark. I developed the methods for the transmission emission microscopy and stopped flow light scattering measurements, Sania developed the methods for the quartz crystal microbalance with dissipation monitoring and zeta-potential measurements, and we worked together to develop the methods for imaging using atomic force microscopy; we both generated data from the different methods and contributed to data analysis, interpretation, and writing.

pure lipid vesicles. Vesicle properties may be adjusted by varying composition, polymer-lipid ratio, and surface and solution chemistry.

4.2 Introduction

Lipid bilayers and biomimetic triblock copolymer membranes are used to investigate membrane protein insertion (157) and activity (54, 158) and show promise for a variety of applications, including screening platforms for drug discovery (159), biosensors (160, 161), and immunoassays (162). Lipids have the advantages of being better understood and more similar to the native environment for incorporation of membrane proteins. However, copolymer membranes are typically more stable and can be engineered for the desired combination of properties (37). For example, polyethyleneoxide-polyethylethylene vesicles are 5-50 times tougher mechanically than lipid membranes (32) and exhibit greater thermal and temporal stability (163). Another promising biomimetic membrane, a triblock hydrophilic-hydrophobic-hydrophilic copolymer (poly-(2-methyloxazoline)-polydimethylsiloxane-poly-(2-methyloxazoline) or PMOXA-PDMS-PMOXA), shows functional incorporation of a variety of transmembrane proteins (16, 18, 28, 38, 54, 55, 122, 158, 164-167). The majority of the work conducted with block copolymer membranes has been with vesicles, but for many biosensor applications and analytical techniques it is desirable to produce planar, solid-supported membranes.

For lipids, planar membranes can be made on a solid support by Langmuir-Blodgett (vertical) or Langmuir-Schäfer (horizontal) transfer from a water-air interface (168) or through vesicle collapse (35). The adsorption and fusion of vesicles from aqueous solution onto solid supports are affected by vesicle properties (size (96, 169), composition (35), and surface charge (35)), support surface properties (surface chemistry (170), cleanliness (91), roughness (91), and charge (100)), and solution chemistry (pH, ionic strength, temperature (171), and osmotic pressure (91, 170)). Calcium has been shown to enhance deposition for anionic and zwitterionic vesicles (35). A free-standing planar lipid membrane can also be made in a single aperture of less than 1 mm in a hydrophobic scaffold either by painting a solvent-containing black lipid membrane across the aperture (88) or by folding solvent-free lipid monolayers across the aperture (172). Recently,

planar lipid membranes (either free-standing (173-175) or on nanoporous supports (92, 176)) covering a larger area have been realized by utilizing aperture arrays in hydrophobic scaffolds.

Recently there has also been some progress in synthesizing planar, solid-supported copolymer membranes using three different approaches: Langmuir-Blodgett transfer (37, 38, 177), synthesis on a gold surface (178), and vesicle deposition (40, 179, 180). In the current work we focused on vesicle deposition because it presents the fewest obstacles for incorporation of membrane proteins. However, the high rupture strength of triblock copolymer vesicles presents some difficulty for this method. This can be resolved by the use of charged or functionalized copolymers to facilitate adsorption (40, 179). There is also one report investigating direct deposition of $PMOXA_7$-$PDMS_{60}$-$PMOXA_7$ polymer onto solid surfaces; in this case a variety of structures were observed using atomic force microscopy (AFM), including spherical and tubular vesicles and areas with a thinner layer, possibly planar polymer membranes (180).

The current work investigates the potential use of mixed or hybrid polymer-lipid vesicles to facilitate formation of a planar membrane through vesicle deposition and to allow tailoring of vesicle properties. The triblock copolymer $PMOXA_{15}$-$PDMS_{110}$-$PMOXA_{15}$ was selected because of its suitability for protein insertion (16, 18, 28, 38, 54, 55, 122, 158, 164-167). The formation of mixed polymer-lipid vesicles has been documented for poly(ethylene oxide)-poly(propylene oxide)-poly(ethylene oxide) (181) and PMOXA-PDMS-PMOXA polymers (182) but to our knowledge the deposition and rupture properties of such vesicles have not been reported before. Mixed polymer-lipid vesicles with different ratios of $PMOXA_{15}$-$PDMS_{110}$-$PMOXA_{15}$ polymer to zwitterionic or positively charged lipids were characterized by transmission electron microscopy (TEM), dynamic light scattering (DLS), electrophoretic light scattering (ELS), and osmotic shock stopped-flow permeability measurements, and their deposition behavior was investigated on quartz with quartz crystal microbalance with dissipation monitoring (QCM-D) and on mica with AFM. These mixed polymer-lipid vesicles show promise for selectively tethering vesicles or forming planar, solid-supported membranes.

4.3 Materials and methods

Materials

$PMOXA_{15}$-$PDMS_{110}$-$PMOXA_{15}$ was obtained from Dr. Wolfgang Meier at the University of Basel, Switzerland (183). 1-palmitoyl-2-oleoyl-*sn*-glycero-3-phosphocholine (POPC, 25 mg/ml in chloroform) and 1,2-dioleoyl-3-trimethylammonium-propane (DOTAP, 10 mg/ml in chloroform) were purchased from Avanti Polar Lipids (Alabaster, USA). Dodecyl maltoside detergent sol grade was purchased from Anatrace (Santa Clara, USA). Sodium azide and chloroform were purchased from Sigma (St. Louis, USA).

Vesicle preparation

Mixed polymer-lipid vesicles were prepared by dissolving $PMOXA_{15}$-$PDMS_{110}$-$PMOXA_{15}$ polymer in chloroform (2 ml) and adding POPC or DOTAP in specified molar ratios (0, 33, 67, 89, 100% lipid), then using a film rehydration technique (16). A thin polymer-lipid film was formed by evaporating the solvent in a round-bottomed flask using a rotary vacuum evaporator (vacuum <110 mbar) at room temperature. Trace chloroform was removed under a high vacuum (<2.5 mbar) for 1- 2 h before the dried polymer-lipid film was rehydrated with 2.8 mM PBS (8 g L^{-1} NaCl, 0.2 g L^{-1} KCl, 0.144 g L^{-1} Na_2HPO_4, 0.24 g L^{-1} KH_2PO_4, pH 7.2) containing 0.04% dodecyl maltoside and 0.13% sodium azide to a final polymer-lipid concentration of 6 mg/ml. The films were sonicated to ensure that the polymer lifted off from the bottom of the flask. The films were rehydrated at 4° C under continuous rotational stirring for 24 h. The resulting vesicles were extruded using a pneumatic thermobarrel extruder (Northern Lipids, Burnaby, Canada) through 0.6 μm and 0.2 μm track-etched Isopore™ membranes (Millipore, Billerica, MA, USA) 5 and 11 times respectively to ensure unilamellar vesicles. The vesicles were purified by size-exclusion with a flow rate of 0.5 ml/min on a Superdex 200 pressurized column (GE Healthcare, Piscataway, NJ, USA) using an Äkta prime plus instrument (GE Healthcare, Piscataway, NJ, USA). The fraction corresponding to the vesicles was typically collected after 10 minutes. Unless otherwise noted, results are from a single preparation of vesicles at each ratio and composition. Vesicles were stored at 4°C for up to 14 days prior to TEM and QCM-D experiments; DLS results did not show a change in average size or size distribution over that time. The POPC vesicles were imaged on AFM after

12 days and the PMOXA-PDMS-PMOXA vesicles after 50 days; again none of these samples showed a change in DLS results over that time. Eleven molar ratio PMOXA-PDMS-PMOXA:89 molar ratio DOTAP and pure DOTAP vesicles used for AFM had been stored for 40 days and by DLS showed an increase in diameter from 109 nm to 186 nm and from 160 nm to 524 nm respectively.

Vesicle characterization

The hydrodynamic diameter and zeta potential of the vesicle preparations were determined using dynamic light scattering (DLS) and electrophoretic light scattering (ELS), respectively, on a 4W Zetasizer Nano-ZS90 (Malvern Instruments, Malvern, UK) with a He-Ne standard laser, wavelength 632.8 nm and 90° scattering angle. The DLS results shown here are the average of three 10-measurement series for each sample taken directly after introducing the sample. The refractive index for the vesicles was set as 1.48 (184). Zeta potential measurements were carried out at 25°C in 2.8 mM PBS pH 7.2 buffer with an equilibration time of 2 minutes and signal processing used M3-PALS (second generation Phase Analysis Light Scattering) to measure the particle electrophoretic mobility. Zeta potential was calculated using a built-in monomodal analysis model assuming the Smoluchowski approximation and a dispersant viscosity of 0.8904 cP (185).

In preparation for TEM, thin film holey carbon grids (Ted Pella, Redding, CA, USA) were treated with a Denton DPG-1 glow-discharge system (Denton Vacuum Inc., Moorestown, NJ, USA) at a glow current of 200 mAmp for 2 minutes to make them hydrophilic. Vesicle samples were allowed to adsorb to the grid surface for 2 minutes, stained with 1% uranyl acetate (SPI, West Chester, PA, USA) for 30 seconds, and air-dried. Drying technique employed in TEM sample preparation can alter the shape of the vesicles (148). Vesicles were viewed with a JEM 2100 transmission electron microscope (JEOL, Tokyo, Japan) with a LaB_6 cathode operated at 200 keV. 15-35 images were collected from each batch of vesicles. TEM experiments at ratios of 11 molar ratio PMOXA-PDMS-PMOXA:69 molar ratio POPC and 100% PMOXA-PDMS-PMOXA were performed with 2 and 3 replicate vesicle preparations respectively. Data shown are from a single vesicle preparation; similar trends were observed in all preparations.

Quartz crystal microbalance with dissipation monitoring

We used a QCM-D300 system and polished AT-cut, 5 MHz quartz crystals with a 50 nm silicon dioxide coating (QSX-303, Q-Sense AB, Gothenburg, Sweden) to measure deposition kinetics of vesicles on a bare silica surface, using the software Q-Soft for data collection. The application of the QCM-D technique for determining deposition kinetics is described by Rodahl *et al*. (186). Briefly, the QCM-D technique monitors the change in frequency (Δf) of vibration due to deposition of wet mass on the quartz crystal sensor in a liquid environment. As wet mass deposits onto the quartz sensor, the frequency of vibration decreases. The change in energy dissipation (ΔD) of the quartz crystal is monitored simultaneously. ΔD gives information about the softness of the adsorbed film – an increase in ΔD corresponds to an increase in the softness of the adsorbed film. Combined frequency and energy dissipation measurements give information about both the adsorbed amount (Δf) and the viscoelastic properties (ΔD) of the adsorbed film. All data shown was measured at the third harmonic, n= 3, i.e., at 15 MHz. For clarity, the frequency response is divided by 3 in all graphs (this makes the data directly comparable to data measured at n = 1, for ideal conditions).

The fractional bilayer coverage (Equation 4.1) was calculated as previously described by Graneli *et al*(187) based on two assumptions: (i) The water-exposed domains on a planar supported lipid bilayer do not contribute significantly to D. (ii) There exists a linear relationship between the dissipation change at saturation and liposome size, as previously demonstrated for pure PC liposomes in the size range of 25 and 200 nm. The fractional bilayer coverage, α, and fractional coverage of intact liposomes, 1 - α, are estimated using

$$\alpha = 1 - \Delta D_{fin} / \Delta D_{sat}$$
$$\Delta D_{sat} = x\Theta$$

Equation 4.1. Fractional bilayer coverage

where ΔD_{sat} is the dissipation value expected when α=0, i.e., for the whole surface covered by intact liposomes, ΔD_{fin} is the actual measured change in D at saturation, Θ is the liposome diameter (Table 1) in nanometers, and x=0.15 is the proportionality constant between ΔD_{sat} for complete surface coverage of intact liposomes on TiO_2 (169) and the liposome diameter (ΔD_{sat} /nm).

The thickness of the adsorbed film was obtained by fitting *f* and *D* at the third and fifth overtones using a built-in Voigt model in the software Q-tools. In this model the adsorbed film is represented by a homogeneous thickness, viscosity, and complex shear modulus. Before each experiment, the silica sensors were soaked in 2% Hellmanex II (Hellma GmbH & Co. KG, Müllheim, Germany) cleaning solution for 30 min, rinsed thoroughly with DI water, dried with ultra high-purity N_2, and treated in an ozone/UV chamber (BioForce Nanosciences Inc., Ames, IA) for 30 min. To ensure that the silica surface was maintained, each sensor was used only seven times. All test solutions were fed into the chamber using a syringe, and adsorption was measured in stagnant conditions. For each experiment, the silica sensor frequency and dissipation in air and in double distilled water were measured as a quality control of the sensor. A baseline was obtained in PBS buffer pH adjusted to 7.2, with the frequency signals stabilized at an approximately 0.2 Hz change in frequency over 10 min. One ml of vesicles were injected and allowed to adsorb onto the silica-coated sensor until the frequency signal stabilized at an approximately 0.2 Hz change in frequency over 10 min. To ensure saturation of the surface with vesicles, more vesicles were injected until no further increase in frequency was observed. PBS buffer was then added to remove any unadsorbed vesicles. Finally, 1 ml of 5 mM $CaCl_2$ was then introduced to encourage formation of planar membranes. The frequency signal was monitored for 10 minutes then equilibrated with PBS buffer again. Adsorption experiments were repeated 2-3 times for a single preparation at most vesicle compositions. QCM-D experiments at ratios of 100% POPC, 11% PMOXA-PDMS-PMOXA:89%POPC, 33% PMOXA-PDMS-PMOXA:67%POPC and 100% PMOXA-PDMS-PMOXA were performed with 2 replicate vesicle preparations. Data shown are from a single vesicle preparation; similar trends were observed in both preparations.

Atomic force microscopy

Visualization of the deposited mixed vesicles on the hydrophilic surface of mica (Structure Probe, Inc., West Chester, PA) was determined with an MFP-3D atomic force microscope (Asylum Research, Santa Barbara, CA, USA) in tapping mode in air with a Si cantilever with aluminum reflex coating (Tap300Al, Budget Sensors, Sofia, Bulgaria) at room temperature. The length of the cantilever was 125 µm, the resonance frequency 300 kHz, and the force constant 40 N/m. Twenty

µl of vesicle solution was incubated on a freshly cleaved mica surface for 2 minutes, rinsed with 1 ml DI water, blotted with a Kimwipe® at the edge of the mica, and allowed to dry for 10 minutes. The thickness of the formed layer was obtained by plotting a histogram with the number of pixels per height for each image, to give two peaks corresponding to the mica surface and the vesicles. The vesicle peak was fit with a Gaussian function to obtain the mean±sd height of the adsorbed vesicles.

Vesicle permeability

Vesicle permeability to water was determined using an SX.18MV-R stopped-flow spectrometer (Applied Photophysics, Surrey, UK) with light scattering (16, 43). The vesicles were subjected to a hyperosmotic shock by mixing them with an equal volume of 1 M NaCl PBS pH 7.2 at 10 °C. Hybrid vesicles were monitored for 2 s, while pure PMOXA-PDMS-PMOXA vesicles were monitored for up to 50 s. The change in vesicle size with water efflux was monitored by light scattering at 600 nm. Six or more light scattering curves for a single vesicle batch at each vesicle composition were averaged and fitted using an exponential rise equation in Origin (v.8.1) to obtain the exponential rise rate constant, *k*. Water permeability was calculated using Equation 4.2**:**

$$P_f = k / \left[\left(S / V_o \right) \times V_w \times \Delta_{osm} \right]$$

Equation 4.2. Water permeability

where S/V_o is the initial vesicle surface area to volume ratio, V_w the molar volume of water (18 cm^3/mol), and Δ_{osm} is the difference in osmolarity (1 osmol/L for DOTAP, POPC, and 11 molar ratio PMOXA-PDMS-PMOXA:89 molar ratio DOTAP and 0.5 osmol/L for 11 molar ratio PMOXA-PDMS-PMOXA:89 molar ratio POPC) driving the shrinkage of the vesicles. The hydrodynamic radius of the vesicles was derived from dynamic light scattering data. Stopped-flow experiments at ratios of 100% POPC, 11 molar ratio PMOXA-PDMS-PMOXA:89 molar ratio POPC, 33 molar ratio PMOXA-PDMS-PMOXA:67 molar ratio POPC, and PMOXA-PDMS-PMOXA were performed with 2 replicate vesicle preparations. Data shown are from a single vesicle preparation; similar trends were observed in both preparations.

4.4 Results

Throughout this work we compared the properties of unilamellar vesicles of different compositions: 100% zwitterionic lipid (POPC), 100% positively charged lipid (DOTAP), 100% biomimetic triblock copolymer (PMOXA-PDMS-PMOXA), and mixtures of 11 molar ratio, 33 molar ratio, and 67 molar ratio of the polymer with each lipid.

Table 4.1. Hydrodynamic diameter and zeta potential
Measurements were made of lipid vesicles, polymer vesicles and mixed lipid-polymer vesicles obtained by DLS and ELS. Abbreviations are as follows: 1-palmitoyl-2-oleoyl-sn-glycero-3-phosphocholine (POPC), 1,2-dioleoyl-3-trimethylammonium-propane (DOTAP), hydrodynamic diameter (D_h), polydispersivity index (PDI), zeta potential (ζ).

Polymer:lipid ratio (molar ratio)			D_h (nm)[a]	PDI	ζ(mV)[a]
polymer	POPC	DOTAP			
-	100	-	159±2	0.13	0.2±0.3
11	89	-	194±3	0.17	-5.7±0.8
33	67	-	217±3	0.19	-2.0±0.3
67	33	-	189±5	0.12	-2.6±0.4
-	-	100	160±3	0.085	35.6±0.4
11	-	89	109±0	0.24	2.5±0.1
33	-	67	105±1	0.21	-1.7±0.9
67	-	33	175±1	0.15	0.8±0.1
100	-	-	198±5	0.12	-4.9±0.8

[a] Numbers shown are the average ± standard deviation from three 10-measurement series.
Abbreviations are as follows:

Characterization of lipid, polymer, and polymer-lipid vesicles by DLS and TEM

DLS measurements showed that all of the vesicle preparations had monodispersed size distributions. The average hydrodynamic diameters for the vesicles used in this work varied between 105 - 217 nm (Table 4.1). The differences in diameters did not correspond to the different compositions, and no trends in size were observed with increasing polymer content. Duplicate batches of the same composition showed considerable variation in size while consistently having a narrow intrabatch size distribution, as illustrated by 33% polymer:67% POPC vesicles, which had hydrodynamic diameters of 126±2 nm and 217±3 nm for duplicate batches. Rather than being characteristic of the different compositions, the size differences generally relate to the extrusion

pressure that was required during preparation, as has been documented previously for lipids (188). Vesicle size influences the water content of vesicles and therefore the adsorbed mass measured in QCM. To eliminate contributions from vesicle size, batch-specific hydrodynamic diameters were used in the calculation of the bilayer coverage (Table 4.2). For polymer:DOTAP mixtures, the zeta potential was greatly reduced upon addition of even 11 molar ratio polymer (Table 4.1), indicating charge screening in the presence of polymer.

In TEM, POPC vesicles formed large collapsed vesicular structures on the hydrophilic grid (Figure 4.1a). DOTAP vesicles were difficult to find on the hydrophilic grid, which we attribute to rupture on the grid, but when present appeared as spherical or fused vesicles (Figure 4.1b). PMOXA-PDMS-PMOXA vesicles appeared as intact spherical particles (Figure 4.1c). All polymer:POPC mixtures resulted in the formation of spheres similar to those obtained for polymer alone (Figure 4.1d); no evidence for two distinct populations of vesicles was observed. Polymer:DOTAP mixtures also formed a single population of spherical vesicles (Figure 4.1e), with the exception of 11 molar ratio PMOXA-PDMS-PMOXA:89 molar ratio DOTAP (Figure 4.1f), which resulted in some spherical vesicles and some fused structures.

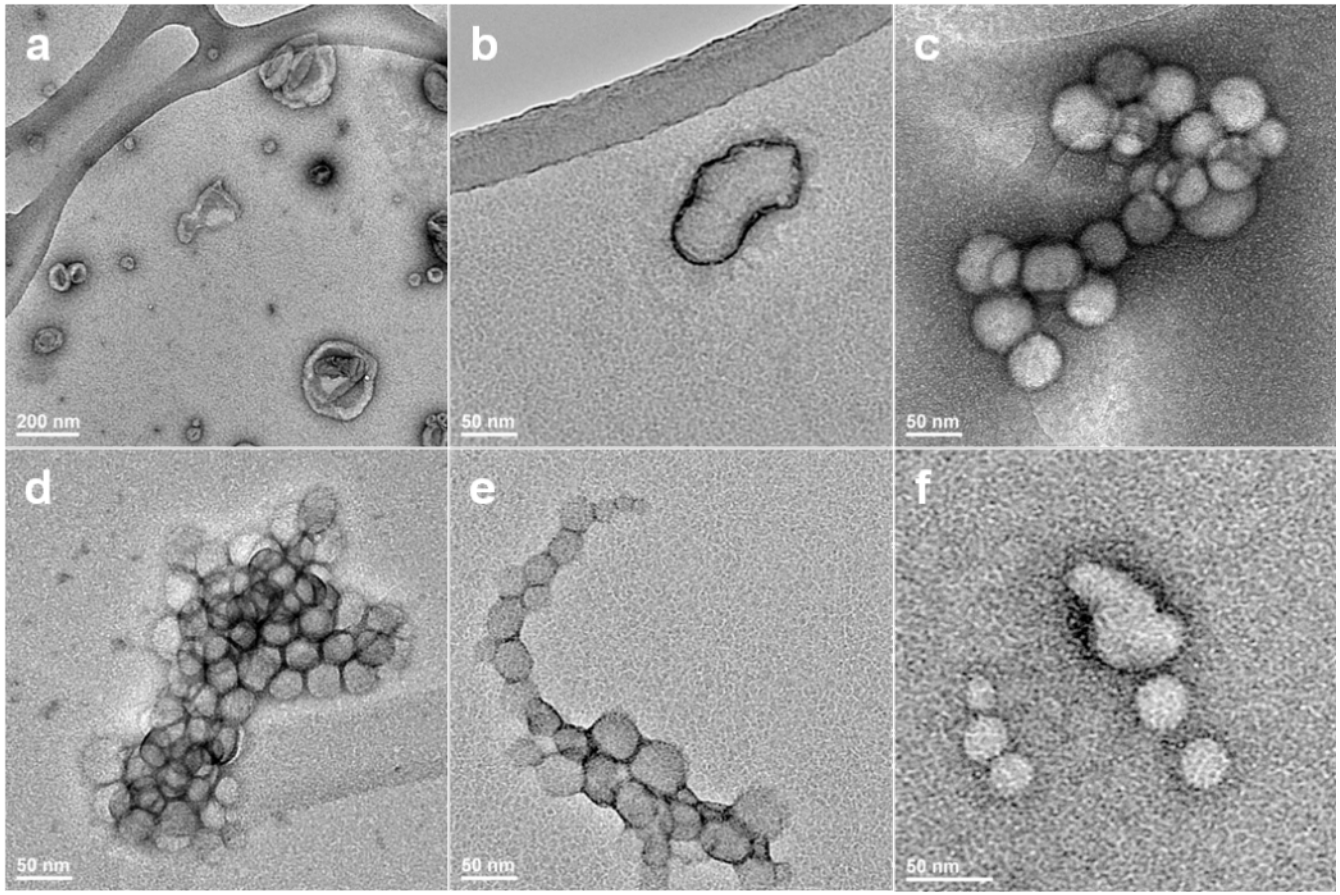

Figure 4.1. TEM of lipid vesicles, polymer vesicles and mixed polymer:lipid vesicles
(a) POPC, (b) DOTAP, (c) PMOXA-PDMS-PMOXA, (d) 11 molar ratio PMOXA-PDMS-PMOXA:89 molar ratio POPC, (e) 33 molar ratio PMOXA PDMS-PMOXA:67 molar ratio DOTAP: and (f) 11 molar ratio PMOXA-PDMS-PMOXA:89 molar ratio DOTAP.

Table 4.2. Adsorption of mixed lipid polymer vesicles on quartz monitored by QCM[a]

Composition	$[Ca^{2+}]$	$-\Delta f_{min}$[b]	$-\Delta f_{fin}$[c]	ΔD_{max}[d]	ΔD_{fin}[e]	α[f]	t_{max}[g]	t_{min}[h]	$-\Delta D_{fin}/\Delta f_{fin}$
(molar ratio)	(mM)	(Hz)	(Hz)	($x10^{-6}$)	($x10^{-6}$)	(%)	(nm)	(nm)	
100% POPC	0	56±9	36±8	5.9±1.2	1.8±1.2	93±6	12±2	9±1	0.05±0.02
89% POPC	5	138±20	55±9	24.4±2.1	9.7±2.7	66±8	33±5	16±3	0.17±0.03
67% POPC	5	188±3	174±16	25.4±4	20.3±2.0	38±6	49±12	47±13	0.12±0.00
33% POPC	5	300±5	300±5	48.6±1.7	48.6±1.7	0	104±2	104±2	0.17±0.00
100% DOTAP	5	30±4	30±4	3.6±1.1	3.6±1.1	86±4	7±2	7±2	0.15±0.02
89% DOTAP	5	70±7	70±7	5.7±0.7	5.7±0.7	79±3	14±1	14±1	0.09±0.02
67% DOTAP	5	115±19	115±19	16.4±3.5	16.4±3.5	17±15	66±15	66±15	0.15±0.04
33% DOTAP	5	120±15	120±15	22.4±12	22.4±12	-6±40	101±28	101±28	0.23±0.06
PMOXA-PDMS-PMOXA	5	42±1	42±1	13.7±3.2	11.8±5.9	---	81±21	81±21	0.33±0.08

[a] All values shown are the average ± standard deviation from 2-3 measurements of one (most) or two (pure POPC and pure PMOXA-PDMS-PMOXA) vesicle preparations per composition.
[b] Δf_{min}, change in frequency from initial buffer baseline to the minimum observed frequency
[c] Δf_{fin}, change in frequency from initial buffer baseline to the final buffer baseline
[d] ΔD_{max}, change in dissipation from initial buffer baseline to the maximum observed dissipation
[e] ΔD_{fin}, change in dissipation from initial buffer baseline to the final buffer baseline
[f] α, fractional bilayer coverage
[g] t_{max}, maximum observed thickness of the adsorbed layer
[h] t_{min}, minimum observed thickness of the adsorbed layer

Vesicle deposition and rupture on quartz

The deposition kinetics and average thickness of lipid, polymer, and mixed polymer:lipid vesicles on a quartz support were studied with QCM-D, where a decrease in resonance frequency corresponds to an increase in adsorbed mass and an increase in dissipation indicates a softer adsorbed layer (Figure 4.2 and Table 4.2). The deformation ratio, $-\Delta D_{fin} / \Delta f_{fin}$, was used as a measure of vesicle flattening. A high ratio corresponds to a low degree of deformation (spherical vesicles) and a low ratio to a high degree of deformation (flattened vesicles or bilayers).

Adsorption of pure POPC vesicles onto silica (Figure 4.2a) was a two-phase process. In the first phase the frequency decreased and the dissipation increased until reaching extremes of Δf=-56 Hz and $\Delta D=5.9\times10^{-6}$ (Table 4.2). This is attributed to vesicle adsorption onto the silica surface. In the second phase, which started spontaneously 11 minutes after vesicle addition, the frequency increased and the dissipation decreased until reaching equilibrium at Δf=-36 Hz and $\Delta D=1.8\times10^{-6}$. These changes are attributed to vesicle rupture and the resulting release of water. The existence of a second stage is indicative of POPC vesicle rupture requiring a critical coverage, as has been proposed previously (35, 170). Onset of the second stage began at a dissipation corresponding to a vesicular coverage of 28 areal %. With vesicle deformation or flattening occurring, as suggested by the deformation ratio, the actual surface area covered at the onset of rupture would be greater than 28%.

Adsorption of pure DOTAP vesicles onto silica (Figure 4.2b) was a one-phase process. Upon adsorption, the frequency decreased to an equilibrium of Δf=-30 Hz and the dissipation increased up to $\Delta D=3.6\times10^{-6}$ (Table 4.2). This is interpreted as immediate DOTAP vesicle rupture upon adsorption to the quartz surface.

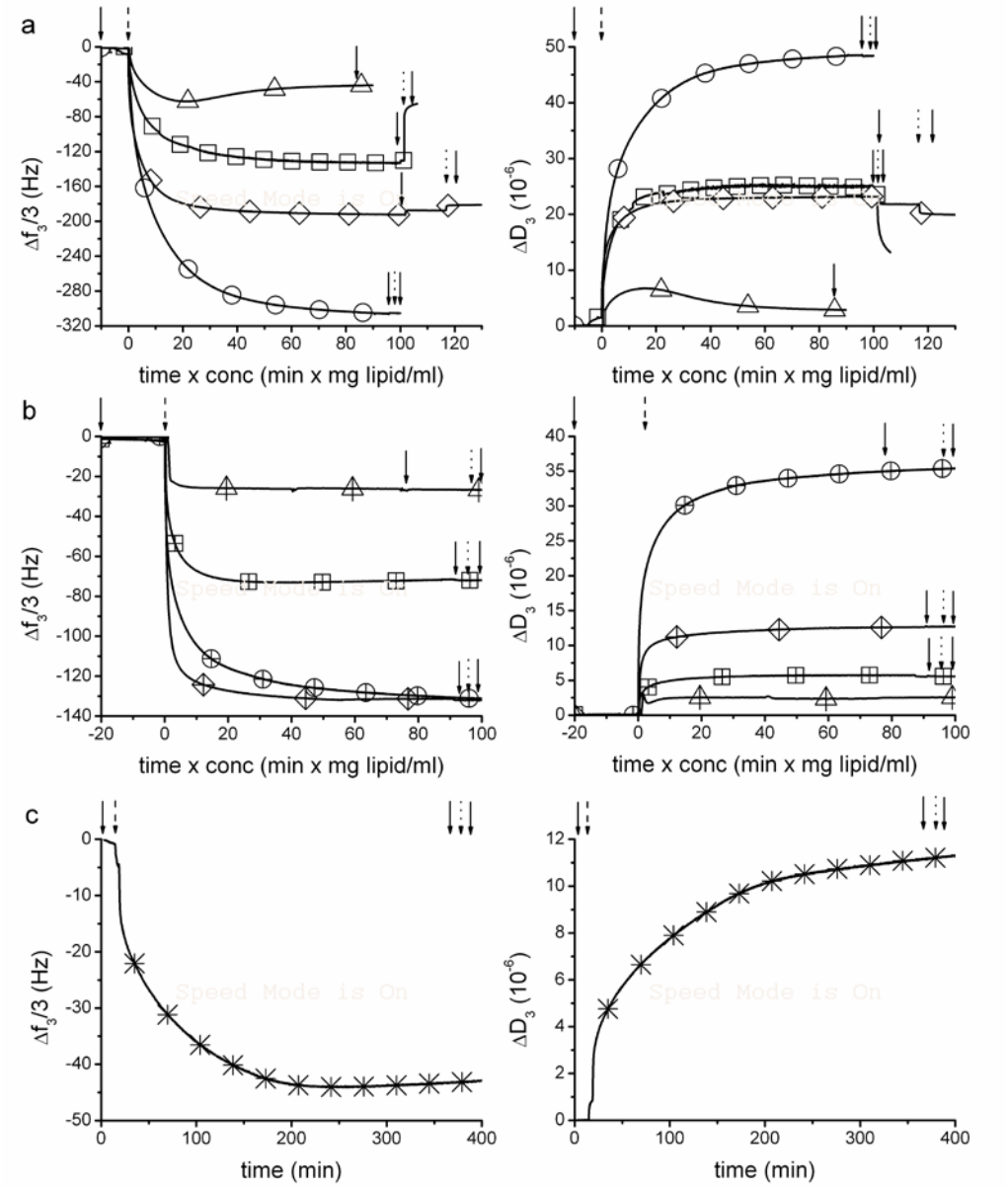

Figure 4.2. QCM-D responses for the deposition of different polymer:lipid mixtures on SiO_2 Solid lines show temporal changes in frequency (left column) and dissipation (right column) at 15 MHz, with symbols added to designate different vesicle compositions. Arrows show addition of PBS (solid), 1ml of vesicles (dashed), or 5mM CaCl2 (dotted). (a) POPC vesicles (100 molar ratio POPC (Δ), 11 molar ratio PMOXA-PDMS-PMOXA:89 molar ratio POPC (□), 33 molar ratio PMOXA-PDMS-PMOXA:67 molar ratio POPC (◊), 67 molar ratio PMOXA-PDMS-PMOXA:33 molar ratio POPC (o)), (b) DOTAP vesicles (100 molar ratio DOTAP (Δ), 11 molar ratio PMOXA-PDMS-PMOXA:89 molar ratio DOTAP (□), 33 molar ratio PMOXA-PDMS-PMOXA:67 molar ratio DOTAP (◊), 67 molar ratio PMOXA-PDMS-PMOXA:33 molar ratio DOTAP (o)), and (c) PMOXA-PDMS-PMOXA vesicles.

PMOXA-PDMS-PMOXA vesicles adsorbed on quartz in a one-phase process (Figure 4.2c), with an equilibrium of Δf=-42 Hz and ΔD=11.8x10^{-6}. Although the equilibrium Δf for PMOXA-PDMS-PMOXA was similar to that for pure lipid vesicles, indicating that a similar adsorbed mass is obtained, the ΔD for PMOXA-PDMS-PMOXA vesicles is 3-7 times larger, indicating that it formed a softer layer. This softness is consistent with a layer containing substantial water, typical of vesicles. PMOXA-PDMS-PMOXA vesicles adsorbed with a mean thickness of 81 nm. Compared to the hydrodynamic diameter of 198 nm from DLS data (Table 4.1), this indicates that PMOXA-PDMS-PMOXA vesicles are flattened on the surface. The deformation ratio of pure polymer vesicles is the highest out of all the vesicle compositions, indicating that they are less deformed than vesicles with lipid content. Both the deformation ratios and the thicknesses indicate that all vesicle compositions are at least partially flattened on the silica surface. Upon addition of calcium to polymer vesicles, the frequency and dissipation remained unchanged (Figure 4.2 and Table 4.2).

Polymer:POPC mixed vesicles (Figure 4.2a) adsorbed on quartz in a one-phase process, rather than the two-phase process observed for pure POPC, with equilibrium adsorption values of -300 Hz<Δf<-138 Hz and 24x10^{-6}<ΔD<49x10^{-6}. The Δf was tenfold higher for mixed polymer:POPC vesicles than for pure POPC or pure PMOXA-PDMS-PMOXA vesicles, which corresponds to a tenfold higher mass coverage. The high ΔD values, 13-27 times higher than ΔD_{fin} for lipid bilayers made from pure POPC vesicles, are indicative of an adsorbed vesicular layer. For mixed polymer:POPC vesicles with 11% and 33% polymer, addition of the known fusogen calcium promoted rupture, based on the changes in frequency (from -138 Hz to -55 Hz and from -188 Hz to -174 Hz respectively), dissipation (from 24.4x10^{-6} to 9.7x10^{-6} and from 25.4x10^{-6} to 20.3x10^{-6} respectively), and mean thickness (from 33 nm to 16 nm and from 49 nm to 47 nm respectively) with and without calcium, while at 67% polymer calcium had no effect.

For mixed polymer:DOTAP vesicles, the adsorption depended on the polymer:lipid ratio. 11 molar ratio PMOXA-PDMS-PMOXA:89 molar ratio DOTAP (Figure 4.2b) had equilibrium values similar to pure lipid vesicles, reaching a low Δf of -70 Hz and ΔD of 5.7x10^{-6}. In contrast, 33 molar ratio PMOXA-PDMS-PMOXA:67 molar ratio DOTAP (Figure 4.2b ◊) and 67 molar ratio PMOXA-PDMS-PMOXA:33 molar ratio DOTAP (Figure 4.2b o) behaved more like

polymer:POPC vesicles, with a high $|\Delta f|$ and a high ΔD, reaching Δf=-115 Hz and Δf=-120 Hz respectively. Upon addition of calcium, the frequency and dissipation remained unchanged, indicating that calcium had no effect on mixed polymer:DOTAP vesicles (Figure 4.2 and Table 4.2).

Vesicle deposition and rupture on mica

To visualize the deposition and rupture indicated by the bulk measurements of QCM-D, AFM imaging was performed on selected samples. To facilitate imaging we switched from quartz to molecularly flat mica. Although silica and mica are both hydrophilic, supported bilayer formation on the two surfaces has been reported to differ (100). AFM control images (PBS without any vesicles, Figure 4.3a) showed small structures of irregular height, so all images were compared to this control.

POPC vesicles on mica formed patches (Figure 4.3b) with a mean thickness of 3.2±1.4 nm, consistent with the thickness of a lipid bilayer (189). When pure DOTAP vesicles were deposited for AFM, no areas of sufficient height to be a vesicle were observed; they appeared to form a continuous bilayer on the surface (Figure 4.3c). PMOXA-PDMS-PMOXA vesicles adsorbed as intact vesicles, just as on silica, although the average thickness was greater, 199.3±39.5 nm, on mica (Figure 4.3d).

The 11 molar ratio PMOXA-PDMS-PMOXA:89 molar ratio POPC (Figure 4.3e) vesicles formed patches with a mean thickness of 5±1.4 nm, even in the absence of calcium. These are interpreted as patches of polymer monolayer and lipid bilayer. In contrast, 33 molar ratio PMOXA-PDMS-PMOXA:67 molar ratio POPC: vesicles gave rise to vesicular structures (Figure 4.3f) with a mean thickness of 26.6±48.4 nm and a broad thickness distribution. Vesicles were still visible following addition of calcium (Figure 4.3g), but the mean thickness of the vesicular structures decreased to 19.4±7.0 nm, which suggests that some flattening and/or rupture occurs when calcium is added.

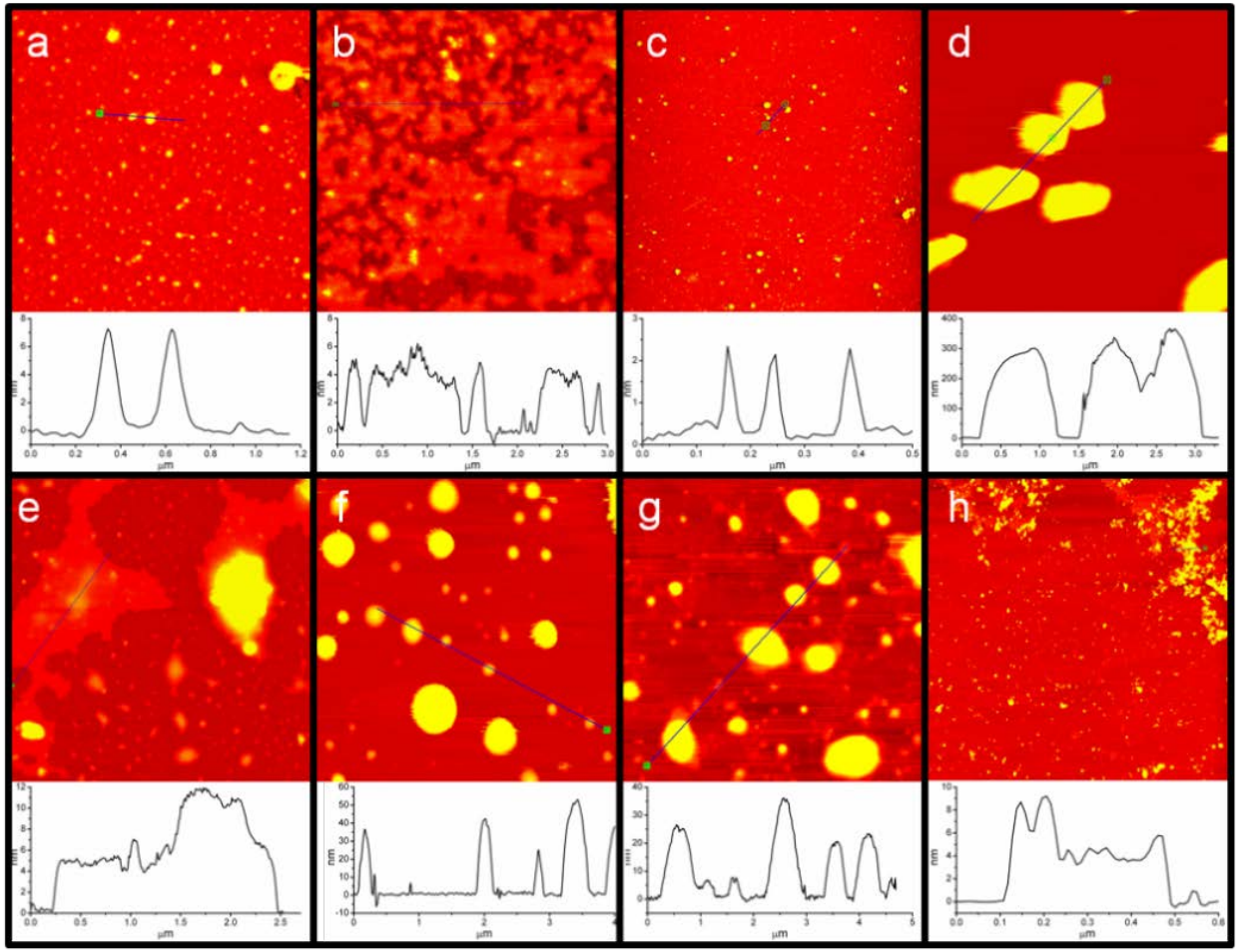

Figure 4.3. AFM images
(a) PBS, (b) POPC, (c) DOTAP, (d) PMOXA-PDMS-PMOXA, (e) 11 molar ratio PMOXA-PDMS-PMOXA:89 molar ratio POPC, (f) 33 molar ratio PMOXA-PDMS-PMOXA:67 molar ratio POPC, (g) 33 molar ratio PMOXA-PDMS-PMOXA:67 molar ratio POPC: with 5 mM $CaCl_2$, (h) 11 molar ratio PMOXA-PDMS-PMOXA:89 molar ratio DOTAP. Each block is 5 µm x 5 µm. A height profile is shown for each figure.

Eleven molar ratio PMOXA-PDMS-PMOXA:89 molar ratio DOTAP: mixtures (Figure 4.3h) did not show any areas of sufficient height to be a vesicle and appeared to make a continuous bilayer on the surface.

Vesicle water permeability

One advantage of the PMOXA-PDMS-PMOXA polymers is their low permeability for water (0.8 μm/s (16)), as compared to lipids (43, 190), so it was of interest to assess the water permeability of hybrid polymer-lipid vesicles. Based on stopped-flow measurements under hyperosmotic shock (Figure 4.4), the zwitterionic POPC vesicles had a P_f of 22.6 μm/s at 10 °C, similar to previous measurements using a fluorescence quenching method (P_f=18.8±4.7 μm/s, converted from 25°C measurements (190) to the 10°C equivalent using an activation energy of 15 kcal/mol). Differences in permeability values could be due to differences in stopped flow instruments. The osmotic water permeability of DOTAP vesicles was 13.2 μm/s at 10 °C, somewhat lower than POPC vesicles. Both lipids gave permeability values roughly similar to those reported for *Escherichia coli* total lipid extracts (20.9 μm/s, based on measurements at 6.5°C (43) converted as above). All hybrid vesicle compositions were less permeable to water than pure lipid vesicles. In fact, a molar content of PMOXA-PDMS-PMOXA exceeding 33% resulted in vesicles that were so impermeable that the results could not be fit to an exponential function and we could not calculate a P_f value (Figure 4.5).

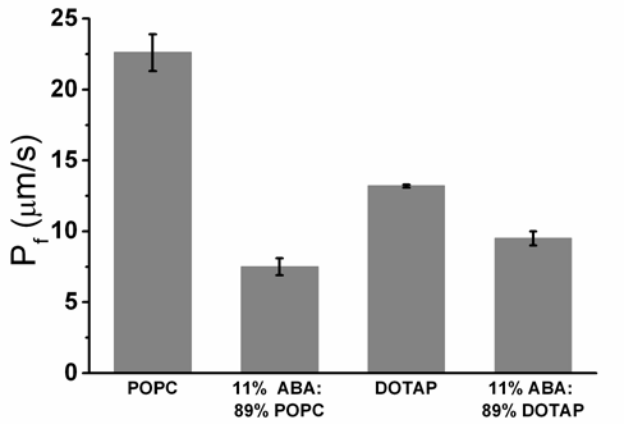

Figure 4.4. Water permeability of hybrid polymer:lipid vesicles from osmotic shock stopped-flow light-scattering experiments
Average and standard deviation calculated from at least 6 injections. Other vesicle compositions, including pure polymer, did not show sufficient water efflux to allow permeability calculations. The reported permeability, P_f, for PMOXA-PDMS-PMOXA is 0.8 μm/s (16).

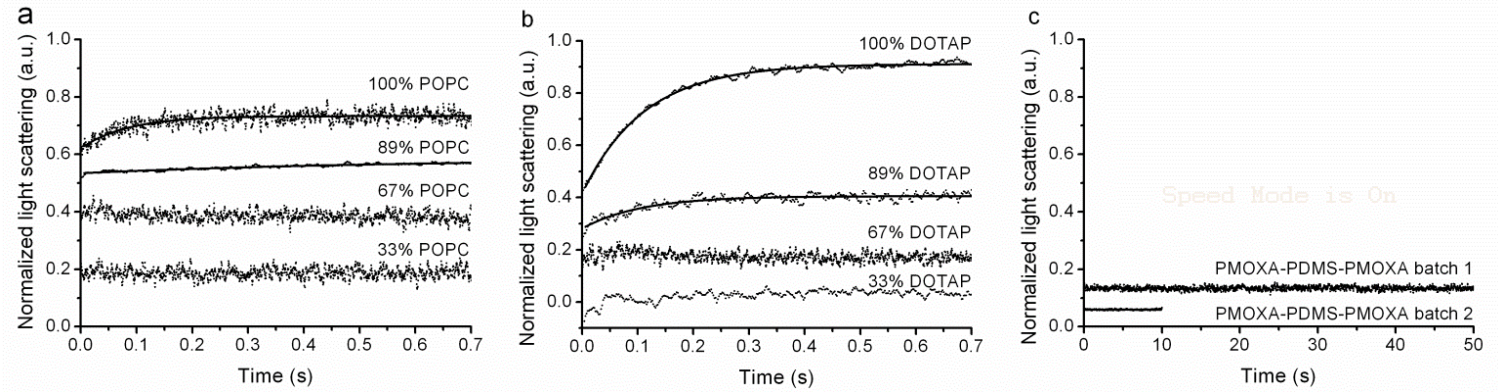

Figure 4.5. Stopped-flow light scattering results
(a) POPC-containing, (b) DOTAP-containing and (c) PMOXA-PDMS-PMOXA vesicles determined by stopped-flow light-scattering experiments. Average and standard deviation calculated from at least 6 injections. Vesicles with at least 89 molar ratio lipid were fitted to an exponential function. Hybrid vesicles containing less than 89 molar ratio lipid showed no slope. PMOXA-PDMS-PMOXA data was collected over 10 and 50 seconds, and no slope was seen during the entire time.

4.5 Discussion

For all ratios tested, PMOXA-PDMS-PMOXA polymer formed hybrid vesicles with POPC and DOTAP lipids, rather than forming two populations of single material vesicles. Evidence for such hybrid vesicles is provided by the screening of the positively charged DOTAP, which is evident in the zeta potential measurements (Table 4.1), the consistent morphologies observed with TEM (Figure 4.1), and the low variation in stopped-flow light scattering measurements (Figure 4.4 and Figure 4.5). Additional evidence for hybrid vesicles is provided by the progressive change in adsorption properties (Figure 4.2 and Figure 4.3) and permeability (Figure 4.4 and Figure 4.5) as the lipid content in the vesicles is decreased. These results are consistent with a previous study (182), which demonstrated the formation of mixed PMOXA-PDMS-PMOXA/egg-PC/egg-PE vesicles and provided evidence that the mixing was homogeneous on a molecular scale.

Vesicle adsorption on quartz followed one of three scenarios (Figure 4.6), based on the mean thickness of the adsorbed layer and the fractional bilayer coverage (Table 4.2). In scenario I, the vesicles ruptured spontaneously to form a planar membrane. This scenario included pure POPC, pure DOTAP, and vesicles consisting primarily of DOTAP (11% and 33% polymer). Formation of bilayers by pure lipids is consistent with previous studies (35, 191). Consistent with the fractional bilayer coverage, which suggests that some vesicles remained intact, the POPC deformation ratios (35), the mean thickness (189) for POPC vesicles, and the DOTAP deformation ratios (35) were all slightly higher than previous reports for the corresponding bilayers (Table 4.2). In scenario II, the vesicles adsorbed as vesicles but could be induced to rupture by the addition of calcium. Mixed polymer:POPC vesicles consisting of predominantly POPC (11% and 33% polymer) followed this scenario. In scenario III vesicles adsorbed until the quartz surface was saturated, but did not rupture even upon addition of the fusogen calcium. Vesicle compositions that followed this scenario contained predominately PMOXA-PDMS-PMOXA (100% and 67% PMOXA-PDMS-PMOXA with POPC or DOTAP). The increased ease of rupturing DOTAP-containing vesicles, as compared to POPC, is consistent with the expected stronger electrostatic interactions between positively charged DOTAP and the negatively charged quartz surface, as compared to the zwitterionic POPC.

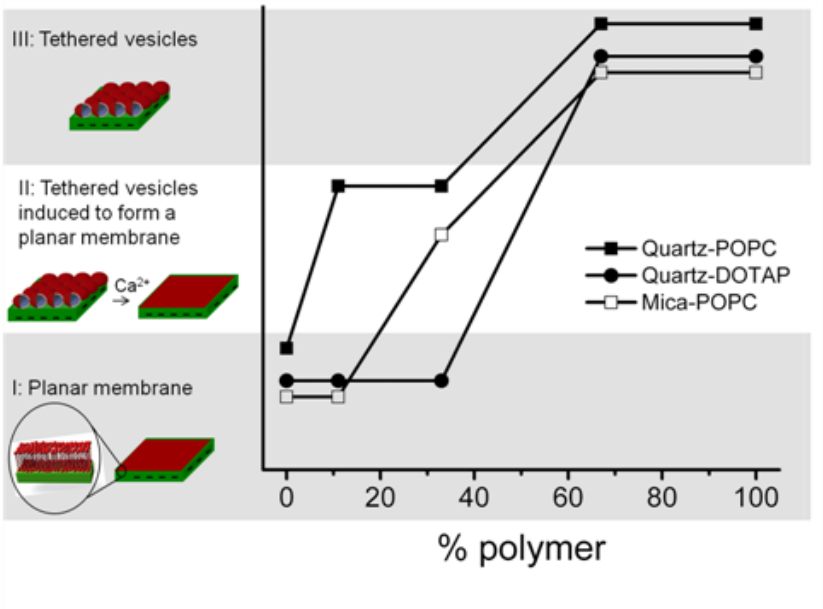

Figure 4.6. The type of supported membrane formed can be controlled by varying the ratio of polymer to lipid and the types of lipids
(I) Planar membrane, (II) tethered vesicles that can be triggered to form a planar membrane by addition of calcium, and (III) tethered vesicles. The data presented here indicate that the surface becomes saturated, but do not distinguish whether or not a continuous layer of vesicles is formed.

The results on mica were generally similar to those on quartz. 100% DOTAP and 11 molar ratio PMOXA-PDMS-PMOXA:89 molar ratio DOTAP vesicles did not produce intact vesicles on mica, consistent with rupture, but inconsistent results were obtained with other ratios of polymer:DOTAP. For POPC-containing vesicles the overall trend was similar on quartz and mica, but the division between scenarios I and II shifted somewhat. On mica the 11 molar ratio polymer:89% POPC vesicles followed scenario I, deposition and rupture, rather than requiring calcium to promote rupture as on quartz. For 33 molar ratio polymer:67% POPC, adsorbed vesicles were detected with and without calcium, but the mean thickness decreased with calcium, suggesting that some rupture was occurring. These vesicles also had a significantly lower thickness on mica than on silica (both with and without calcium). Together these results show a trend for lower resistance to rupture, or stronger lipid-surface interactions, of polymer:POPC vesicles on mica than on silica. This is consistent with the results of Richter et al., where charged lipid vesicles experienced stronger interactions with mica than with silica, and suggests that mica is more strongly negatively charged than silica under these conditions (100).

For both POPC and DOTAP, the addition of a relatively low molar percentage polymer provided higher rupture stability and decreased water permeability. On quartz the transition from rupture to stability occurred between 11 and 33% PMOXA-PDMS-PMOXA for polymer:DOTAP vesicles and between 0 and 11% PMOXA-PDMS-PMOXA for polymer:POPC vesicles. Similarly, for mixed vesicles with 33% and higher polymer content, the water permeability values were low, similar to those of the polymer vesicles. This relatively large effect from a low molar percentage of polymer may be explained by its larger size. Assuming that individual PMOXA-PDMS-PMOXA molecules span the membrane, that one PMOXA-PDMS-PMOXA polymer molecule has a surface area of 4 nm^2 (from surface pressure isotherm measurements (177)), and that one lipid has a head group area of 0.68 nm^2,(192) then 11 molar ratio PMOXA-PDMS-PMOXA corresponds to 59% of the vesicle surface area and 33 molar ratio PMOXA-PDMS-PMOXA corresponds to 85% of the surface area.

Several properties of the PMOXA-PDMS-PMOXA polymer may be contributing to the observed increases in resistance to rupture and decreases in water permeability in hybrid vesicles. First, the increased thickness of the hydrophobic block of the polymer is likely to be affecting both properties. In the PMOXA-PDMS-PMOXA polymer used here, the hydrophobic PDMS block has a thickness of 10 nm (182), whereas a typical lipid membrane has a hydrophobic region around 3 nm thick (189). The longer polymer length may also allow the PMOXA to physically shield the lipids, resulting in steric repulsion between vesicles and reducing fusion. Second, in mixed DOTAP/PMOXA-PDMS-PMOXA vesicles, the polymer screens the positive charge of the DOTAP, based on zeta potential measurements. This is expected to decrease the electrostatic attraction of DOTAP to the quartz and mica surfaces, reducing vesicle-surface interactions and thereby increasing vesicle stability. Third, with PMOXA-PDMS-PMOXA a single molecule may span the entire membrane. As compared to the bilayer structure formed by lipids, this should make the membrane more rigid and provide stability from mechanical stress. This is analogous to some archaeal membranes, which have increased structural stability (193) due to membrane spanning, bipolar bolalipids (193, 194). Fourth, the block copolymers can be stretched by up to 21% of their original area (163), whereas lipid membranes cannot be stretched beyond 5% without rupture under osmotic or other stresses (195).

4.6 Conclusions

Mixing PMOXA-PDMS-PMOXA polymer and lipids produced hybrid vesicles containing both lipids and polymers. Either adsorbed vesicles or supported planar membranes were formed on negatively charged quartz and mica surfaces, depending on the polymer:lipid ratio of the depositing vesicles. Hybrid vesicles exhibited characteristic attributes of both lipid and polymer vesicles: adsorption and surface-induced or calcium-induced rupture similar to lipids and polymer characteristics of surface-induced rupture stability and low water permeability. Hybrid vesicles and planar membranes formed through vesicle deposition should be compatible with incorporation of functional transmembrane proteins, and the properties demonstrated here for hybrid vesicles are attractive for a variety of applications, including drug delivery and formation of solid-supported polymer-lipid membranes for biosensors or water purification membranes.

4.7 Acknowledgments

We thank Drs. Mariusz Grzelakowski and Wolfgang P. Meier (University of Basel) for polymer and Dr. Christian Rein (University of Copenhagen), Prof. Erik Reimhult (University of Natural Resources and Life Sciences, Vienna), Dr. Wacek Swiech (Frederick Seitz Materials Research Laboratory Central Facilities, University of Illinois) and Dr. Scott McLaren (Frederick Seitz Materials Research Laboratory Central Facilities, University of Illinois) for valuable discussions. AFM and TEM experiments were carried out in the Frederick Seitz Materials Research Laboratory Central Facilities, University of Illinois. Glow-discharging of copper grids for TEM was carried out at the Microscopy Suite in the Beckman Institute, University of Illinois.

Support for this work was provided by the US National Science Foundation (CBET 08-28512 and CBET-1336620), and the Graduate Assistance in Areas of National Need (GAANN) and the University of Illinois SURGE fellowships. In addition, this work was supported through MEMBAQ, a Specific Targeted Research Project by the European Commission under the Sixth Framework Programme (NMP4-CT-2006-033234), through the US National Science Foundation (CBET 08-28512), through the Danish National Advanced Technology Foundation (023-2007-1), and through a grant to DTU Physics from the Danish National Research Foundation. This work

was also supported by the Environment & Water Industry Programme Office of Singapore (EWI) through project #MEWR 651/06/169.

CHAPTER 5: PH EFFECT ON PERMEABILITY AND SURVIVAL OF *ESCHERICHIA COLI*[3]

5.1 Abstract

Aquaporins exist across all domains of life and are essential for satisfying water transport needs in mammalian and plant cells. The physiological relevance of bacterial aquaporins (AqpZ), however, is unknown. Previous work demonstrated that AqpZ-polymer vesicles exhibited reduced permeability under acid shock conditions, and presented preliminary evidence that this phenomenon might also occur in whole cells of *E. coli*. The current work therefore examines *Escherichia coli* permeability under acid shock, and survival under acid, hypoosmotic, and combined acid and osmotic shock. I found that at neutral pH, the presence of AqpZ increased *E. coli* permeability compared to *aqpZ* null mutants due to AqpZ facilitating rapid water egress under an osmotic gradient. Additionally, *aqpZ* reduced *E. coli.* survival under acid and combined acid and osmotic shocks. This work provides insight into the physiological role of AqpZ.

5.2 Introduction

Existing across all domains of life, aquaporins facilitate rapid and selective water transport across membranes (106, 196). They are essential for the water transport needs of mammalian and plant cells. Yet, in microorganisms, their physiological relevance is unknown. The large surface area to volume ratio of microorganisms can supply the necessary water transport via diffusion (106). Additionally, aquaporins are not present in all types of microorganisms (106, 107); for example, they are less represented across Gram-positive than gram-negative bacteria (107). Even in bacteria where aquaporins are present, they do not seem to be essential. When the aquaporin gene was

[3] Author contributions: I performed all of the experiments described in this chapter, except for the survival experiments. I mentored the undergraduate researchers who performed the survival experiments. I analyzed and interpreted all of the data.

knocked out, it was not lethal to *Escherichia coli* (109) or *Brucella abortus* (110). Therefore, in bacteria, aquaporins are not essential.

In attempting to uncover the role of bacterial aquaporins (AqpZ), studies have eliminated *aqpZ* genes and found, at most, subtle changes in cellular growth or function (106, 108, 109). In one study, *aqpZ* null mutant colonies were smaller than *aqpZ* wild type colonies. When *aqpZ* wild type and null mutants were co-cultured in hypoosmolar conditions, the *aqpZ* null mutant colonies were also smaller in size and less viable. Additionally, gene expression levels of *aqpZ* were higher in hypoosmotic environments and lower in hyperosmotic environments (109). In another study, no changes in growth were observed at hypoosmotic or hyperosmotic conditions, or when changed from one condition to the other (108). While these data are contradictory, cryoelectron microscopy experiments demonstrated that osmotically shocked *E. coli* exhibited AqpZ-mediated water transport (197). Unlike the *aqpZ* wild type strain, cytoplasm shrinkage and rehydration did not occur for *aqpZ* null mutants when subjected to hyperosmotic followed by hypoosmotic shock (197). However, *aqpZ* null mutants containing a plasmid with *aqpZ* allowed for cytoplasm changes under these conditions, implicating *aqpZ* in osmolarity regulation. In eukaryotic microorganisms and in plants, aquaporins have generally been implicated in providing freeze tolerance and survival under hypoosmotic conditions (106, 109, 110).

Some clues to AqpZ's physiological role in Bacteria may arise from its characteristics. In previous work in our lab, AqpZ was found to reversibly close under acidic conditions. The permeability of AqpZ reconstituted in biomimetic triblock copolymer vesicles decreased when pH was reduced from 7.2 to 4.0. At acidic pH, vesicles only exhibited 19% of the permeability at 7.2. When the pH was restored to neutral, permeability returned to 123% of the permeability before the acid shock manipulation (41). In initial experiments with whole cells, the effect of acid shock was less pronounced than in the synthetic environment. In whole cells, permeability at pH 4.0 was 84% of permeability at neutral pH. The permeability of an *aqpZ* null strain (JW0859) was even less affected by acidic conditions, exhibiting 95% of its permeability at neutral pH. In addition, even at neutral pH, absolute permeability values vary from group to group, ranging from 2020 μm/s (198) to 691 μm/s (199) for *aqpZ* wild type in the same strain background (NCM3105). Thus, differences in strain background were not the mere cause of the lower permeability observed in

our lab (190 μm/s (41) in a different strain background). Surprisingly, not only did the absolute permeability values differ, the percent difference between the permeability values of the parent and *aqpZ* null strain differed, especially in our lab. Previous reports noted an *aqpZ* null mutant exhibited only 3% (198) and 1.3% (199) of the permeability of the wild type. Previous work in our lab found the *aqpZ* null strain exhibited 84% of the permeability of the wild type (41) in a different strain background. These very different findings show that in our lab, *aqpZ* had much less effect (by an order of magnitude) on permeability than previous reports (198, 199). However, these studies were carried out in different strains.

Based on the potential closure at low pH, previous work also investigated the effects of eliminating or overexpressing *aqpZ* on acid shock. Of all strains tested, the most permeable strain, JM109 pTrc10HisAqpZ, was the most susceptible to acid shock (41). However, based on the observed differences in permeability, a key control was missing in those survival experiments. While survival of parent ME9062 was reported, the survival of the relevant control strain for the overexpression strain (JM109 pTrc10His1) was not tested. These findings and limitations demand further investigation into the effect of *aqpZ* on cell permeability and survival.

In this work, my objectives were to quantify the effects of *aqpZ* on *E. coli* permeability and survival under acid shock. Based on the reversible gating behavior reported previously (41), I expect *aqpZ* to cause reduced permeability under acid shock compared to neutral pH. Additionally, I expect reduced survival for these strains. By investigating the impact of *aqpZ* on permeability and survival in *E. coli*, this work provides insight into the physiological role of AqpZ. While the benefit in *E. coli* is unknown, this work demonstrates that AqpZ must provide one.

5.3 Materials and Methods

Preparation of strains and cell growth

The *E. coli* strains used in this study are described in Table 5.1. Plasmids were introduced by electroporation (Bio-Rad MicroPulser, Hercules, CA) according to the Bio-Rad MicroPulser *E. coli* standard procedure (200). Cells were grown and prepared according to Mallo and Ashby (198) with slight modifications. For the majority of this work, starter cultures were grown on Lennox

Luria-Bertani (LB) (5 g/L NaCl, 10 g/L tryptone, 5 g/L yeast extract) media, and subcultured in LB with a total concentration of 0.2 M NaCl (11.7 g/L NaCl, 10 g/L tryptone, 5 g/L yeast extract) with antibiotics at 30 μg/ml kanamycin (Km), 25 μg/ml chloramphenicol (Cm), or 50 μg/ml Amp as appropriate. Starter cultures were inoculated with a single colony from a freshly grown streak plate and incubated at 37°C with agitation for 15 h. Strains with plasmids were grown with 50 μg/ml ampicillin (Amp). The *aqpZ* null mutant NCM3306 strain was also reconstructed; see APPENDIX C.

Table 5.1. Strains used in this study

Strain	Type	Origin	Antibiotic resistance	Genotype	Ref
ME9062	parent	National BioResource Project (Japan)	---	*F-, Δ(araD-araB)567, ΔlacZ4787(::rrnB-3), λ-, rph-1, Δ(rhaD-rhaB)568, hsdR514*	(201)
JW0859	AqpZ null mutant	Keio collection	Km	*F-, Δ(araD-araB)567, ΔlacZ4787(::rrnB-3), λ-, rph-1, Δ(rhaD-rhaB)568, hsdR514, ΔaqpZ*	(201)
NCM3105 (MG1655)	parent	Kustu Lab	---	*ilvG, rfb-50, rph-1, fnr-267 eut*	(202)
NCM3105 pTrc10HisAqpZ	Parent with AqpZ overexpression plasmid	this work	Amp	*ilvG, rfb-50, rph-1, fnr-267 eut*, pTrc10HisAqpZ	
NCM3105 pTrc10His1	Parent with control plasmid	this work	Amp	*ilvG, rfb-50, rph-1, fnr-267 eut*, pTrc10His1	
NCM3306	AqpZ null mutant	Kustu Lab	Cm	*ilvG, rfb-50, rph-1, fnr-267 eut, ΔaqpZ*	(202)
NCM3306 pTrc10HisAqpZ	Parent with AqpZ overexpression plasmid	this work	Cm, Amp	*ilvG, rfb-50, rph-1, fnr-267 eut*, ΔAqpZ, pTrc10HisAqpZ	
NCM3306 pTrc10His1	Parent with control plasmid	this work	Cm, Amp	*ilvG, rfb-50, rph-1, fnr-267 eut*, ΔAqpZ, pTrc10His1	
JM109	AqpZ null mutant	Purchased from Promega	Amp	endA1, recA1, gyrA96, thi, hsdR17 (rk–, mk+), relA1, supE44, Δ(lac-proAB), [F′ traD36, proAB, laqIqZΔM15]	
JM109 pTrc10HisAqpZ	Parent with AqpZ overexpression plasmid	this work	Amp	endA1, recA1, gyrA96, thi, hsdR17 (rk–, mk+), relA1, supE44, Δ(lac-proAB), [F′ traD36, proAB, laqIqZΔM15], pTrc10HisAqpZ	(41)
JM109 pTrc10His1	Parent with control plasmid	this work	Amp	endA1, recA1, gyrA96, thi, hsdR17 (rk–, mk+), relA1, supE44, Δ(lac-proAB), [F′ traD36, proAB, laqIqZΔM15], pTrc10His1	(41)

Whole cell permeability measurements

The standard procedure for permeability measurements is presented here. Modifications were also tested as described in Section 5.4. Starter cultures were diluted 1:100 into fresh LB media (0.086 M NaCl) with antibiotics as needed. These subcultures were incubated with agitation for 8 to 13 h, and until cells were in stationary phase as measured by optical density (O.D., λ=600) of 1.8-2.0. For the last 4 hours of the 8-13 hours of incubation, strains containing plasmids were induced with 1 mM isopropyl β-D-1-thiogalactopyranoside (IPTG) for overexpression of AqpZ. On the pTrc10HisAqpZ plasmid, when transcription of the lac operon is activated by IPTG, protein overexpression occurs. All cells were harvested by centrifugation (5 min, 4°C at 10,000 × g) and pellets were rinsed three times with 10 ml of ice cold 100 mM phosphate buffered saline (PBS) at the specified pH (pH 7.4 or 4.0) and with 50 μg/ml tetracycline. Cell pellets were finally resuspended in ice cold PBS buffer with tetracycline to achieve 70±1% transmittance. Thirty to 60 min elapsed between cell harvest and stopped-flow measurement.

Cell permeability was determined using stopped-flow spectrometry (SX.18MV-R, Applied Photophysics, Surrey, UK) with light scattering according to Borgnia et al. (43). Prepared cells were mixed with an equal volume of 1 M L-Proline in PBS osmotic agent at 10^{o} C. Change in cellular size (volume) due to water efflux was monitored by light scattering at 600 nm emission wavelength. The light scattering curves (at least 7) were averaged and fitted using an exponential rise equation in MATLAB (v.8.3.0.532) or Origin (v.8.1) software, and water permeability (P_f) was calculated using Equation 5.1 (198):

$$P_f = k \times \left[V_o / \left(S \times V_w \times \Delta_{osm} \right) \right]$$

Equation 5.1. Water permeability

where k is the exponential rise rate constant or change in cell volume ($d[V/V_o]$), V_o and S are the respective initial cellular volume and surface area, assuming similarity to the average K-12 *E. coli* strains grown in LB from exponential to the beginning of stationary phases (198, 203). Assuming a length of 5 μm and a diameter of 1 μm (198, 203) gives values of V_o= 3.93 μm^3 and S = 16.49 μm^2. V_w is the molar volume of water (18 cm^3/mol), and Δ_{osm} is the imposed osmolar gradient.

Mixing cells with an equal volume of 1 M proline, the resulting osmolar gradient imposed was 5×10^4 mol/cm^3. The number of independent biological replicates are noted in the presentation of the data. A two sample t-test was used to determine significance using Origin (v.8.1) software. The stopped flow instrument used is noted in presentation of the data. Whole cell permeability data is tabulated in APPENDIX C.

E. coli survival measurements

Survival was measured following Levina et al. (204) with slight modifications. Starter cultures were diluted 1:50 into LB media with a total concentration of 0.2 M NaCl and appropriate antibiotics as needed. The subcultures were incubated at 37°C with agitation for 8 h before 1:100 dilution into an appropriate buffer for the desired shock condition: 0.2 M NaCl pH 7.4 LB for the control, 0.2 M NaCl pH 4.0 LB for the acidic condition, 0 M NaCl pH 7.4 LB for the osmotic condition, 0 M NaCl pH 4.0 LB for the combined acidic and osmotic condition. The cultures were incubated at 37°C with agitation in the test conditions for 30 min before they were diluted in LB (10^4-10^7 dilution) and plated. The number of independent biological replicates are noted in the presentation of the data. In the survival data presented in this chapter (2011), one plate was prepared for each biological replicate. In additional survival data (2014) presented in APPENDIX C, three plates were prepared for each dilution of each biological replicate. Colonies were counted manually after 12-16 h incubation at 37°C. Only plates with 25-250 colonies were included in this study (205), except when plates with 20-25 colonies allowed inclusion of an independent biological replicate. All survival data is tabulated in APPENDIX C.

5.4 Results

Factors influencing permeability measurements

To investigate permeability differences observed in previous reports, I identified differences between my protocol and those of previous reports. I tested the impact of the following: presence of an antibiotic to suppress protein synthesis during processing of cells, time on ice from harvest to stopped-flow analysis, and growth phase.

In my experiments, tetracycline was added to suppress protein synthesis after harvest and during the washing and resuspension preparation steps, but antibiotic was not added in previous reports (198, 199). In previous experiments in our lab kanamycin was used for ME9062 and JM109 derived strains, and chloramphenicol was used for JW0859 (41). However, tetracycline did not substantially impact the permeability of NCM3105 (Figure 5.1A). Based on these results, tetracycline was used in subsequent experiments.

One previous report kept time on ice prior to stopped-flow measurement to 10 min (198). Because of the location of one of the stopped-flow instruments, I tested longer times. I did not observe a substantial effect with respect to time on ice prior to measurement ((Figure 5.1B). Time on ice was minimized and was between 30-60 min.

The phase of growth was previously reported as important (198). In testing the effect of phase of growth on permeability, no clear trend emerged between growth phase and permeability ((Figure 5.1C-D). Therefore, in this work, cells were harvested in stationary phase based on previous reports (198).

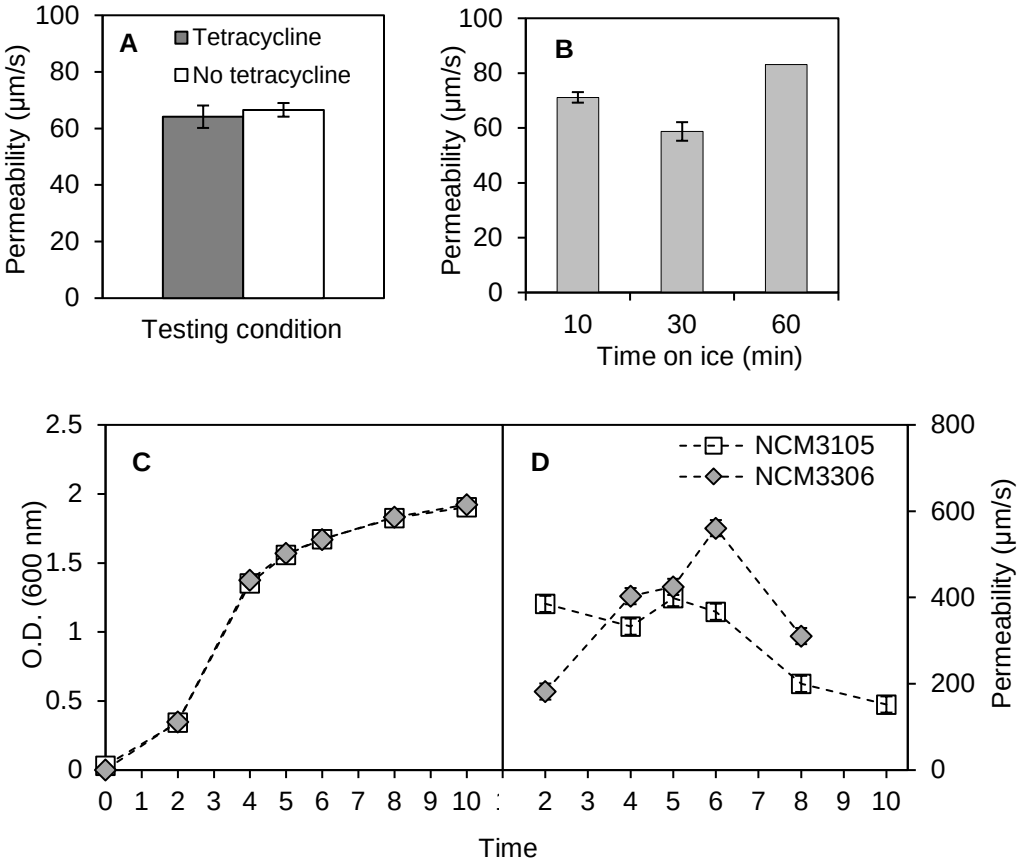

Figure 5.1. Factors that did not impact the permeability of NCM3105
(A) Presence or absence of tetracycline during cell preparation: Chart shows the permeability of NCM3105 with and without tetracycline added to suppress protein synthesis during processing. Error bars denote propagated error from curve fitting of multiple (at least 2) preparations from the same biological replicate. (B) Processing Time: Permeability of NCM3105 after 10-60 min spent on ice between harvest and measurement. Error bars denote propagated error from curve fitting of two biological replicates for 10 and 30 min; no error bars shown for 60 min data because only one biological replicate was tested. (C) Phase of Growth: Growth of strains in neutral pH LB media with agitation at 37^0C, as measured by O.D. at 600 nm and (D) Permeability of strains as a function of growth. Error bars denote error from curve fitting from one biological replicate. All data in this figure was obtained using stopped flow instrument 1.

Permeability

Literature reports conflicting phenotypes in *aqpZ* null mutants (197-199). I therefore tested the permeability of different *E. coli* strains at neutral pH. The *aqpZ* null mutants exhibited reduced permeability than the *aqpZ* wild type strains (Figure 5.2). NCM3306 exhibited 68% of the permeability of NCM3105, and ME9062 exhibited 86% of the permeability of JW0859. However,

the differences in permeability were only statistically significant for NCM3105 and NCM3306. The *aqpZ* overexpression strain (JM109 pTrc10HisAqpZ) had the highest permeability. Surprisingly, the strain background of the overexpression system also seemed to affect permeability. The control strain without *aqpZ* on the plasmid (JM109 pTrc10His1) had 80-85% increased permeability over that of the other wild type *aqpZ* strains NCM3105 and ME9062.

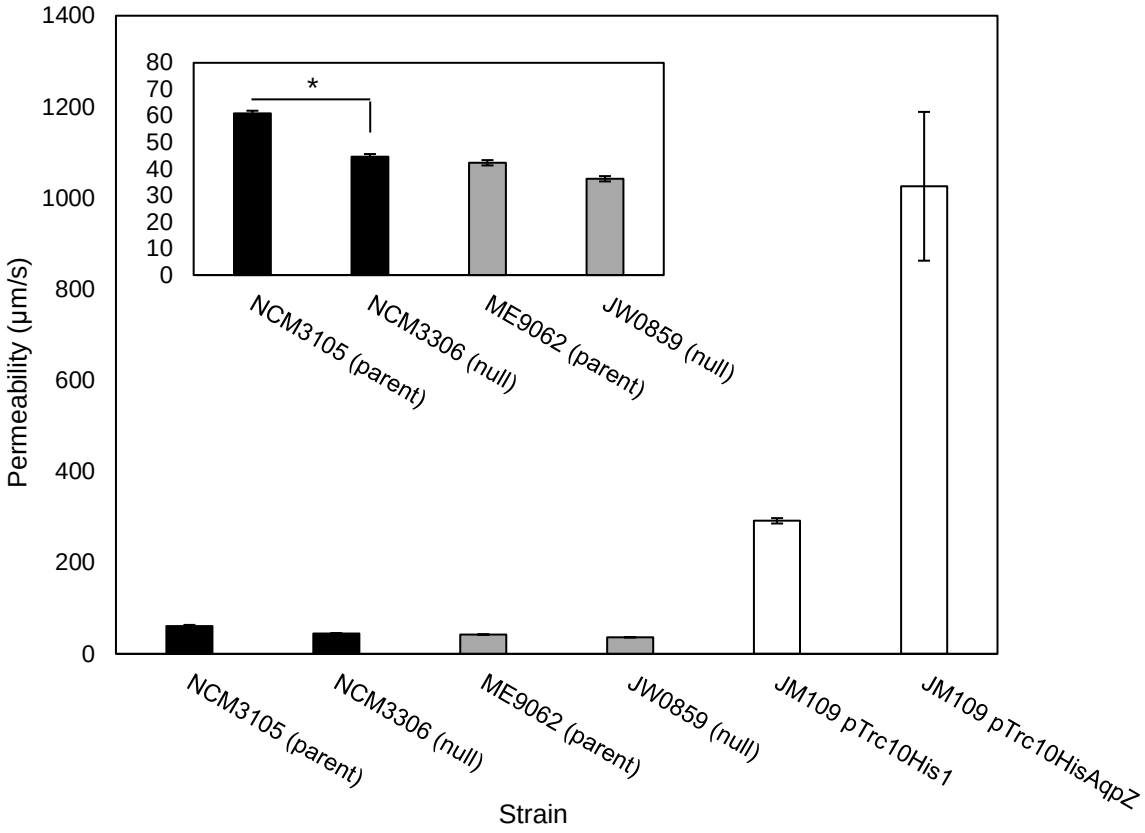

Figure 5.2. Permeability at pH 7.4 of *E. coli* strains
The inset provides a more detailed view of the less permeable strains. *Indicates significantly different permeability ($p < 0.05$). Error bars represent propagated error from curve fitting of independent biological replicates (9 for NCM3105; 7 for NCM3306; 3 for ME9062 and JW0859; and 2 for JM109 pTrc10His1 and JM109 pTrc10HisAqpZ). All data in this figure was obtained using stopped flow instrument 1.

Effect of pH on permeability

Since AqpZ has been shown to reversibly close under acidic conditions in a synthetic membrane, I also tested the permeability of *E. coli* under acidic conditions (Figure 5.3). The *aqpZ* wild type

strain ME9062, which had been tested previously in our lab, behaved as expected, having reduced permeability at pH 4.0 compared to pH 7.4. However, in contrast to previous results (41), the corresponding *aqpZ* null mutant (JW0859) showed a similar phenotype. Furthermore, the permeability of strains in the NCM3105 background was typically greater at pH 4.0 than at pH 7.4, regardless of the presence, absence, or overexpression of *aqpZ*. The sole exception was the overexpression strain, NCM3105 pTrc10HisAqpZ after expression was induced. Additionally, the presence of the overexpression plasmid pTrc10HisAqpZ and its control seemed to increase cell permeability at pH 4, with the exception of NCM3105 pTrc10His1 uninduced. This effect was even more pronounced after induction, even when no gene had been introduced into the overexpression locus.

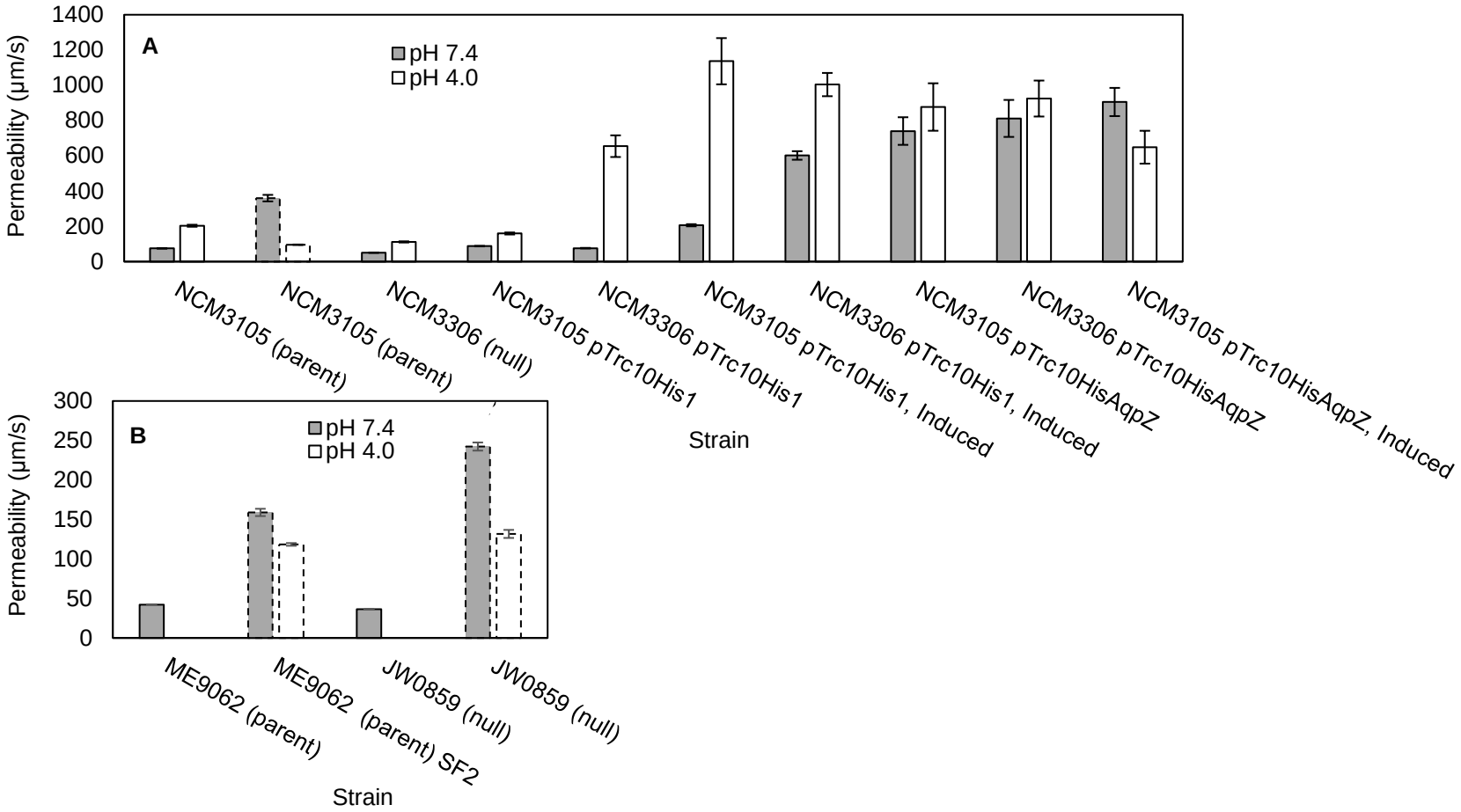

Figure 5.3. pH effect on permeability
(A) Permeability of strains derived from NCM3105 at pH 7.4 and 4.0. (B) Permeability of strains derived from ME9062. Error bars denote error from curve fitting of stopped-flow measurements for one biological replicate; exception: NCM3105 from stopped-flow 2 includes 2 biological replicates. There is no data for NCM3306 pTrc10HisAqpZ under induced conditions. Dashed borders note that cells were grown on Miller LB (0.017 M NaCl) and measured on stopped-flow 2.

Effect of stopped-flow instrument on permeability

Over the course of this work I tested cell permeability on two different stopped-flow instruments. Although the difference was only statistically significant for NCM3105, at pH 7.4, permeability values for all strains tested were consistently higher using stopped-flow instrument 2 (Figure 5.4). Conversely, at pH 4.0, the permeability of NCM3105 was greater on stopped-flow instrument 1. ME9062 and JW0859 were not tested on stopped-flow instrument 1 at pH 4.0. These measurements were not made with the same biological preparations and were separated by time because the instruments were not available at the same time; they are presented here simply to illustrate a potential confounding factor. Additionally, cells measured on stopped-flow instrument 2 were grown on Miller LB (0.017 M NaCl) as opposed to Lennox LB (0.086 M NaCl).

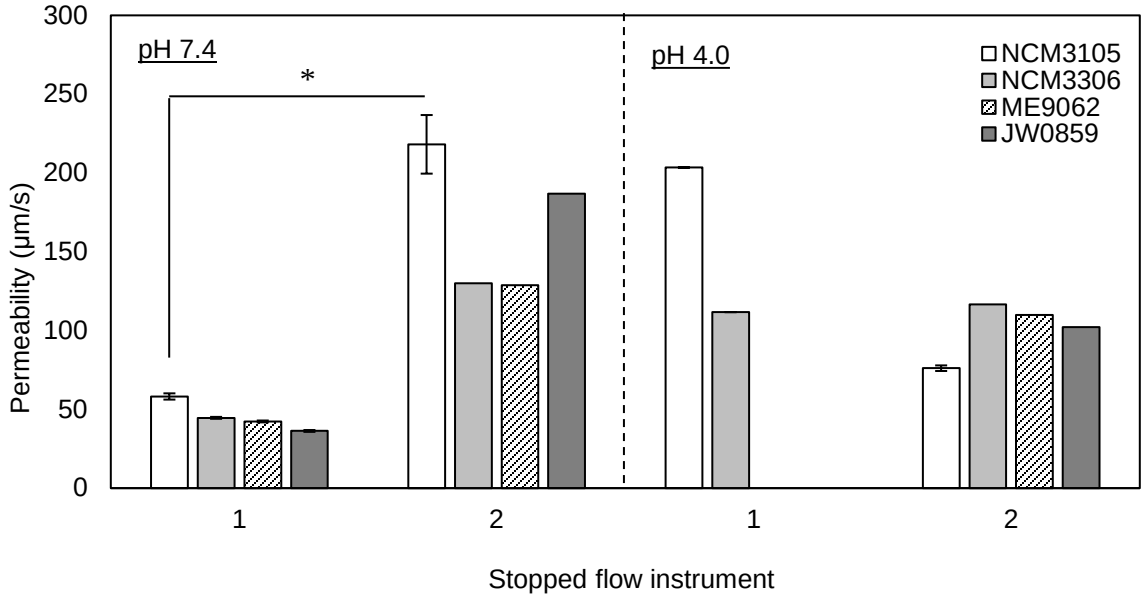

Figure 5.4. Effect of stopped-flow instrument on permeability
These measurements on two different stopped-flow instruments were not made with the same biological preparations and were separated by time. ME9062 and JW0859 were not tested on stopped-flow 1 at pH 4.0. Error bars denote propagated error of at least two independent biological replicates. *Indicates significantly different permeability ($p < 0.05$) in the same strain across the two instruments. No statistical analyses were performed for the other strains. The number of independent biological replicates is as follows for pH 7.4: NCM3105: 8 (SF1) and 2 (SF2), NCM3306: 6 (SF1) and 1 (SF2), ME9062 and JW0859: 3 (SF1) and 1 (SF2); for pH 4.0: NCM3105: 1 (SF1) and 2 (SF2), NCM3306: 1 (SF1) and 1 (SF2), ME9062 and JW0859: 0 (SF1) and 1 (SF2).

Effect of varying AqpZ level on survival

To investigate the effects of varying *aqpZ* expression levels on *E. coli*, I tested survival of different strain pairs under acid, hypoosmotic, and combined acid and hypoosmotic shock conditions (Figure 5.5).

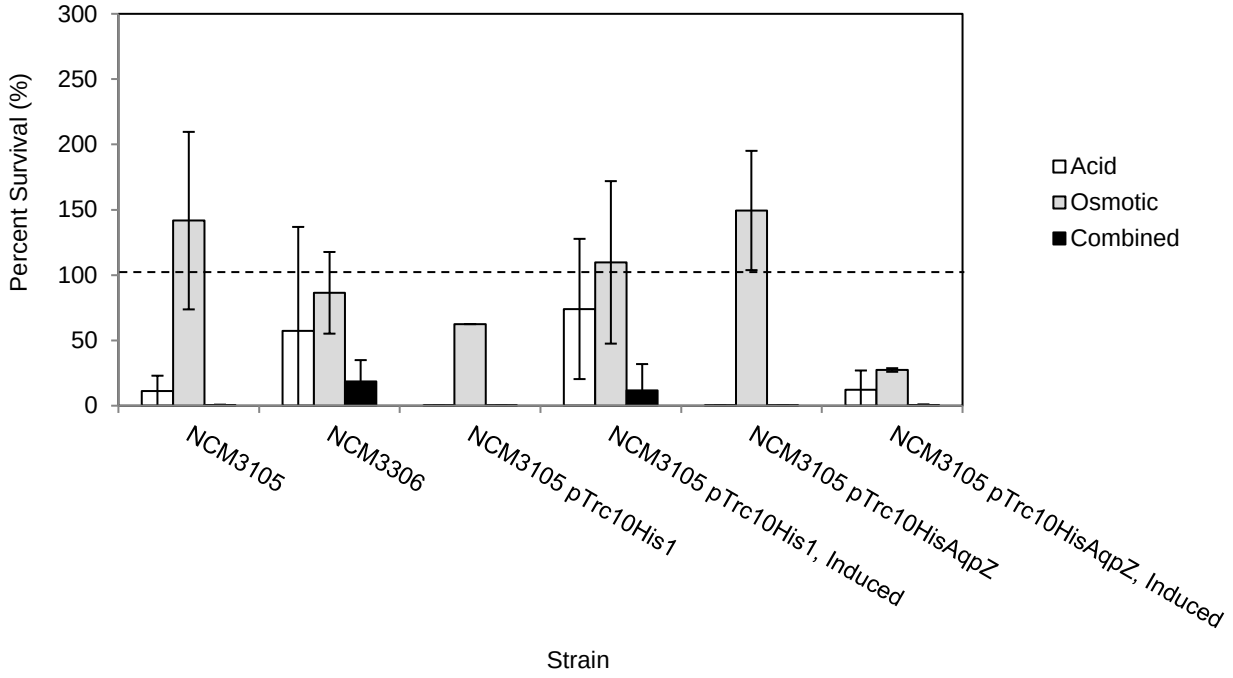

Figure 5.5. Percent survival of parent and null strains after exposure to various shock types
The acid shock was from pH 7.4 to 4.0 and the osmotic shock was from 300 to 100 mOsm (hypoosmotic); all conditions were for 30 min. Survival at the shock conditions were normalized to survival of respective strains at control conditions (0.2 M NaCl pH 7.4 LB), indicated by the dashed line at 100%. Error bars denote standard deviations between replicates. The number of independent biological replicates for each strain is as follows: NCM3105: 4 for acid and osmotic, 3 for combined; NCM3306: 4 for acid and osmotic, 3 for combined; NCM3105 pTrc10His1: 2 for acid, 1 for combined, 2 for osmotic; NCM3105 pTrc10His1 induced: 3 for acid and combined, 2 for osmotic; NCM3105 pTrc10HisAqpZ: 4 for acid and osmotic, 3 for combined; NCM3105 pTrc10HisAqpZ induced: 2 for all conditions.

Strains that contained *aqpZ* typically had reduced survival under acid and combined acid and osmotic shock. These include strains with the NCM3105 background. The overexpression system to produce more AqpZ required the addition of a chemical to induce expression and these strains were induced during stationary phase. Strains with the control plasmid were treated similarly.

Surprisingly, induction increased survival under acid shock even when no *aqpZ* gene had been introduced into the overexpression locus. The sole exception was the induced strain with the control plasmid (NCM3105 pTrc10His1).

5.5 Discussion

The physiological relevance of AqpZ is unknown and clues to its purpose may be discoverable by testing the behavior of AqpZ under different conditions and in *E. coli* with and without *aqpZ*. In this work I found that at neutral pH, the presence of AqpZ increased permeability. Additionally, under acid shock conditions, AqpZ reduced survival. In this section I will also discuss data related to these conclusions and unexpected findings.

I found reduced permeability for the *aqpZ* null mutant NCM3306 compared to parent NCM3105. This conclusion is based on my extensive experimentation with NCM3105 and the *aqpZ* null mutant NCM3306 at neutral pH (stopped-flow 1). Nine and seven independent biological replicates were tested for NCM3105 and NCM3306, respectively (Figure 5.2). The opposite trend was observed using stopped-flow 2 (Figure 5.3), but in that experiment only 2 biological replicates were tested for NCM3105 and only 1 for NCM3306. This trend of reduced permeability in the *aqpZ* null mutant is in agreement with previous reports (41, 198, 199). However, absolute permeability values varied across reports (41, 198, 199) (Table 5.2). I found lower permeability values for NCM3105 compared to previous reports (198, 199). Permeability values were bounded by previously reported values for NCM3306 (stopped-flow 1). The mutations present in the strains tested should not impact permeability. The reasons for these inconsistencies in permeability phenotypes is unclear, but not unexpected, given previous variability and the variability I found using different stopped-flow instruments.

To investigate the effect of *aqpZ* on permeability despite differences in absolute permeability values, I compared the ratios of the *aqpZ* null and parent strains. I found that the ratios of permeability values between these strains also differed (Table 5.2). The *aqpZ* null mutant NCM3306 had 73% and 60% (stopped-flow 1 and 2, respectively) of NCM3105 permeability (Table 5.2). However, previous studies found ≤ 3% of NCM3105 permeability for NCM3306 (198, 199). The *aqpZ* null mutant JW0859 exhibited 86% and 145% of the permeability detected for

parent ME9062 (stopped-flow 1 and 2), whereas previous work in our lab found JW0859 to have 83% of the permeability of ME9062 (41). The reason for these differences has not been determined, but could reflect differences in stopped flow instruments or secondary mutations.

Table 5.2. Permeability values measured at neutral pH by investigator for parent NCM3105 and *aqpZ* null NCM3306, and parent ME9062 and *aqpZ* null JW0859
Pf denotes permeability.

Strain pair	P_f Parent (μm/s)	P_f Null (μm/s)	% P_f (null:parent)	Source
NCM3105 & NCM3306	2020.2 ± 50.5	63.1 ± 5.1	3.1	(198)
NCM3105 & NCM3306	691.4 ± 15.9	8.8 ± 0.2	1.3	(199)
NCM3105 & NCM3306	61.0 ± 2.6	44.6 ± 0.6	73.2	stopped-flow 1
NCM3105 & NCM3306	218.2 ± 18.6	130.0 ± 2.7	59.6	stopped-flow 2
ME9062 & JW0859	190 ± 5	157 ± 3	82.6	(41)
ME9062 & JW0859	42.3 ± 0.3	36.3 ± 0.3	85.7	stopped-flow 1
ME9062 & JW0859	128.8 ± 3.8	186.9 ± 3.9	145.0	stopped-flow 2

The results of the pH effect on permeability (Figure 5.3) were inconclusive. Several factors contribute to the ambiguity: data was collected from only one biological replicate, I observed differences between stopped flow instruments, and the salt concentrations during growth also differed between experiments. Based on previous work in our lab which found evidence of AqpZ closure under acidic conditions (41), I expected reduced permeability for all strains with *aqpZ* at pH 4.0 compared to their permeability at neutral pH. However, I did not observe that trend. Reasons for the different permeability responses to low pH is unexpected and unclear. It is possible that AqpZ is not fully closing at acidic pH. Increases in permeability, and any differences in permeability of *aqpZ* null mutants under acidic conditions is especially surprising. Testing additional replicates may allow trends to emerge. In addition, testing the permeability of an AqpZ mutant without the ability to close at low pH may provide insight on the closure capability of AqpZ. It is also possible that between biological replicates, differences arising from secondary mutations to rescue stressed cells could affect permeability or acid survival differently. In fact, NCM3105 was derived from MG1655 from the *E. coli* Genetic Stock Center (CGSC). MG1655 was found to exhibit more growth defects than expected based on its genotype (202). For example, MG1655 from CGSC grew slowly on galactose, and the supposed cross regulation of gene expression between the metabolism of galactose and lactose, and galactose and *N*-acetylglucosamine, was the result of fast growing mutants (15% of cells) with high levels of *lac*

expression. Stocks from other laboratories and stock centers were found to differ (202). These differences could result in variability between biological replicates and across strain backgrounds. Finally, redundancy in water transport mechanisms combined with these mutations might explain the lack of apparent necessity of AqpZ in bacteria.

Surprisingly, permeability was not only increased by increased presence of AqpZ, but also the induced overexpression plasmid pTrc10His conditions at neutral pH. While this data was from a single biological replicate, it suggests that the plasmid itself may have an effect at pH 4.0. The general impact of pTrc10His on permeability is unclear because of the conflicting findings between parent NCM3105 and *aqpZ* null NCM3306. No effect is observed in NCM3105, whereas the presence of the control plasmid increased permeability in NCM3306. The reason for this increase in permeability with the presence of a control plasmid is unclear. Because of these results, it is difficult to distinguish between the effect of the strain background and that of the plasmid. Based on the plasmid construction, no unintended gene expression should occur under induced conditions. Previous work did not compare strains with the overexpression and control plasmids to the *aqpZ* wild type JM109 strain (41).

In addition, *aqpZ* reduced cell survival under acid and simultaneous acid and osmotic shocks (Figure 5.6); the sole exception was NCM3105 pTrc10His1 under induced conditions. For both shock conditions, NCM3105 had reduced survival compared to *aqpZ* null NCM3306, and the induced AqpZ overexpression strain had reduced survival compared to its control. These findings are in agreement with previous work in our lab where more permeable strains had reduced survival under acid and combined acid and osmotic shocks (41). Specifically, the highly permeable overexpression strain JM109 pTrc10HisAqpZ (uninduced) had reduced survival compared to that of parent ME9062 and *aqpZ* null mutant JW0859 (41). However, in the previous work, survival of the control strain JM109 pTrc10His1 was not reported. Acidic conditions were critical in reducing survival since osmotic shock alone was not especially detrimental. Since the presence of AqpZ reduced survival under acidic conditions, this work demonstrates that AqpZ must provide an important benefit to *E. coli*.

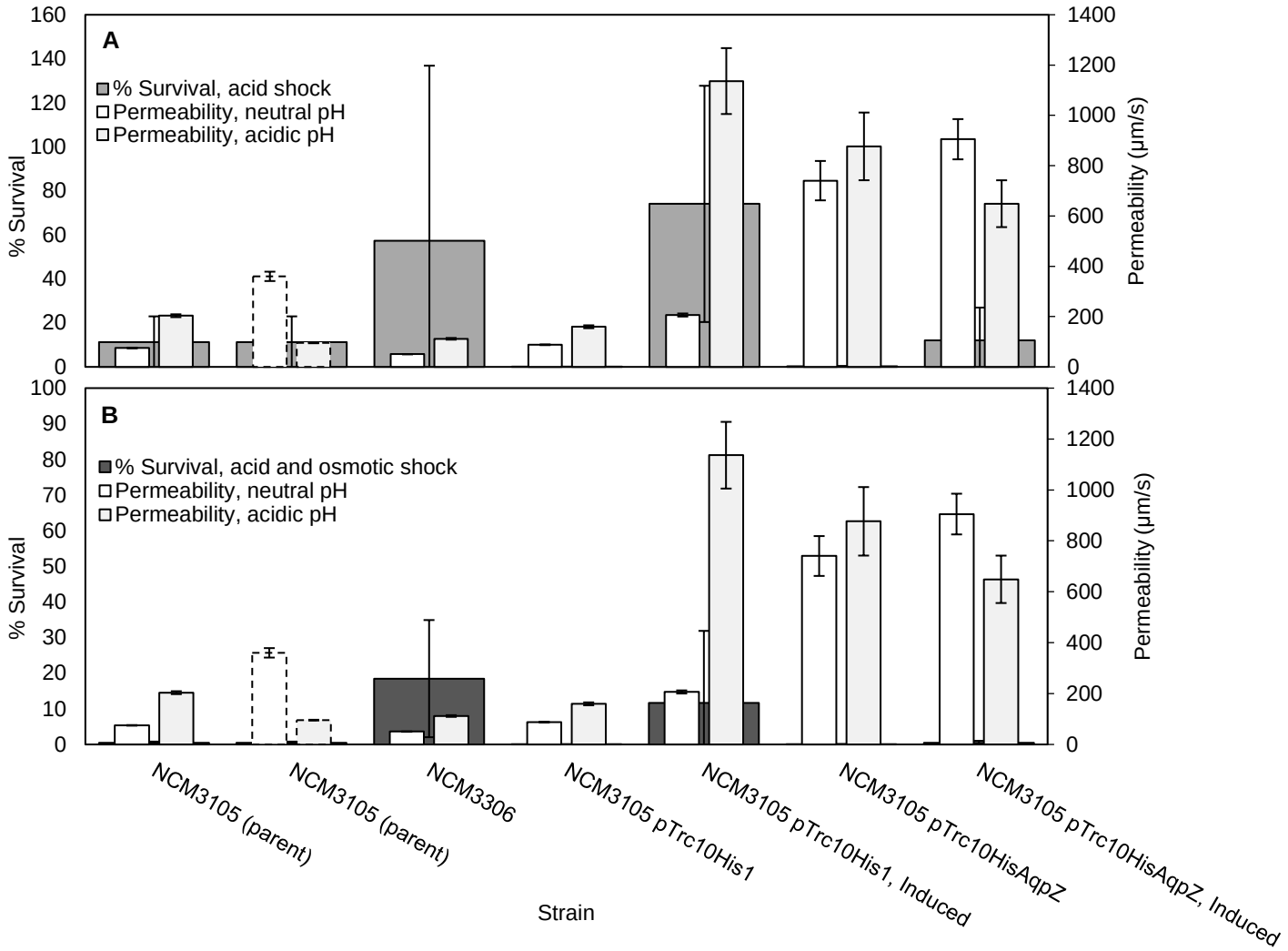

Figure 5.6. Comparison of survival and permeability
(A) % survival is survival under acid shock, and (B) % survival is under combined acid and osmotic shock. Note that the scales differ between the panels. Permeability data is identical between the panels. Survival data is presented for all strains. Dashed borders note use of stopped-flow 2, and ind denotes induction of the plasmid. All conditions and replicates are as noted in previous presentation of data.

5.6 Conclusions

- At neutral pH, *aqpZ* increased *E. coli* permeability compared to *aqpZ* null mutants. This behavior is due to AqpZ mediating water transport across the cell membrane in response to an osmotic gradient.

- Overall, *aqpZ* reduced *E. coli.* survival under acid and combined acid and osmotic shocks. This finding establishes that AqpZ must provide an important benefit to *E. coli*.

5.7 Acknowledgements

Support for this work was provided by the US National Science Foundation (CBET 08-28512 and CBET-1336620), and the Graduate Assistance in Areas of National Need (GAANN) and the University of Illinois SURGE fellowships. I thank Dr. Benito Marinas (Department of Civil and Environmental Engineering, University of Illinois) and Dr. Robert Gennis (Department of Civil and Environmental Engineering, University of Illinois) for use of their stopped-flow instruments, Dr. Sydney Kustu (Department of Plant and Microbial Biology, University of California, Berkeley) for providing the NCM3105 and NCM3306 strains for our use, Dr. Christopher Rao (Department of Chemical and Biomolecular Engineering, University of Illinois) and his research group for providing the wild-type P1 lysate, and Dr. Eric Reyes (Department of Mathematics, Rose-Hulman Institute of Technology) for helpful discussions about error propagation. Undergraduate research assistants Kenny Long and Joseph Chang (University of Illinois) conducted the survival experiments.

CHAPTER 6: CONCLUSIONS AND FUTURE DIRECTIONS

6.1 Conclusions

To investigate the relationship between protein insertion and membrane permeability, I developed a method utilizing FCS to quantify membrane proteins in an average vesicle. I found that membrane permeability was related to protein insertion. Additionally, DDM concentrations greater than 0.3% (w/v) substantially inhibited protein insertion. Insertion and permeability behavior varied by protein preparation for AqpZ. I suggest that the aggregation state of AqpZ may be responsible for this variation. These contributions provide a basis for optimizing membrane permeability for a variety of environmental applications.

To develop stable membranes with good insertion capability, I demonstrated that hybrid polymer-lipid vesicles could be synthesized. I found that these hybrid material vesicles exhibited characteristics of both lipid and polymer vesicles including surface or calcium-induced vesicle collapse – a lipid attribute – and low permeability to water – a polymer attribute. To develop planar membranes, I synthesized hydrophilic solid-supported planar hybrid lipid-polymer membranes. Increasing the ratio of polymer to lipid increased the polymer-mimicking behavior of the vesicles. The properties demonstrated for these hybrid vesicles are attractive for a variety of applications, including drug delivery and environmental remediation in vesicular form, and water purification or biosensors in the solid-supported planar form.

To characterize the effect of acidic conditions on AqpZ and investigate the physiological relevance of AqpZ, I demonstrated that in *E. coli*, presence of AqpZ increased cell permeability at neutral pH. This behavior is due to AqpZ allowing for rapid egress of water under an osmotic shock. Additionally, I found that the presence of AqpZ caused *E. coli* to be more susceptible, in terms of survival, to acid shock and simultaneous acid and osmotic shock. While the physiological

relevance of AqpZ is still unknown, this finding proves that AqpZ provides a benefit for *E. coli*. These findings contribute to understanding of the behavior of AqpZ under neutral and acidic pH conditions, which is important for development of AqpZ-based membranes.

6.2 Future directions

Hybrid protein-synthetic membranes have the potential to allow for development of new water sources by increasing membrane permeability without sacrificing selectivity. While several important questions were examined in this work, further work is needed before hybrid protein-synthetic membranes can be developed commercially. For water purification, remediation and sensing applications, a membrane must be highly permeable, but it also must be highly stable. Commercial membranes are routinely subjected to environmental and membrane cleaning stresses. Hybrid protein-synthetic membranes must also be able to withstand these operating stresses.

In this work I demonstrated that hybrid lipid-polymer membranes can form. Because they exhibit both lipid and polymer attributes, they are a promising platform for protein insertion in a more stable membrane environment. However, neither functional protein insertion nor membrane stability has been quantified for these systems. To optimize biomimetic membrane materials for both permeability and stability, it is crucial to know the relationship between protein insertion and membrane integrity. To achieve this goal, it is first necessary to quantify and optimize insertion efficiency in hybrid lipid-polymer membranes. Additionally, it is critical to quantify the effect of increasing protein insertion on membrane integrity over time and under membrane cleaning conditions. Investigation of these topics will elucidate factors controlling insertion and ultimately allow the engineer to optimize membrane permeability and stability.

In this work I also demonstrated that AqpZ is harming *E. coli* under acid and combined acid and osmotic shock by reducing survival under these conditions. Since the *aqpZ* gene has not been lost despite this negative impact means that it must have some benefit for *E. coli* under some condition. However, I additionally obtained conflicting results for the effect of *aqpZ* on the permeability of *E. coli* under acidic conditions and propose that AqpZ is only partially closing in acidic conditions. Investigation of the effect of pH on AqpZ permeability in a synthetic environment would allow

elucidation of the mechanism of AqpZ closure under acidic conditions, allowing for better design and implementation of AqpZ-based membranes.

Insertion efficiency of membrane proteins

Highly-permeable, selective, and stable membranes are needed for environmental applications. In this work, I demonstrated that planar, hybrid lipid-polymer membranes can be formed that exhibit advantageous attributes of both lipid and polymer. Functional protein insertion efficiency has not been quantified in hybrid lipid-polymer membranes. Additionally in this work, I discovered that AqpZ multimer state appeared to affect insertion and thus permeability in lipid vesicles. Development of both selective and highly-permeable membranes demands high protein insertion, requiring investigation into the impact of AqpZ multimer state on insertion.

i. Quantify AqpZ insertion in hybrid lipid-polymer membranes

Protein insertion efficiency and the relationship between insertion and permeability in hybrid lipid-polymer membranes should be assessed by measuring AqpZ insertion and the resulting membrane permeability. Because AqpZ insertion has been demonstrated in both lipid and polymer membranes, I hypothesize that AqpZ should functionally insert in hybrid membranes. I hypothesize that the permeability of hybrid vesicles will depend on AqpZ insertion as demonstrated in chapter 3. The permeability of these membranes could be measured using stopped flow light scattering (vesicles) as reported in this work, or using the forward or reverse osmosis setups (planar membranes) as previously reported (46, 63). Finally, to quantify insertion and the relationship between insertion and permeability, the resolubilization FCS method reported previously (47) could be modified for planar membranes.

In this approach, the brightness of vesicles would be measured using FCS and then a sample would be resolubilized to measure the brightness of the resolubilized protein (47). After vesicle collapse to form the planar membranes, the planar membrane would also be resolubilized to measure the brightness of the resolubilized protein from the planar membrane. If the number of proteins measured from the resolubilized planar member is less than the number from the resolubilized

vesicles, then the insertion was less in the planar membrane. If the number is similar, then insertion was similar.

ii. Quantify the effect of AqpZ multimer state on insertion and permeability

The multimer state of AqpZ should be assessed using native (non-denaturing) gel electrophoresis and compared to insertion and membrane permeability measurements. Although it is unclear why, in this work, I found that AqpZ that appeared to exist in higher multimer states inserted more efficiently at high protein to membrane material ratios, and thus produced more permeable membranes. As my data suggested, I hypothesize that aggregated AqpZ will more readily insert at high molar ratios. Native polyacrylamide gel electrophoresis can be used to analyze unlabeled AqpZ, or high resolution clear native electrophoresis can be used to analyze fluorescently-labeled AqpZ (206, 207). Native, or non-denaturing, gel electropohoresis is run in the absence of SDS and can allow for examination of protein multimer state. Careful observations regarding culture growth, AqpZ purification, yield, and storage should also be made to investigate factors that could affect AqpZ aggregation. Understanding these factors would allow for more precise control over AqpZ-membrane synthesis, allowing the engineer to optimize insertion and thus, membrane permeability.

Characterize the membrane integrity of AqpZ-based vesicles

To be useful, hybrid protein-synthetic membranes must be able to withstand environmental and membrane cleaning conditions. In this work, I investigated the behavior of AqpZ in *E. coli* under various stress conditions, but it is necessary to know the behavior of the assembled membrane system when exposed to these stress conditions. In addition, as membrane permeability is optimized, the tradeoff between membrane permeability and stability is necessary. I expect that membrane integrity will decrease with increasing protein insertion. With varying amounts of AqpZ inserted in hybrid lipid-polymer membranes, membrane integrity should be quantified in several ways: membrane selectivity, leakage, and elasticity. By modifying the protein insertion quantification methods developed in this and other work (47), AqpZ insertion can be measured using FCS.

i. Monitor the selectivity of vesicles over time

The temporal stability of AqpZ-containing vesicles should be quantified by measuring changes in vesicle selectivity and ion rejection over time. Hybrid lipid-polymer vesicles with varying ratios of AqpZ can be subjected to osmotic solutes (NaCl, Na_2SO_4, $MgCl_2$ and glucose). Glucose can be assumed to have a reflection coefficient of 1.0 and serve as the reference solute. Reflection coefficients for the other solutes can quantify selectivity and ion rejection properties of the various vesicle preparations. In addition, vesicles should be tested under conditions typical for cleaning reverse osmosis membranes such as acid (0.2 wt% HCl, pH 2) and base (0.1 wt% NaOH, pH 12) conditions and in the presence of 0.1 mg/L free chlorine (208). These experiments would allow quantification of membrane integrity by comparing changes in selectivity with insertion over time.

ii. Monitor the leakage rate of AqpZ/lipid vesicles with varying AqpZ insertion

Membrane integrity should be assessed by measuring the leak-in rate of fluorescent markers through AqpZ/lipid vesicles. Fluorescence leakage is routinely used to measure membrane integrity by measuring the dequenching, or the reduction in the fluorescence intensity, of encapsulated fluorescent markers using fluorimetry (209). I propose monitoring the leak-in rate (34) from exposure to the fluorescent marker calcein. Previous work has demonstrated calcein leak-out and leak-in through lipid vesicle membranes at measurable rates (34, 210-212). A proposed experimental plan would involve adding 60 mM calcein at a ratio of 2:1 by volume to AqpZ/lipid vesicles (34). At weekly intervals for up to 3 months, aliquots would be size excluded, and after immediate treatment with 1% Triton X-100, fluorescence would be measured using a fluorescence microplate reader (34, 210-212).

iii. Measure the elasticity of vesicles and planar membranes with varying AqpZ insertion

Mechanical properties of vesicle membranes, such as elasticity and bending rigidity, determine vesicle structure and interaction behaviors, including membrane fusion and adhesion (213-215). Previous results demonstrate that gramicidin-AC2-containing lipid vesicles were more rigid than pure lipid vesicles when probed using atomic force microscopy (AFM) (216). As such, I hypothesize that membranes with the highest AqpZ insertion would display the least membrane

elasticity. AFM can directly evaluate these mechanical properties (213-215). In this approach, the sample surface is probed by a sharp tip at the end of a cantilever to measure deviations in heights and surface properties at the atomic scale (215, 217, 218). AFM liquid tapping mode (219) should be optimized for imaging vesicles. Specifically, Young's Modulus should be compared across vesicles with varying AqpZ insertion to assess the elastic properties as a function of AqpZ insertion. To obtain these data, the initial slope of the approach force curve measured with AFM would be fit to the Hertz model (220) or the Shell model (213) using the force-distance plot method as described in Mao et al. (220). Force-distance measurements should also be obtained for planar membranes to evaluate the relationship between membrane elasticity and protein insertion in the planar membrane configuration as well.

Investigate the behavior of AqpZ under acidic conditions

In water treatment, AqpZ-based membranes would be exposed to environmental and membrane cleaning conditions, including acidic conditions. Understanding the potential closure mechanism of AqpZ would allow suitable applications and membrane cleaning procedures to be identified. In this work, I investigated the behavior of AqpZ in *E. coli* under acidic and osmotic shock where I found that *aqpZ* reduced *E. coli* survival. However, I found the effect of pH on permeability to be inconclusive. Previous research in our lab suggested that AqpZ closed at low pH conditions (41). However, based on my findings, I hypothesize that AqpZ remains partially open at low pH. While this work focused on investigating the impact of *aqpZ* in *E. coli*, the function of AqpZ in a synthetic environment is important from a water treatment perspective and should be investigated. Additionally, use of a synthetic environment would eliminate the possibility of other transport proteins interfering with permeability measurements under different conditions.

To determine the ability of AqpZ to close at low pH, the permeability of vesicles containing an AqpZ mutant that remains open at low pH should be compared to the permeability of vesicles containing the wildtype AqpZ. Site-directed mutagenesis could be used to modify amino acids to identify the residues involved in the potential gating mechanism. Residues sensitive to pH and important for proposed gating in mammalian and plant aquaporins include histidine, tyrosine, serine and leucine (221-225). Due to its basic side chain at neutral pH, histidine may be involved

in the potential AqpZ gating mechanism under acidic pH conditions. Additionally, using the FCS method I developed, AqpZ insertion could be quantified and the permeability per AqpZ monomer calculated for the AqpZ mutant and wildtype under acidic conditions. Elucidating the behavior of AqpZ under acidic conditions will further development of biomimetic membranes for water treatment.

REFERENCES

1. Jackson RB, Carpenter SR, Dahm CN, McKnight DM, Naiman RJ, Postel SL, et al. Water in a changing world. Ecological Applications. 2001;11(4):1027-45.
2. Harrison P. AAAS atlas of population & environment. Berkeley: University of California Press; 2000. 204 p.
3. Hightower M, Pierce SA. The energy challenge. Nature. 2008;452(7185):285-6.
4. Matsura T. Progress in membreane science and technology for desalination - a review. Desalination. 2001;134:47-54.
5. Bohdziewicz J, Bodzek M, Wąsik E. The application of reverse osmosis and nanofiltration to the removal of nitrates from groundwater. Desalination. 1999;121(2):139-47.
6. Judd S. The MBR book: principles and applications of membrane bioreactors for water and wastewater treatment: Elsevier; 2006.
7. Del Pino MP, Durham B. Wastewater reuse through dual-membrane processes: Opportunities for sustainable water resources. Desalination. 1999;124(1-3):271-7.
8. Goldstein J. Sustainable water supplies with wastewater recycling. BioCycle. 2006;47(1):24-5.
9. Kimura K, Amy G, Drewes JE, Heberer T, Kim TU, Watanabe Y. Rejection of organic micropollutants (disinfection by-products, endocrine disrupting compounds, and pharmaceutically active compounds) by NF/RO membranes. Journal of Membrane Science. 2003;227(1-2):113-21.
10. Koplin DW, Furlong ET, Meyer MT, Thurman EM, Zaugg SD, Barber LB, et al. Response to comment on "pharmaceuticals, hormones, and other organic wastewater contaminants in US streams, 1999-2000: a national reconnaissance". Environmental Science & Technology. 2002;36(18):4004-.
11. Buchanan JR, Mote CR, Robinson RB. Thermodynamics of struvite formation. Transactions of the American Society of Agricultural Engineers. 1994;37(2):617-21.
12. Pearce GK. UF/MF pre-treatment to RO in seawater and wastewater reuse applications: a comparison of energy costs. Desalination. 2008;222(1-3):66-73.
13. Agency UEP. Drinking water contaminant candidate list 3 - final. USEPA. 2009.
14. Fritzmann C, Löwenberg J, Wintgens T, Melin T. State-of-the-art of reverse osmosis desalination. Desalination. 2007;216(1-3):1-76.
15. Elimelech M, Phillip WA. The future of seawater desalination: energy, technology, and the environment. Science. 2011;333(6043):712-7.
16. Kumar M, Grzelakowski M, Zilles J, Clark M, Meier W. Highly permeable polymeric membranes based on the incorporation of the functional water channel protein Aquaporin Z. Proceedings of the National Academy of Sciences of the United States of America. 2007;104(52):20719-24.
17. Grzelakowski M, Cherenet MF, Shen Y-x, Kumar M. A framework for accurate evaluation of the promise of aquaporin based biomimetic membranes. Journal of Membrane Science. 2015;479:223-31.

18. Nardin C, Thoeni S, Widmer J, Winterhalter M, Meier W. Nanoreactors based on (polymerized) ABA-triblock copolymer vesicles. Chemical Communications. 2000(15):1433-4.
19. Nardin C, Meier W. Hybrid materials from amphiphilic block copolymers and membrane proteins. Reviews in Molecular Biotechnology. 2002;90(1):17-26.
20. Axthelm F, Casse O, Koppenol WH, Nauser T, Meier W, Palivan CG. Antioxidant nanoreactor based on superoxide dismutase encapsulated in superoxide-permeable vesicles. Journal of Physical Chemistry B. 2008;112(28):8211-7.
21. Winterhalter M, Hilty C, Bezrukov SM, Nardin C, Meier W, Fournier D. Controlling membrane permeability with bacterial porins: Application to encapsulated enzymes. Talanta. 2001;55(5):965-71.
22. Coates JD, Achenbach LA. Microbial perchlorate reduction: rocket-fuelled metabolism. Nature Reviews Microbiology. 2004;2(7):569-80.
23. Hutchison JM, Poust SK, Kumar M, Cropek DM, MacAllister IE, Arnett CM, et al. Perchlorate reduction using free and encapsulated *Azospira oryzae* enzymes. Environmental Science & Technology. 2013;47(17):9934-41.
24. Alshawabkeh AN. Electrokinetic soil remediation: challenges and opportunities. Separation Science and Technology. 2009;44(10):2171-87.
25. Zhu Y, Fan L, Yang B, Du J. Multifunctional homopolymer vesicles for facile immobilization of gold nanoparticles and effective water remediation. ACS Nano. 2014;8(5):5022-31.
26. Braha O, Gu L-Q, Zhou L, Lu X, Cheley S, Bayley H. Simultaneous stochastic sensing of divalent metal ions. Nat Biotech. 2000;18(9):1005-7.
27. Braha O, Walker B, Cheley S, Kasianowicz JJ, Song L, Gouaux JE, et al. Designed protein pores as components for biosensors. Chemistry and Biology. 1997;4(7):497-505.
28. Wong D, Jeon TJ, Schmidt J. Single molecule measurements of channel proteins incorporated into biomimetic polymer membranes. Nanotechnology. 2006;17(15):3710-7.
29. Nielsen C. Biomimetic membranes for sensor and separation applications. Anal Bioanal Chem. 2009;395(3):697-718.
30. Minami H, Sugawara M, Odashima K, Umezawa Y, Uto M, Michaelis EK, et al. Ion channel sensors for glutamic acid. Analytical Chemistry. 1991;63(23):2787-95.
31. Separovic F, Cornell B. Gated ion channel-based biosensor device. In: Chung S-H, Andersen O, Krishnamurthy V, editors. Biological Membrane Ion Channels: Springer New York; 2007. p. 595-621.
32. Discher BM, Won YY, Ege DS, Lee JCM, Bates FS, Discher DE, et al. Polymersomes: Tough vesicles made from diblock copolymers. Science. 1999;284(5417):1143-6.
33. González-Pérez A, Stibius KB, Vissing T, Nielsen CH, Mouritsen OG. Biomimetic triblock copolymer membrane arrays: a stable template for functional membrane proteins. Langmuir. 2009;25(18):10447-50.
34. Grit M, Crommelin DJA. Chemical stability of liposomes: implications for their physical stability. Chemistry and Physics of Lipids. 1993;64(1-3):3-18.
35. Richter R, Mukhopadhyay A, Brisson A. Pathways of lipid vesicle deposition on solid surfaces: a combined QCM-D and AFM study. Biophysical journal. 2003;85(5):3035-47. Epub 2003/10/29.
36. Reimhult E, Höök F, Kasemo B. Vesicle adsorption on SiO_2 and TiO_2: dependence on vesicle size. Journal of Chemical Physics. 2002;117(16):7401.

37. Belegrinou S, Dorn J, Kreiter M, Kita-Tokarczyk K, Sinner EK, Meier W. Biomimetic Supported Membranes from Amphiphilic Block Copolymers. Soft Matter. 2010;6(1):179-86.
38. Ho D, Chu B, Lee H, Montemagno CD. Protein-driven energy transduction across polymeric biomembranes. Nanotechnology. 2004;15(8):1084-94.
39. Kita-Tokarczyk K, Itel F, Grzelakowski M, Egii S, Rossbach P, Meier W. Monolayer interactions between lipids and amphiphilic block copolymers. Langmuir. 2009;25(17):9847-56.
40. Rakhmatullina E, Meier W. Solid-supported block copolymer membranes through interfacial adsorption of charged block copolymer vesicles. Langmuir. 2008;24(12):6254-61.
41. Kumar M. Biomimetic membranes as new materials for applications in environmental engineering and biology: University of Illinois at Urbana-Champaign; 2010.
42. Calamita G, Bishai WR, Preston GM, Guggino WB, Agre P. Molecular cloning and characterization of AqpZ, a water channel from *Escherichia coli*. Journal of Biological Chemistry. 1995;270(49):29063-6.
43. Borgnia MJ, Kozono D, Calamita G, Maloney PC, Agre P. Functional reconstitution and characterization of AqpZ, the *E. coli* water channel protein. Journal of Molecular Biology. 1999;291(5):1169-79.
44. Zhong PS, Chung T-S, Jeyaseelan K, Armugam A. Aquaporin-embedded biomimetic membranes for nanofiltration. Journal of Membrane Science. 2012;407:27-33.
45. Wang H, Chung T-S, Tong YW, Jeyaseelan K, Armugam A, Chen Z, et al. Highly permeable and selective pore-spanning biomimetic membrane embedded with aquaporin Z. Small. 2012;8(8):1185-90.
46. Wang HL, Chung TS, Tong YW, Meier W, Chen ZC, Hong MH, et al. Preparation and characterization of pore-suspending biomimetic membranes embedded with Aquaporin Z on carboxylated polyethylene glycol polymer cushion. Soft Matter. 2011;7(16):7274-80.
47. Erbakan M, Shen Y-x, Grzelakowski M, Butler PJ, Kumar M, Curtis WR. Molecular cloning, overexpression and characterization of a novel water channel protein from *Rhodobacter sphaeroides*. PLoS ONE. 2014;9(1):e86830.
48. Nakae T. Outer membrane of *Salmonella*: isolation of protein complex that produces transmembrane channels. Journal of Biological Chemistry. 1976;251(7):2176-8.
49. Benz R. Structure and function of porins from gram-negative bacteria. Annual Reviews in Microbiology. 1988;42(1):359-93.
50. Nikaido H, Nakae T. The outer membrane of gram-negative bacteria. Advances in Microbial Physiology. 1980;20:163-250.
51. Tanner P, Baumann P, Enea R, Onaca O, Palivan C, Meier W. Polymeric vesicles: from drug carriers to nanoreactors and artificial organelles. Accounts of Chemical Research. 2011;44(10):1039-49.
52. Tanner P, Onaca O, Balasubramanian V, Meier W, Palivan CG. Enzymatic cascade reactions inside polymeric nanocontainers: a means to combat oxidative stress. Chemistry – A European Journal. 2011;17(16):4552-60.
53. Renggli K, Baumann P, Langowska K, Onaca O, Bruns N, Meier W. Selective and responsive nanoreactors. Advanced Functional Materials. 2011;21(7):1241-59.
54. Nardin C, Widmer J, Winterhalter M, Meier W. Amphiphilic block copolymer nanocontainers as bioreactors. European Physical Journal E. 2001;4(4):403-10.

55. Grzelakowski M, Onaca O, Rigler P, Kumar M, Meier W. Immobilized protein-polymer nanoreactors. Small. 2009;5(22):2545-8.
56. Klara SS, Saboe PO, Sines IT, Babaei M, Chiu P-L, DeZorzi R, et al. Magnetically directed two-dimensional crystallization of OmpF membrane proteins in block copolymers. Journal of the American Chemical Society. 2016;138(1):28-31.
57. Shen Y-x, Saboe PO, Sines IT, Erbakan M, Kumar M. Biomimetic membranes: a review. Journal of Membrane Science. 2014;454:359-81.
58. Licsandru E, Kocsis I, Shen Y-x, Murail S, Legrand Y-M, van der Lee A, et al. Salt-excluding artificial water channels exhibiting enhanced dipolar water and proton translocation. Journal of the American Chemical Society. 2016;138(16):5403-9.
59. Pohl P, Saparov SM, Borgnia MJ, Agre P. Highly selective water channel activity measured by voltage clamp: analysis of planar lipid bilayers reconstituted with purified AqpZ. Proceedings of the National Academy of Sciences. 2001;98(17):9624-9.
60. Li X, Wang R, Tang C, Vararattanavech A, Zhao Y, Torres J, et al. Preparation of supported lipid membranes for aquaporin Z incorporation. Colloids and Surfaces B: Biointerfaces. 2012;94(0):333-40.
61. Sun G, Chung T-S, Jeyaseelan K, Armugam A. Stabilization and immobilization of aquaporin reconstituted lipid vesicles for water purification. Colloids and Surfaces B: Biointerfaces. 2013;102(0):466-71.
62. Wang HL, Chung TS, Tong YW, Jeyaseelan K, Armugam A, Chen ZC, et al. Highly Permeable and Selective Pore-Spanning Biomimetic Membrane Embedded with Aquaporin Z. Small. 2012;8(8):1185-90.
63. Zhao Y, Qiu C, Li X, Vararattanavech A, Shen W, Torres J, et al. Synthesis of robust and high-performance aquaporin-based biomimetic membranes by interfacial polymerization-membrane preparation and RO performance characterization. Journal of Membrane Science. 2012;423–424(0):422-8.
64. Pata V, Dan N. The effect of chain length on protein solubilization in polymer-based vesicles (polymersomes). Biophysical Journal. 2003;85(4):2111-8.
65. Ho D, Chang S, Montemagno CD. Fabrication of biofunctional nanomaterials via *Escherichia coli* OmpF protein air/water interface insertion/integration with copolymeric amphiphiles. Nanomedicine: Nanotechnology, Biology and Medicine. 2006;2(2):103-12.
66. Kumar M, Habel JEO, Shen Y-x, Meier WP, Walz T. High-density reconstitution of functional water channels into vesicular and planar block copolymer membranes. Journal of the American Chemical Society. 2012;134(45):18631-7.
67. Killian JA. Hydrophobic mismatch between proteins and lipids in membranes. Biochimica Et Biophysica Acta-Reviews on Biomembranes. 1998;1376(3):401-16.
68. Dumas F, Lebrun MC, Tocanne J-F. Is the protein/lipid hydrophobic matching principle relevant to membrane organization and functions? FEBS Letters. 1999;458(3):271-7.
69. Bloom ME, Evan; Mouritsen, Ole G. . Physical properties of the fluid lipid-bilayer component of cell membranes: a perspective. Q Rev Biophys. 1991;24(3):293-397.
70. Mouritsen OG, Biltonen RL. Chapter 1: protein-lipid interactions and membrane heterogeneity. New Comprehensive Biochemistry. 1993;25:1-39.
71. Gil T, Ipsen JH, Mouritsen OG, Sabra MC, Sperotto MM, Zuckermann MJ. Theoretical analysis of protein organization in lipid membranes. Biochimica et Biophysica Acta (BBA) - Reviews on Biomembranes. 1998;1376(3):245-66.

72. Srinivas G, Discher DE, Klein ML. Key roles for chain flexibility in block copolymer membranes that contain pores or make tubes. Nano Letters. 2005;5(12):2343-9.
73. Kita-Tokarczyk K, Grumelard J, Haefele T, Meier W. Block copolymer vesicles - using concepts from polymer chemistry to mimic biomembranes. Polymer. 2005;46(11):3540-63.
74. Privé GG. Detergents for the stabilization and crystallization of membrane proteins. Methods. 2007;41(4):388-97.
75. Seddon AM, Curnow P, Booth PJ. Membrane proteins, lipids and detergents: not just a soap opera. Biochimica et Biophysica Acta (BBA) - Biomembranes. 2004;1666(1–2):105-17.
76. Hasler L, Heymann JB, Engel A, Kistler J, Walz T. 2D crystallization of membrane proteins: rationales and examples. Journal of Structural Biology. 1998;121(2):162-71.
77. Raunser S, Walz T. Electron crystallography as a technique to study the structure on membrane proteins in a lipidic environment. Annual Review of Biophysics. 2009;38(1):89-105.
78. Hite RK, Raunser S, Walz T. Revival of electron crystallography. Current Opinion in Structural Biology. 2007;17(4):389-95.
79. Dolder M, Engel A, Zulauf M. The micelle to vesicle transition of lipids and detergents in the presence of a membrane protein: towards a rationale for 2D crystallization. FEBS Letters. 1996;382(1):203-8.
80. Montal M, Mueller P. Formation of bimolecular membranes from lipid monolayers and a study of their electrical properties. Proceedings of the National Academy of Sciences. 1972;69(12):3561-6.
81. Chandrawati R, Caruso F. Biomimetic liposome- and polymersome-based multicompartmentalized assemblies. Langmuir. 2012;28(39):13798-807.
82. Ho D, Chu B, Schmidt JJ, Brooks EK, Montemagno CD. Hybrid protein-polymer biomimetic membranes. IEEE Transactions on Nanotechnology. 2004;3(2):256-63.
83. Graff A, Winterhalter M, Meier W. Nanoreactors from polymer-stabilized liposomes. Langmuir. 2001;17(3):919-23.
84. Kaur L, Kaur P, Khan M. Liposome as a drug carrier—a review. IJRPC. 2013;3:121-8.
85. Akbarzadeh A, Rezaei-Sadabady R, Davaran S, Joo SW, Zarghami N, Hanifehpour Y, et al. Liposome: classification, preparation, and applications. Nanoscale Res Lett [Internet]. 2013 2013; 8(1):[102 p.]. Available from: http://europepmc.org/abstract/MED/23432972
http://europepmc.org/articles/PMC3599573?pdf=render
http://europepmc.org/articles/PMC3599573
http://www.pubmedcentral.nih.gov/picrender.fcgi?tool=EBI&pubmedid=23432972&action=stream&blobtype=pdf
http://www.pubmedcentral.nih.gov/articlerender.fcgi?tool=EBI&pubmedid=23432972
https://doi.org/10.1186/1556-276X-8-102.
86. Graff A, Fraysse-Ailhas C, Palivan CG, Grzelakowski M, Friedrich T, Vebert C, et al. Amphiphilic copolymer membranes promote nadh: ubiquinone oxidoreductase activity: towards an electron-transfer nanodevice. Macromolecular Chemistry and Physics. 2010;211(2):229-38.
87. Cruz A, Pérez-Gil J. Langmuir films to determine lateral surfacepressure on lipid segregation. In: Dopico AM, editor. Methods in Membrane Lipids. Totowa, NJ: Humana Press; 2007. p. 439-57.
88. Mueller P, Rudin DO, Ti Tien H, Wescott WC. Reconstitution of cell membrane structure in vitro and its transformation into an excitable system. Nature. 1962;194(4832):979-80.

89. Hansen JS, Perry M, Vogel J, Groth JS, Vissing T, Larsen MS, et al. Large scale biomimetic membrane arrays. Anal Bioanal Chem. 2009;395(3):719-27.
90. Hansen JS, Perry M, Vogel J, Vissing T, Hansen CR, Geschke O, et al. Development of an automation technique for the establishment of functional lipid bilayer arrays. Journal of Micromechanics and Microengineering. 2009;19(2).
91. Castellana ET, Cremer PS. Solid supported lipid bilayers: from biophysical studies to sensor design. Surface Science Reports. 2006;61(10):429-44.
92. Roerdink Lander M, Ibragimova S, Rein C, Vogel J, Stibius K, Geschke O, et al. Biomimetic membrane arrays on cast hydrogel supports. Langmuir. 2011;27(11):7002-7.
93. Ibragimova S, Stibius K, Szewczykowski P, Perry M, Bohr H, Hélix-Nielsen C. Hydrogels for in situ encapsulation of biomimetic membrane arrays. Polymers for Advanced Technologies. 2012;23(2):182-9.
94. McConnell HM, Watts TH, Weis RM, Brian AA. Supported planar membranes in studies of cell-cell recognition in the immune system. Biochimica et Biophysica Acta (BBA) - Reviews on Biomembranes. 1986;864(1):95-106.
95. Watts TH, Brian AA, Kappler JW, Marrack P, McConnell HM. Antigen presentation by supported planar membranes containing affinity-purified I-Ad. Proceedings of the National Academy of Sciences. 1984;81(23):7564-8.
96. Reviakine I, Brisson A. Formation of supported phospholipid bilayers from unilamellar vesicles investigated by atomic force microscopy. Langmuir. 2000;16(4):1806-15.
97. Reimhult E, Höök F, Kasemo B. Intact vesicle adsorption and supported biomembrane formation from vesicles in solution: Influence of surface chemistry, vesicle size, temperature, and osmotic pressure. Langmuir. 2003;19(5):1681-91.
98. Reimhult E, Höök F, Kasemo B. Intact vesicle adsorption and supported biomembrane formation from vesicles in solution: influence of surface chemistry, vesicle size, temperature, and osmotic pressure. Langmuir. 2003;19(5):1681-91.
99. Stelzle M, Weissmüller G, Sackmann E. On the application of supported bilayers as receptive layers for biosensors with electrical detection. The Journal of Physical Chemistry. 1993;97(12):2974-81.
100. Richter RP, Brisson AR. Following the formation of supported lipid bilayers on mica: a study combining AFM, QCM-D, and ellipsometry. Biophysical journal. 2005;88(5):3422-33. Epub 2005/02/26.
101. Schönherr H, Johnson JM, Lenz P, Frank CW, Boxer SG. Vesicle adsorption and lipid bilayer formation on glass studied by atomic force microscopy. Langmuir. 2004;20(26):11600-6.
102. King LS, Kozono D, Agre P. From structure to disease: the evolving tale of aquaporin biology. Nat Rev Mol Cell Biol. 2004;5(9):687-98.
103. Agre P. Aquaporin water channels (Nobel lecture). Angewandte Chemie International Edition. 2004;43(33):4278-90.
104. Murata K, Mitsuoka K, Hirai T, Walz T, Agre P, Heymann JB, et al. Structural determinants of water permeation through aquaporin-1. Nature. 2000;407(6804):599-605.
105. Agre P, Kozono D. Aquaporin water channels: molecular mechanisms for human diseases1. FEBS Letters. 2003;555(1):72-8.
106. Tanghe A, Van Dijck P, Thevelein JM. Why do microorganisms have aquaporins? Trends in Microbiology. 2006;14(2):78-85.

107. Zardoya R. Phylogeny and evolution of the major intrinsic protein family. Biology of the Cell. 2005;97(6):397-414.
108. Soupene E, King N, Lee H, Kustu S. Aquaporin Z of *Escherichia coli*: reassessment of its regulation and physiological role. Journal of Bacteriology. 2002;184(15):4304-7.
109. Calamita G, Kempf B, Bonhivers M, Bishai WR, Bremer E, Agre P. Regulation of the *Escherichia coli* water channel gene *aqpZ*. Proceedings of the National Academy of Sciences of the United States of America. 1998;95(7):3627-31.
110. Hernández-Castro R, Rodríguez MC, Seoane A, García Lobo JM. The aquaporin gene aqpX of Brucella abortus is induced in hyperosmotic conditions. Microbiology. 2003;149(11):3185-92.
111. Calamita G. The *Escherichia coli* aquaporin-Z water channel. Molecular Microbiology. 2000;37(2):254-62.
112. Cowan SW, Schirmer T, Rummel G, Steiert M, Ghosh R, Pauptit RA, et al. Crystal structures explain functional properties of two *E. coli* porins. Nature. 1992;358(6389):727-33.
113. Koebnik R, Locher KP, Van Gelder P. Structure and function of bacterial outer membrane proteins: barrels in a nutshell. Molecular Microbiology. 2000;37(2):239-53.
114. Nikaido H, Rosenberg EY. Porin channels in *Escherichia coli*: studies with liposomes reconstituted from purified proteins. Journal of Bacteriology. 1983;153(1):241-52.
115. Csonka LN. Physiological and genetic responses of bacteria to osmotic stress. Microbiological Reviews. 1989;53(1):121-47.
116. Csonka LN, Hanson AD. Prokaryotic osmoregulation: genetics and physiology. Annual Reviews in Microbiology. 1991;45(1):569-606.
117. Ding J, Liu G. Water-soluble hollow nanospheres as potential drug carriers. Journal of Physical Chemistry B. 1998;102(31):6107-13.
118. Poust SK. Engineered vesicles for perchlorate degradation. Urbana, IL: University of Illinois at Urbana-Champaign; 2010.
119. Eray M, Dogan NS, Reiken SR, Sutisna H, Van Wie BJ, Koch AR, et al. A highly stable and selective biosensor using modified nicotinic acetylcholine receptor (nAChR). Biosystems. 1995;35(2–3):183-8.
120. Discher DE, Eisenberg A. Polymer vesicles. Science. 2002;297(5583):967-73.
121. Wang HL, Chung TS, Tong YW, Jeyaseelan K, Armugam A, Chen ZC, et al. Highly Permeable and Selective Pore-Spanning Biomimetic Membrane Embedded with Aquaporin Z (vol 8, pg 1185, 2012). Small. 2012;8(13):1969-.
122. Choi HJ, Germain J, Montemagno CD. Effects of different reconstitution procedures on membrane protein activities in proteopolymersomes. Nanotechnology. 2006;17(8):1825-30.
123. Bacia K, Haustein E, Schwille P. Fluorescence correlation spectroscopy: principles and applications. Cold Spring Harbor Protocols. 2014;2014(7):pdb.top081802.
124. Thompson NL. Fluorescence correlation spectroscopy. In: Lakowicz JR, editor. Topics in Fluorescence Spectroscopy: Techniques. Boston, MA: Springer US; 1999. p. 337-78.
125. Elson EL, Magde D. Fluorescence correlation spectroscopy: conceptual basis and theory. Biopolymers. 1974;13(1):1-27.
126. Ries J, Schwille P. Fluorescence correlation spectroscopy. BioEssays. 2012;34(5):361-8.
127. Magde D, Elson EL, Webb WW. Fluorescence correlation spectroscopy. II. An experimental realization. Biopolymers. 1974;13(1):29-61.

128. Oleg K, Grégoire B. Fluorescence correlation spectroscopy: the technique and its applications. Reports on Progress in Physics. 2002;65(2):251.
129. Hess ST, Huang S, Heikal AA, Webb WW. Biological and chemical applications of fluorescence correlation spectroscopy: a review. Biochemistry. 2002;41(3):697-705.
130. Rigler P, Meier W. Encapsulation of fluorescent molecules by functionalized polymeric nanocontainers: Investigation by confocal fluorescence imaging and fluorescence correlation spectroscopy. Journal of the American Chemical Society. 2006;128(1):367-73.
131. Cabane E, Malinova V, Menon S, Palivan CG, Meier W. Photoresponsive polymersomes as smart, triggerable nanocarriers. Soft Matter. 2011;7(19):9167-76.
132. Egli S, Nussbaumer MG, Balasubramanian V, Chami M, Bruns N, Palivan C, et al. Biocompatible functionalization of polymersome surfaces: a new approach to surface immobilization and cell targeting using polymersomes. Journal of the American Chemical Society. 2011;133(12):4476-83.
133. Itel F, Chami M, Najer A, Lörcher S, Wu D, Dinu IA, et al. Molecular organization and dynamics in polymersome membranes: a lateral diffusion study. Macromolecules. 2014;47(21):7588-96.
134. Onaca O, Hughes DW, Balasubramanian V, Grzelakowski M, Meier W, Palivan CG. SOD antioxidant nanoreactors: influence of block copolymer composition on the nanoreactor efficiency. Macromolecular Bioscience. 2010;10(5):531-8.
135. Erokhova L, Horner A, Kügler P, Pohl P. Monitoring single-channel water permeability in polarized cells. Journal of Biological Chemistry. 2011;286(46):39926-32.
136. Hoomann T, Jahnke N, Horner A, Keller S, Pohl P. Filter gate closure inhibits ion but not water transport through potassium channels. Proceedings of the National Academy of Sciences. 2013.
137. Knyazev DG, Lents A, Krause E, Ollinger N, Siligan C, Papinski D, et al. The bacterial translocon SecYEG opens upon tibosome binding. Journal of Biological Chemistry. 2013;288(25):17941-6.
138. Corporation LT. Amine-reactive probes 2013.
139. Probes IM. Alexa fluor succinimidyl esters, MP 00143. 2009.
140. Biolabs NE. Factor Xa. 2014.
141. Kaufmann TC, Engel A, Rémigy H-W. A novel method for detergent concentration determination. Biophysical Journal. 2006;90(1):310-7.
142. Bacia K, Schwille P. A dynamic view of cellular processes by in vivo fluorescence auto- and cross-correlation spectroscopy. Methods. 2003;29(1):74-85.
143. Ramadurai S, Duurkens R, Krasnikov VV, Poolman B. Lateral diffusion of membrane proteins: consequences of hydrophobic mismatch and lipid composition. Biophysical Journal. 2010;99(5):1482-9.
144. Panchuk-Voloshina N, Haugland RP, Bishop-Stewart J, Bhalgat MK, Millard PJ, Mao F, et al. Alexa dyes, a series of new fluorescent dyes that yield exceptionally bright, photostable conjugates. Journal of Histochemistry & Cytochemistry. 1999;47(9):1179-88.
145. Nardin C, Hirt T, Leukel J, Meier W. Polymerized ABA triblock copolymer vesicles. Langmuir. 2000;16(3):1035-41.
146. Walde P, Ichikawa S. Enzymes inside lipid vesicles: preparation, reactivity and applications. Biomolecular Engineering. 2001;18(4):143-77.

147. Borgnia MJ, Agre P. Reconstitution and functional comparison of purified GlpF and AqpZ, the glycerol and water channels from *Escherichia coli*. Proceedings of the National Academy of Sciences of the United States of America. 2001;98(5):2888-93.
148. Sundar SK, Tirumkudulu MS. Novel method for synthesizing monodisperse dispersion of nanometer liposomes. In: Joshi YM, Khandekar S, editors. Nanoscale and Microscale Phenomena: Fundamentals and Applications. New Delhi: Springer India; 2015. p. 3-16.
149. Petzold G, Dutschk V, Mende M, Miller R. Interaction of cationic surfactant and anionic polyelectrolytes in mixed aqueous solutions. Colloids and Surfaces A: Physicochemical and Engineering Aspects. 2008;319(1):43-50.
150. Antonietti M, Förster S. Vesicles and liposomes: a self-assembly principle beyond lipids. Advanced Materials. 2003;15(16):1323-33.
151. Vink M, Derr KD, Love J, Stokes DL, Ubarretxena-Belandia I. A high-throughput strategy to screen 2D crystallization trials of membrane proteins. Journal of Structural Biology. 2007;160(3):295-304.
152. Fotiadis D, Engel A. Two-dimensional crystallisation of membrane proteins and structural assessment. eLS: John Wiley & Sons, Ltd; 2001.
153. Jensen MO, Mouritsen OG. Single-channel water permeabilities of Escherichia coli aquaporins AqpZ and GlpF. Biophysical Journal. 2006;90(7):2270-84.
154. Jensen MØ, Mouritsen OG. Single-channel water permeabilities of Escherichia coli aquaporins AqpZ and GlpF. Biophysical Journal. 2006;90(7):2270-84.
155. Hashido M, Kidera A, Ikeguchi M. Water transport in aquaporins: osmotic permeability matrix analysis of molecular dynamics simulations. Biophysical Journal. 2007;93(2):373-85.
156. Hashido M, Ikeguchi M, Kidera A. Comparative simulations of aquaporin family: AQP1, AQPZ, AQP0 and GlpF. FEBS Letters. 2005;579(25):5549-52.
157. Nielsen CH. Biomimetic membranes for sensor and separation applications. Anal Bioanal Chem. 2009;395(3):697-718. Epub 2009/07/29.
158. Meier W, Nardin C, Winterhalter M. Reconstitution of channel proteins in (polymerized) ABA triblock copolymer membranes. Angewandte Chemie-International Edition. 2000;39(24):4599-602.
159. Kelety B, Diekert K, Tobien J, Watzke N, Dorner W, Obrdlik P, et al. Transporter assays using solid supported membranes: A novel screening platform for drug discovery. Assay and Drug Development Technologies. 2006;4(5):575-82.
160. Eray M, Dogan NS, Reiken SR, Sutisna H, Vanwie BJ, Koch AR, et al. A Highly Stable and Selective Biosensor using Modified Nicotinic Acetylcholine-Receptor (nAChR). Biosystems. 1995;35(2-3):183-8.
161. Nikolelis DP, Siontorou CG. Bilayer-Lipid Membranes for Flow-Injection Monitoring of Acetylcholine, Urea, and Penicillin. Analytical Chemistry. 1995;67(5):936-44.
162. Moran-Mirabal JM, Edel JB, Meyer GD, Throckmorton D, Singh AK, Craighead HG. Micrometer-sized supported lipid bilayer arrays for bacterial toxin binding studies through total internal reflection fluorescence microscopy. Biophysical Journal. 2005;89(1):296-305.
163. Lee JCM, Bermudez H, Discher BM, Sheehan MA, Won YY, Bates FS, et al. Preparation, stability, and in vitro performance of vesicles made with diblock copolymers. Biotechnology and Bioengineering. 2001;73(2):135-45.

164. Sauer M, Haefele T, Graff A, Nardin C, Meier W. Ion-carrier controlled precipitation of calcium phosphate in giant ABA triblock copolymer vesicles. Chemical Communications. 2001(23):2452-3.
165. Onaca O, Sarkar P, Roccatano D, Friedrich T, Hauer B, Grzelakowski M, et al. Functionalized Nanocompartments (Synthosomes) with a Reduction-Triggered Release System. Angewandte Chemie - hrsg von der Gesellschaft deutscher Chemiker. 2008;120(37):7137-9.
166. Graff A, Sauer M, Van Gelder P, Meier W. Virus-assisted loading of polymer nanocontainer. Proceedings of the National Academy of Sciences of the United States of America. 2002;99(8):5064-8.
167. Graff A, Fraysse-Ailhas C, Palivan CG, Grzelakowski M, Friedrich T, Vebert C, et al. Amphiphilic Copolymer Membranes Promote NADH:Ubiquinone Oxidoreductase Activity: Towards an Electron-Transfer Nanodevice. Macromolecular Chemistry and Physics. 2010;211(2):229-38.
168. Cruz A, Perez-Gil J. Langmuir films to determine lateral surface pressure on lipid segregation. Methods in Molecular Biology. 2007;400:439-57. Epub 2007/10/24.
169. Reimhult E, Hook F, Kasemo B. Vesicle adsorption on SiO2 and TiO2: Dependence on vesicle size. Journal of Chemical Physics. 2002;117(16):7401-4.
170. Reimhult E, Hook F, Kasemo B. Intact Vesicle Adsorption and Supported Biomembrane Formation from Vesicles in Solution: Influence of Surface Chemistry, Vesicle Size, Temperature, and Osmotic Pressure. Langmuir : the ACS journal of surfaces and colloids. 2003;19(5):1681-91.
171. Reimhult E, Hook F, Kasemo B. Temperature dependence of formation of a supported phospholipid bilayer from vesicles on SiO2. Physical Review E, Statistical, Nonlinear, and Soft Matter Physics. 2002;66(5 Pt 1):051905. Epub 2003/01/07.
172. Montal M, Mueller P. Formation of bimolecular membranes from lipid monolayers and a study of their electrical properties. Proceedings of the National Academy of Sciences of the United States of America. 1972;69(12):3561-6.
173. Hansen JS, Perry M, Vogel J, Groth JS, Vissing T, Larsen MS, et al. Large scale biomimetic membrane arrays. Anal Bioanal Chem. 2009;395(3):719-27. Epub 2009/08/13.
174. Hansen JS, Perry M, Vogel J, Vissing T, Hansen CR, Geschke O, et al. Development of an automation technique for the establishment of functional lipid bilayer arrays. J Micromech Microeng. 2009;19(2):025014.
175. Vogel J, Perry M, Hansen JS, Bolinger PY, Nielsen CH, Geschke O. A support structure for biomimetic applications. J Micromech Microeng. 2009;19(2):025026.
176. Ibragimova S, Stibius K, Szewczykowski P, Perry M, Bohr H, Hélix-Nielsen C. Hydrogels for in situ Encapsulation of Biomimetic Membrane Arrays. Polym Adv Technol.doi 10.1002/pat.850.
177. Kita-Tokarczyk K, Itel F, Grzelakowski M, Egli S, Rossbach P, Meier W. Monolayer interactions between lipids and amphiphilic block copolymers. Langmuir. 2009;25(17):9847-56. Epub 2009/08/27.
178. Rakhmatullina E, Mantion A, Burgi T, Malinova V, Meier W. Solid-Supported Amphiphilic Triblock Copolymer Membranes Grafted from Gold Surface. Journal of Polymer Science Part a-Polymer Chemistry. 2009;47(1):1-13.
179. Dorn J, Belegrinou S, Kreiter M, Sinner EK, Meier W. Planar Block Copolymer Membranes by Vesicle Spreading. Macromolecular Bioscience. 2011;11(4):514-25.

180. Gonzalez-Perez A, Castelletto V, Hamley IW, Taboada P. Biomimetic triblock copolymer membranes: from aqueous solutions to solid supports. Soft Matter. 2011;7(3):1129-38.
181. Wang JY, Chin JM, Marks JD, Lee KYC. Effects of PEO-PPO-PEO Triblock Copolymers on Phospholipid Membrane Integrity under Osmotic Stress. Langmuir. 2010;26(15):12953-61.
182. Ruysschaert T, Sonnen AF, Haefele T, Meier W, Winterhalter M, Fournier D. Hybrid nanocapsules: interactions of ABA block copolymers with liposomes. Journal of the American Chemical Society. 2005;127(17):6242-7. Epub 2005/04/28.
183. Nardin C, Hirt T, Leukel J, Meier W. Polymerized ABA Triblock Copolymer Vesicles. Langmuir : the ACS journal of surfaces and colloids. 2000;16(3):1035-41.
184. Jin YL, Chen JY, Xu L, Wang PN. Refractive index measurement for biomaterial samples by total internal reflection. Physics in Medicine and Biology. 2006;51(20):N371.
185. Weast RC, Astle MJ, Beyer WH. CRC Handbook of Chemistry and Physics. Boca Raton, FL: CRC Press Inc; 1985.
186. Rodahl M, Hook F, Fredriksson C, Keller CA, Krozer A, Brzezinski P, et al. Simultaneous frequency and dissipation factor QCM measurements of biomolecular adsorption and cell adhesion. Faraday Discuss. 1997(107):229-46. Epub 1997/01/01.
187. Graneli A, Rydstrom J, Kasemo B, Hook F. Formation of supported lipid bilayer membranes on SiO2 from proteoliposomes containing transmembrane proteins. Langmuir. 2003;19(3):842-50.
188. Kölchens S, Ramaswami V, Birgenheier J, Nett L, O'Brien DF. Quasi-elastic light scattering determination of the size distribution of extruded vesicles. Chem Phys Lipids. 1993;65:1-10.
189. Lewis BA, Engelman DM. Lipid Bilayer Thickness Varies Linearly with Acyl Chain-Length in Fluid Phosphatidylcholine Vesicles. Journal of Molecular Biology. 1983;166(2):211-7.
190. Lande MB, Donovan JM, Zeidel ML. The Relationship between Membrane Fluidity and Permeabilities to Water, Solutes, Ammonia, and Protons. Journal of general physiology. 1995;106:67-84.
191. Keller CA, Kasemo B. Surface specific kinetics of lipid vesicle adsorption measured with a quartz crystal microbalance. Biophysical journal. 1998;75(3):1397-402. Epub 1998/09/03.
192. Kucerka N, Tristram-Nagle S, Nagle JF. Structure of Fully Hydrated Fluid Phase Lipid Bilayers with Monounsaturated Chains. Journal of Membrane Biology. 2006;208(3):193-202.
193. Dannenmuller O, Arakawa K, Eguchi T, Kakinuma K, Blanc S, Albrecht AM, et al. Membrane properties of archaeal macrocyclic diether phospholipids. Chemistry-a European Journal. 2000;6(4):645-54.
194. Chang EL. Unusual Thermal-Stability of Liposomes Made From Bipolar Tetraether Lipids. Biochemical and Biophysical Research Communications. 1994;202(2):673-9.
195. Needham D, Zhelev D. The mechanochemistry of lipid vesicles examined by micropipet manipulation techniques. Surfactant science series. 1996;62:373-444.
196. Preston GM, Agre P, et. Appearance of water channels in *Xenopus Oocytes* expressing red cell CHIP28 protein. Science. 1992;256(5055):385.
197. Delamarche C, Thomas D, Rolland JP, Froger A, Gouranton J, Svelto M, et al. Visualization of AqpZ-mediated water permeability in *Escherichia coli* by cryoelectron microscopy. Journal of Bacteriology. 1999;181(14):4193-7.

198. Mallo RC, Ashby MT. AqpZ-mediated water permeability in *Escherichia coli* measured by stopped-flow spectroscopy. Journal of Bacteriology. 2006;188(2):820-2.
199. Romantsov T, Battle AR, Hendel JL, Martinac B, Wood JM. Protein localization in *Escherichia coli* cells: comparison of the cytoplasmic membrane proteins ProP, LacY, ProW, AqpZ, MscS, and MscL. Journal of Bacteriology. 2010;192(4):912-24.
200. Laboratories B-R. MicroPulser electroporation apparatus operating instructions and applications guide. Contract No.: 165-2100.
201. Baba T, Ara T, Hasegawa M, Takai Y, Okumura Y, Baba M, et al. Construction of Escherichia coli K-12 in-frame, single-gene knockout mutants: the Keio collection. Molecular systems biology. 2006;2(1).
202. Soupene E, van Heeswijk WC, Plumbridge J, Stewart V, Bertenthal D, Lee H, et al. Physiological studies of *Escherichia coli* strain MG1655: growth defects and apparent cross-regulation of gene expression. Journal of Bacteriology. 2003;185(18):5611-26.
203. Van De Merwe WP, Czégé J, Milham ME, Bronk BV. Rapid optically based measurements of diameter and length for spherical or rod-shaped bacteria in vivo. Appl Opt. 2004;43(28):5295-302.
204. Levina N, Tötemeyer S, Stokes NR, Louis P, Jones MA, Booth IR. Protection of *Escherichia coli* cells against extreme turgor by activation of MscS and MscL mechanosensitive channels: identification of genes required for MscS activity. The EMBO Journal. 1999;18(7):1730-7.
205. Maturin LP, James T. Bacteriological analytical manual chapter 3: aerobic plate count. U.S. Food and Drug Administration; 2001 [April 21, 2017]; Available from: https://www.fda.gov/food/foodscienceresearch/laboratorymethods/ucm063346.htm#r10-Zipkes.
206. Wittig I, Beckhaus T, Wumaier Z, Karas M, Schägger H. Mass estimation of native proteins by blue native electrophoresis: principles and practical hints. Molecular & Cellular Proteomics. 2010;9(10):2149-61.
207. Schägger H, von Jagow G. Blue native electrophoresis for isolation of membrane protein complexes in enzymatically active form. Analytical biochemistry. 1991;199(2):223-31.
208. Dow. Water and process solutions: FILMTEC reverse osmosis membranes, technical manual. Technical Manual. 2009 Contract No.: 609-00071-1009.
209. Crommelin DJA, van Bommel EMG. Stability of liposomes on storage: freeze dried, frozen or as an aqueous dispersion. Pharmaceutical Research. 1984;1(4):159-63.
210. Allen TM, Romans AY, Kercret H, Segrest JP. Detergent removal during membrane reconstitution. Biochimica et Biophysica Acta (BBA) - Biomembranes. 1980;601(0):328-42.
211. Ariën A, Henry-Toulmé N, Dupuy B. Calcitonin-loaded liposomes: stability under acidic conditions and bile salts-induced disruption resulting in calcitonin-phospholipid complex formation. Biochimica et Biophysica Acta (BBA) - Biomembranes. 1994;1193(1):93-100.
212. Ariën A, Toulmé-Henry N, Dupuy B. Cholate-induced disruption of calcitonin-loaded liposomes: formation of trypsin-resistant lipid-calcitonin-cholate complexes. Pharmaceutical Research. 1995;12(9):1289-92.
213. Delorme N, Fery A. Direct method to study membrane rigidity of small vesicles based on atomic force microscope force spectroscopy. Physical Review E. 2006;74(3):030901.
214. Lipowsky R. The morphology of lipid membranes. Current Opinion in Structural Biology. 1995;5(4):531-40.

215. Fotiadis D, Scheuring S, Müller SA, Engel A, Müller DJ. Imaging and manipulation of biological structures with the AFM. Micron. 2002;33(4):385-97.
216. Leonenko ZV, Carnini A, Cramb DT. Supported planar bilayer formation by vesicle fusion: the interaction of phospholipid vesicles with surfaces and the effect of gramicidin on bilayer properties using atomic force microscopy. Biochimica et Biophysica Acta (BBA) - Biomembranes. 2000;1509(1–2):131-47.
217. Hansma HG, Hoh JH. Biomolecular imaging with the atomic force microscope. Annual Review of Biophysics and Biomolecular Structure. 1994;23(1):115-40.
218. Dufrêne YF. Atomic force microscopy, a powerful tool in microbiology. Journal of Bacteriology. 2002;184(19):5205-13.
219. Hansma PK, Cleveland JP, Radmacher M, Walters DA, Hillner PE, Bezanilla M, et al. Tapping mode atomic force microscopy in liquids. Applied Physics Letters. 1994;64(13):1738-40.
220. Mao GL, Xuemei; Mg, K. Y. Simon. Direct force measurement of liposomes by atomic force microscopy. Dekker Encyclopedia of Nanoscience and Nanotechnology. New York: Marcel Dekker, Inc.; 2004. p. 933-42.
221. Németh-Cahalan KL, Kalman K, Hall JE. Molecular Basis of pH and Ca²⁺ Regulation of Aquaporin Water Permeability. The Journal of General Physiology. 2004;123(5):573-80.
222. Zelenina M, Bondar AA, Zelenin S, Aperia A. Nickel and Extracellular Acidification Inhibit the Water Permeability of Human Aquaporin-3 in Lung Epithelial Cells. Journal of Biological Chemistry. 2003;278(32):30037-43.
223. Tournaire-Roux C, Sutka M, Javot H, Gout E. Cytosolic pH regulates root water transport during anoxic stress through gating of aquaporins. Nature. 2003;425(6956):393.
224. Törnroth-Horsefield S, Wang Y, Hedfalk K, Johanson U, Karlsson M, Tajkhorshid E, et al. Structural mechanism of plant aquaporin gating. Nature. 2006;439(7077):688.
225. Hedfalk K, Törnroth-Horsefield S, Nyblom M, Johanson U, Kjellbom P, Neutze R. Aquaporin gating. Current Opinion in Structural Biology. 2006;16(4):447-56.
226. Thomason LC, Costantino N, Court DL. *E. coli* genome manipulation by P1 transduction. Current Protocols in Molecular Biology: John Wiley & Sons, Inc.; 2001.

APPENDIX A: ALEXA FLUOR 488 LABELING FOR AQPZ AND OMPF

This appendix describes the protocol that was developed to label membrane proteins as described in chapter 3 for measurement using fluorescence correlation spectroscopy (FCS). This protocol was based on the Amine-Reactive Probes Protocol from Invitrogen (138).

Prepare chemical solutions:

1. 1 M sodium bicarbonate (Na HCO_3) buffer stock, pH 8.3.
2. 10 mg/ml Alexa Fluor 488 carboxylic acid, succinimidyl ester *mixed isomers* (Thermo-Fisher Scientific, Pittsburgh, PA)
    a. For 1 g (Cat # A20000), add 100 µl DMSO. Cover vial in aluminum foil and freeze unused stock.
    b. For 5 g (Cat # A20100), add 500 µl DMSO. Cover vial in aluminum foil and freeze unused stock.
3. Dialysis buffer for size exclusion chromatography (SEC):

    <u>For AqpZ, 2L</u>:

Dodecyl maltoside (DDM) (0.05%)	1.000 g
K_2HPO_4 (0.1 M)	34.836 g
2-Mercaptoethanol (BME) (5 mM)	0.6944 ml
NaCl (0.2 M)	23.4 g
Glycerol (10%)	200 ml
water	make up to 2 L
Adjust to pH 7	

    <u>For OmpF (20 mM phosphate buffer), 2L</u>:

$NaH_2PO_4*H_2O$	4.47 g
Na_2HPO_4	1.08 g
n-Octyl-oligo-oxyethylene (Octyl-POE) (1%)	20 ml
Adjust to pH 7.4	

Labeling reaction:

1. From 1 M stock, add $NaHCO_3$, pH 8.3 for a final concentration of 0.1 M. Vortex.
2. Add dye (from 10 mg/ml freezer stock), for a protein:dye molar ratio between $8.6x10^{-2}$. Protein must be at least 2 mg/ml. The appropriate nolecular weights of 28,000 g/mol for AqpZ and 38,000 g/mol for OmpF were used.
3. Shake for 4 hours at room temperature. Wash the SEC column.
4. Size exclude using a Superdex 200 pressurized Tricorn 50 ml column with an Äkta prime plus instrument (GE Healthcare, Chicago, IL) at a flowrate of 0.5 ml/min.
5. Add sodium azide (NaN_3) for a final concentration of 2 mM. Store at 2-6°C.

Table A.1. Sample calculations for labeling AqpZ

init AqpZ conc	2	mg/ml		
init AqpZ vol	2	ml		
Add 0.1 ml NaHCO3 to every 1 ml solution				
added NaHCO3 vol	0.2	ml		
new AqpZ conc	1.82	mg/ml		
new AqpZ vol	2.2	ml		
MW AqpZ	28000	mg/mmol		
moles AqpZ	1.43E-04	mmol AqpZ		
stock dye conc	10	mg/ml		
molar ratio protein:dye	8.58E-02			
	4.29E-02			
added mmol dye	1.67E-03	mmol dye		
	3.33E-03	mmol dye		
added dye vol	1.07E-01	ml dye	107.14	ul dye
	2.14E-01	ml dye	214.29	ul dye
rxn AqpZ conc	1.73	mg/ml		
	1.66	mg/ml		
rxn vol	2.307	ml		
	2.414	ml		

APPENDIX B: FLUORESCENCE CORRELATION SPECTROSCOPY THEORY AND METHOD FOR QUANTIFYING MEMBRANE PROTEIN IN VESICLES

This appendix describes the theory behind fluorescence correlation spectroscopy (FCS) and the method that was developed as described in chapter 3. This FCS method was developed to quantify AqpZ and OmpF membrane protein insertion in lipid and polymer vesicles. The number of fluorescent molecules and total counts can be obtained from an FCS measurement. Measurement using FCS allows for measurement of small fluctuations in fluorescence intensity within a small (~ 1 femtoliter) confocal volume over a short period of time (10 s). The fluctuations of the fluorescence signal are defined as the deviations of intensity measured at time t, *I(t),* from the temporal average of the fluorescence signal, $\langle I(t) \rangle$, shown in Equation B.1 (123, 124, 142).

$$\delta I(t) = I(t) - \langle I(t) \rangle$$

Equation B.1. Temporal average of fluorescent signal

These intensity changes were fit to an autocorrelation function which provided a measure of the self-similarity of a temporal signal. Fitting to the normalized autocorrelation function shown in Equation B.2.

$$G(\tau) = \frac{\langle \delta I(t) \rangle \langle \delta I(t+\tau) \rangle}{\langle I(t) \rangle^2}$$

Equation B.2. Normalized autocorrelation function

The autocorrelation function allows for calculation of various items including the number of molecules, molecular diffusion coefficient, diffusion time and excitation volume. δI(t) is the time-

dependent fluorescence intensity fluctuation, and δI(t+τ) is the intensity fluctuation after a lag time of τ. Autocorrelation data for 10 ten-second measurements were averaged and fit by a single species 3D Gaussian diffusion model described by Equation B.3:

$$G(\tau) = \frac{1}{N} \cdot \frac{1}{1+\tau/\tau_D} \cdot \frac{1}{\left[1+\left(w_o/z_o\right)^2\left(\tau/\tau_D\right)\right]^{1/2}}$$

Equation B.3. 3D Gaussian diffusion model

where N is the average particle number in the focal volume which can be calculated by the amplitude of the of the autocorrelation curve knowing the radius and half-height dimensions w_o and z_o from calibration measurements. The number of molecules within a focal volume at any time is governed by the Poisson distribution. When τ = 0, G(0) = 1/N, which is the variance of the fluorescence intensity fluctuation and allows us to know N. τ_D is the 2D lateral diffusion time in the focal volume or the characteristic decay time of the correlation function. The diffusion time, τ_D, is related to the particle's diffusion coefficient, D, as shown in Equation B.4. The diffusion coefficient for a given particle is based on the particle size (123, 142).

$$\tau_D = \frac{w_o^{\,2}}{4D}$$

Equation B.4. Diffusion time

The average concentration of a single species multiplied by the effective volume is also the average particle number (Equation B.5):

$$N = \langle C \rangle \cdot V_{eff}$$

Equation B.5. Average particle number

and the effective volume is defined in Equation B.6.

$$V_{eff} = \pi^{3/2} w_o^{\,2} z_o$$

Equation B.6. Effective volume

Vesicle fluorescence intensity was measured using single-photon FCS with an Alba fluorescence correlation spectrometer (ISS, Champaign, IL) with a wavelength of 467 nm. The instrument was calibrated using nanomolar aqueous solutions of Alexa-fluor 488 with a pinhole of 50. Three aliquots of each sample were measured for 100 seconds at 30 or 50% power three times in fluorescence fluctuation spectroscopy (FFS) mode. Measurements at 50% power were corrected to 30% power during fitting by measuring labeled AqpZ at both powers. Measurements yielded smooth autocorrelation curves. No decrease in signal intensity was observed during these measurements, indicating that bleaching was not a problem.

Data was analyzed using confocal spectroscopy and imaging application, VistaVision (version 4.0 build 00144; ISS, Champaign, IL, USA). Data was separated into 10, 10-second measurements and the correlation curves were averaged into one correlation curve per measurement per aliquot. Correlation curves for all measurements were fit using a single species 3D Gaussian autocorrelation function and the range of each correlation curve fit was at least 0-0.2 seconds. For fitting free label data, the diffusion coefficient was fixed to the known value for Alexa-fluor 488 in water at 20°C of 380 $\mu m^2 s^{-1}$ (143), dye concentrations were fixed, and the excitation volume parameters, ω_o and z_o, were linked to determine the ω_o and z_o values for each measurement session. For fitting labeled-protein micelles data, the excitation volume parameters, ω_o and z_o, were fixed and initial values for diffusion coefficients and concentrations were set to 30 $\mu m^2 s^{-1}$ and 1 nM, respectively. For fitting labeled-protein in vesicles data, ω_o and z_o, were also fixed and initial values for vesicle diffusion coefficients and concentrations were set to 5 $\mu m^2 s^{-1}$ and 1 nM, respectively.

Distinct diffusion coefficients were obtained for three diffusing species ranging from 380 $\mu m^2/s$ (143) for free fluorescent label, 34±8.8 $\mu m^2/s$ for AqpZ micelles, 19.8±6.0 $\mu m^2/s$ for OmpF micelles, and 2.5±1.9 $\mu m^2/s$ for vesicles. Each of these species were measured independently and yielded smooth autocorrelation curves.

The number of protein inserted in an average vesicle was subsequently determined by comparing the counts (or brightness) per molecule per second (CPMS) of the vesicle to that of the labeled protein (130). The CPMS for vesicles was calculated by Equation B.7.

$$CPMS = CPS/[1/G(0)]$$

Equation B.7. CPMS for vesicles

where CPS is the counts per second and 1/G(0) is the number of fluorescent molecules. The CPMS for protein was calculated by Equation B.8:

$$CPMS = CPS/[1/G(0)\times DOL]$$

Equation B.8. CPMS for protein

where DOL is the degree of labeling. The degree of labeling ranged from 1.2-2.6 mol dye/mol AqpZ monomer and 0.3-0.7 mol dye/mol OmpF monomer. As first described by Rigler and Meier (130) for quantifying the number of encapsulated soluble proteins in polymer vesicles, the number of protein present in an average vesicle was determined by the ratio of the counts per molecule of the vesicle to the counts per molecule of the labeled AqpZ, as shown in Equation B.9.

$$\#\ \text{protein per vesicle} = CPMS_{vesicle}/CPMS_{protein}$$

Equation B.9. Number protein/vesicle

Due to the high photo stability of Alexa Fluor 488 (144), differences in fluoresce intensity in buffer and in the vesicle membrane were not expected nor identified by data collected.

APPENDIX C: DATA TABLES

This appendix lists the data used to generate the plots in Chapter 3 to describe the effect of DDM detergent on insertion and permeability of AqpZ/lipid vesicles (Figure 3.4), the effect of the amount of protein added on insertion and permeability of OmpF/lipid vesicles (Figure 3.6), and AqpZ/lipid vesicles (Figure 3.8). This appendix also lists the data used to generate plots in Chapter 5 to describe the pH effect on permeability of *E. coli* (Figures 5.2, 5.3, 5.4, 5.6) and percent survival of *E. coli* under acid shock (Figures 5.5, 5.6) as well as additional survival data not included in those figures.

Tables comprised of insertion data (Table C.1, Table C.3, Table C.5) first list key sample differences including detergent concentration, protein batch, membrane material, and/or protein/membrane material molar ratio. Data is divided into replicate measurements of each vesicle preparation. For FCS measurements, multiple samples of each vesicle replicate were measured, three times each. These multiple samples were used to avoid any bleaching that could occur with extended measurement of a given sample (none was observed). The autocorrelation curves were fit for each of these samples, and the diffusion coefficient (D), number of particles (1/G0), counts per second (CPS) and the Chi squared values were obtained. Data presented in these tables are the fitted data. The diffusion coefficient was not used in the calculation for the number of protein/vesicle, but allowed confirmation of the size of the diffusing species; particle size is inversely related to diffusion coefficient. Comparing brightness of vesicles to the brightness of the freely diffusing protein allowed calculation of the number of protein/vesicle as described in Section 3.3 and APPENDIX B. For these calculations, protein was assumed to exist in its most common form (tetramer for AqpZ, trimer for OmpF). For AqpZ-containing vesicles, the calculated protein/vesicle values were averaged for each vesicle preparation replicate, and then averaged across replicates for each AqpZ batch. For OmpF-containing vesicles, the calculated protein/vesicle values were averaged for each vesicle preparation, then averaged for each OmpF batch, and finally, because trends were similar between OmpF batches, data was averaged across OmpF batches. Error was propagated in each step.

Tables comprised of vesicle permeability data (Table C.2, Table C.4, Table C.6) also first list key sample differences including detergent concentration, protein batch, membrane material, and/or protein/membrane material molar ratio. Data is divided into replicate measurements of each vesicle preparation. For stopped flow measurements, multiple samples of each vesicle replicate were measured by mixing the sample with a hyperosmotic solution (NaCl for AqpZ-containing vesicles, sucrose for OmpF-containing vesicles, and proline for whole *E. coli* cells). The osmolyte concentration listed in these tables is the concentration of the osmolyte prior to the measurement where mixing occurs. The imposed osmolar gradient, Δ_{osm}, was calculated as described in Equation C.1:

$$\Delta_{osm} = \varphi n C / 2$$

Equation C.1. Osmolar gradient

where the osmotic coefficient, φ, accounts for the degree of non-ideality in the solution. Concentrations were small enough that ideal conditions and complete dissolution were assumed. The number of particles into which a molecule dissociates, n, is 2 for NaCl and 1 for sucrose and proline. The concentration of the solute, C, was the stock concentration of the osmotic solution prior to mixing. This value is then divided in half as described in Equation C.1 because there was 1:1 mixing between the sample and osmotic solution for each measurement. For each replicate, at least 5 curves were averaged into a single curve for fitting. The curves were fit using an exponential rise equation and the exponential rise rate constant (k) and the standard deviation of the fit (SD) was obtained. Data presented in these tables are the fitted data. The water permeability was calculated as described in Sections 3.3. For AqpZ-containing vesicles, the calculated permeability values were averaged for each vesicle preparation replicate, and then averaged across replicates for each AqpZ batch. For OmpF-containing vesicles, the calculated permeability values were averaged for each vesicle preparation, then averaged for each OmpF batch, and finally, because trends were similar between OmpF batches, data was averaged across OmpF batches. The variances of the permeability values were used to calculate the standard deviation across replicates since variance is the square of the standard deviation.

For whole cells of *E. coli*, data in Table C.7 is organized by date, strain, which stopped flow instrument was used, and the pH of the sample. The data presented is as described above except for the following: proline was used as the osmolyte, at least 7 curves were averaged into a single curve for fitting for each replicate, water permeability was calculated as described in Section 5.3, and data was averaged for each replicate measurement of each independent biological preparation and subsequently averaged for each strain. Due to significant differences observed between stopped flow instruments, data were separated by the stopped flow instrument used.

E. coli survival data (Table C.8) is organized by *E. coli* strain and date. Each date represents a different biological replicate. The raw plate count data and the calculated % survival is shown. Different dilutions were from the same shocked culture. The % survival is the percent ratio of the counts from the shocked condition to the counts from the control condition. For 2011 data, the one plate with acceptable counts (as described in Section 5.3) for each shock condition was averaged across biological replicates for each strain. Additionally, data from 2014 is also presented in Table C.8. In 2014, triplicate plates were prepared for each dilution.

Table C.1. Insertion data for the effect of DDM detergent on AqpZ tetramer insertion in AqpZ/lipid vesicles (Figure 3.4)
Abbreviations are as follows: replicate (rep), sample (smpl), diffusion coefficient (D), number of molecules (1/G0), counts per second (CPS), channel (ch), Chi square (chi-sqr), vesicle (ves).

[DDM] (%)	Rep	Smpl	D ($\mu m^2/s$)	1/G(0)	CPS-ch1	CPS-ch2	Chi-sqr of fit	# AqpZ/ves
0.01	1	1	2.31	0.16	3236	2343	0.50	828.71
			1.96	0.25	2843	2008	0.10	452.15
			1.86	0.22	3120	2229	0.09	575.73
			2.70	0.49	2657	1842	0.05	213.84
		2	2.50	0.54	2520	1757	0.19	185.81
			2.16	0.32	2878	2018	0.16	352.10
			2.39	0.24	2901	2016	0.39	483.20
		3	2.80	0.36	2633	1787	0.32	283.52
			2.13	0.56	2484	1715	0.17	173.75
			3.66	0.33	2806	1923	0.62	331.05

Table C.1. cont'd

[DDM] (%)	Rep	Meas	D (μm²/s)	1/G0	CPS-ch1	CPS-ch2	Chi-sqr	# AqpZ/ves
0.09	1	1	2.45	1.67	9092	6900	0.62	223.23
			2.44	1.40	9404	7098	0.29	275.15
			1.58	1.46	9182	6988	0.09	258.62
		2	1.90	1.13	9648	6869	0.04	341.42
			1.81	1.67	9409	6746	0.18	226.15
			1.44	1.14	9894	7104	0.29	347.25
		3	2.77	1.22	9703	6885	0.14	316.53
			2.77	1.50	9688	6872	0.20	257.27
			1.36	1.14	10180	7237	0.15	355.43
0.3	1	1	2.13	0.86	8280	5884	0.22	383.44
			0.69	0.58	9026	6364	0.15	617.91
			1.51	0.80	8257	5827	0.44	412.92
		2	0.92	0.92	8411	5896	0.38	363.57
			1.37	1.26	8240	5825	0.19	260.54
			1.45	1.35	7657	5365	0.13	225.63
		3	0.93	0.85	8960	6390	0.19	422.61
			1.53	0.98	9245	6628	0.27	376.14
			1.29	1.00	8796	6253	0.21	350.26
0.6	1	1	3.58	9.39	3867	2615	0.34	16.11
			8.27	8.40	3821	2597	0.40	17.82
			3.71	7.74	3855	2605	0.16	19.47
		2	5.47	7.81	3897	2650	0.33	19.57
			3.97	9.20	3955	2676	0.29	16.81
			3.49	4.79	3967	2695	0.37	32.45
		3	2.90	6.11	3986	2670	0.12	25.42
			2.67	4.51	3999	2678	0.10	34.52
			3.96	8.32	3934	2629	0.14	18.41
1	1	1	6.83	47.64	7148	4845	0.71	0.17
			9.04	52.20	7176	4850	0.81	1.00
			9.05	57.80	7187	4856	1.27	0.92
		2	6.52	39.83	7576	4978	0.55	0.83
			9.16	52.05	7501	4927	0.76	1.25
			9.79	47.09	7532	4940	1.02	0.95
		3	6.59	66.75	7096	4983	0.41	1.05
			7.24	57.04	7148	5016	0.48	0.72
			7.26	87.55	7122	4992	1.29	0.85

Table C.1. cont'd

[DDM] (%)	Rep	Meas	D ($\mu m^2/s$)	1/G(0)	CPS-ch1	CPS-ch2	Chi-sqr of fit	# AqpZ/ves
0.01	2	1	2.70	0.45	15158	10135	0.33	1322.05
			1.70	0.41	16122	10854	0.10	1518.52
			1.97	0.52	15537	10468	0.20	1169.52
			2.70	0.45	15158	10135	0.33	1322.05
		2	2.49	0.57	18068	12485	0.33	1252.91
			1.67	0.66	22524	15451	0.24	1333.28
			2.23	0.74	22081	15132	0.39	1180.85
		3	1.49	0.60	17134	12899	0.34	1160.51
			1.42	0.56	9026	6364	0.12	646.96
			1.77	0.47	18024	13441	0.33	1556.69
0.09	2	1	2.16	0.48	11036	7918	0.33	916.92
			1.36	0.48	11341	8133	0.30	954.10
			2.22	0.59	10251	7406	0.10	699.35
		2	0.68	7.94	2007	1251	0.30	9.57
			0.55	9.87	1975	1226	0.23	7.57
			0.91	12.19	1966	1225	0.20	6.11
		3	1.98	0.49	10453	7638	0.71	863.34
			1.52	0.38	12097	8833	0.16	1298.13
			2.46	0.46	12582	9191	0.65	1107.03
0.3	2	1	4.15	1.75	2108	1474	0.17	47.72
			2.52	1.06	2290	1627	0.30	86.53
			2.95	0.98	2208	1569	0.13	90.01
			2.34	0.81	2292	1622	0.38	112.22
		2	1.29	0.18	4250	3163	0.01	986.09
			2.97	1.24	2446	1721	0.23	78.66
			1.81	0.83	2556	1824	0.07	122.96
		3	2.75	0.54	2453	1746	0.81	180.94
			2.65	1.44	2315	1639	0.28	63.97
			1.70	0.40	2748	1956	0.34	275.25
0.6	2	1	1.51	3.17	21644	15738	0.26	0.00
			2.38	6.43	20928	15235	0.08	1.00
			2.23	7.12	20747	15153	0.13	0.04
		2	1.44	7.54	21142	15426	0.02	0.04
			0.86	4.34	21369	15661	0.03	0.04
			1.06	7.80	21455	15718	0.18	0.04
		3	2.04	5.07	22001	15822	0.25	0.04
			1.76	4.37	22225	16029	0.21	0.04
			1.15	5.97	21798	15707	0.22	0.05

Table C.1. cont'd

[DDM] (%)	Rep	Meas	D ($\mu m^2/s$)	1/G0	CPS-ch1	CPS-ch2	Chi-sqr	# AqpZ/ves
1	2	1	9.66	4.67	1167	745	0.19	9.55
			4.78	3.61	1202	764	0.52	12.72
			17.87	1.50	1219	786	0.20	31.10
		2	7.08	4.80	975	626	0.83	7.79
			9.13	52.06	7501	4927	0.76	5.57
			8.15	5.24	973	624	0.56	7.12
		3	8.31	6.53	919	580	0.43	5.36
			9.33	7.07	959	590	1.30	5.11

Table C.2. Permeability data for the effect of DDM detergent on permeability of AqpZ/lipid vesicles (Figure 3.4)
Abbreviations are as follows: n-Dodecyl β-D-maltoside (DDM), replicate (rep), exponential fitting parameter (k), permeability (P_f), standard deviation (SD), variance (var).

AqpZ/lipid molar ratio	[DDM] (%)	Rep	[NaCl] (M)	k	P_f (μm/s)	SD of fit	Var of P_f $(\mu m/s)^2$
0	0.01	1	1	11.64	1.79	0.044	4.88E-10
	0.09	1	1	17.97	2.80	0.157	6.32E-09
	0.3	1	1	13.62	2.27	0.052	7.83E-10
	0.6	1	1	26.69	2.61	0.497	2.48E-08
	1	1	1	16.87	2.11	0.820	1.11E-07
	0.01	2	1	10.14	1.55	0.043	4.45E-10
	0.09	2	1	11.73	1.82	0.037	3.44E-10
	0.3	2	1	8.83	1.24	0.028	1.66E-10
	0.6	2	1	18.06	1.34	0.319	5.91E-09
	1	2	1	16.59	1.24	0.802	3.76E-08
1/100	0.01	1	1	83.18	13.66	9.654	2.638E-05
	0.09	1	1	141.10	22.63	6.931	1.297E-05
	0.3	1	1	118.17	19.85	2.321	1.595E-06
	0.6	1	1	69.84	6.98	1.507	2.379E-07
	1	1	1	24.93	1.45	0.689	1.678E-08
	0.01	2	1	112.63	21.09	4.495	7.440E-06
	0.09	2	1	100.06	18.39	45.795	7.437E-04
	0.3	2	1	126.86	22.22	17.256	9.593E-05
	0.6	2	1	24.58	4.37	0.432	6.184E-08
	1	2	1	41.15	4.18	2.308	5.762E-07

Table C.3. Data for the effect of the amount of protein added on insertion in OmpF/lipid vesicles (Figure 3.6)
Abbreviations are as follows: replicate (rep), sample (smpl), diffusion coefficient (D), number of molecules (1/G0), counts per second (CPS), channel (ch), Chi square (chi-sqr), vesicle (ves).

OmpF batch	OmpF/lipid molar ratio	Rep	Smpl	D ($\mu m^2/s$)	1/G0	CPS-ch1	CPS-ch2	Chi-sqr	# AqpZ /ves
1	1/3000	1	1	2.74	0.60	1533	1138	0.14	6.87
				4.12	2.08	1293	961	0.22	1.67
				4.77	1.84	1268	941	0.24	1.84
			2	5.05	1.42	1319	978	0.29	2.49
				5.69	1.44	1307	972	0.52	2.42
				4.20	1.67	1351	1016	0.12	2.18
			3	3.55	1.61	1310	960	0.10	2.16
				3.40	1.45	1332	979	0.16	2.45
				5.53	1.54	1306	963	0.71	2.25
	1/1000	1	1	5.96	0.38	1421	1055	0.49	9.96
				6.31	0.77	1316	978	0.51	4.60
				8.50	0.44	1358	1005	0.46	8.21
			2	12.70	0.44	1444	1068	1.31	8.81
				6.25	0.44	1475	1111	0.27	9.03
				3.03	0.30	1592	1181	0.11	14.25
			3	6.86	0.60	1468	1110	0.41	6.61
				7.83	0.52	1439	1054	0.35	7.34
				6.35	0.36	1403	1039	0.28	10.32
	1/250	1	1	5.00	0.84	4257	3308	0.37	13.87
				4.09	0.55	4713	3665	0.17	23.26
				5.12	0.77	4046	3208	0.34	14.47
			2	5.86	0.57	4589	3768	0.51	22.35
				5.43	0.62	4875	4009	0.27	21.98
				6.30	0.63	4774	3906	0.44	21.10
			3	6.39	0.47	5186	4280	0.35	30.59
				5.28	0.61	5086	4216	0.18	23.60
				5.22	0.59	4794	3944	0.21	22.67

Table C.3. cont'd

OmpF batch	OmpF/lipid molar ratio	Rep	Smpl	D ($\mu m^2/s$)	1/G0	CPS-ch1	CPS-ch2	Chi-sqr	# AqpZ /ves
1	1/100	1	1	5.03	1.51	20123	17054	0.27	37.80
				5.32	1.98	19047	16131	0.15	27.29
				5.06	1.59	19934	16891	0.45	35.60
			2	4.91	1.69	18646	15491	0.31	30.93
				6.05	1.76	18152	15062	0.22	29.02
				5.84	1.51	18316	15148	0.18	34.04
			3	4.84	1.79	21564	18344	0.46	34.14
				4.77	1.74	21368	18122	0.35	34.88
				4.83	1.60	21532	18253	0.33	38.07
1	1/50	1	1	2.61	1.54	47820	41690	1.00	89.34
				2.39	1.31	49086	42489	0.13	106.93
				2.82	1.52	44495	38525	0.18	84.01
			2	2.96	1.46	47761	41758	0.16	94.34
				2.74	1.36	48986	42746	0.18	103.50
				2.73	1.38	48844	42606	0.08	101.37
			3	2.33	1.45	50294	43893	0.49	99.47
				2.69	1.43	54607	47523	0.14	109.54
				2.97	1.34	49223	42773	0.12	105.68
1	1/3000	2	1	5.48	2.16	925	621	0.31	1.10
				6.60	2.63	942	639	0.60	0.92
				4.02	1.01	961	660	0.28	2.46
			2	5.37	2.19	925	621	0.30	1.09
				6.69	1.91	916	598	0.23	1.22
				5.78	1.44	918	612	0.23	1.64
			3	9.88	0.69	948	638	0.30	3.55
				11.31	1.20	929	627	0.31	1.99
1	1/1000	2	1	5.03	0.54	1937	1616	0.08	10.17
				4.50	0.24	2193	1891	0.08	26.41
				5.96	0.55	1915	1598	0.23	9.75
			2	5.71	0.68	1861	1545	0.23	7.74
				6.96	0.96	1778	1469	0.83	5.19
				5.80	0.50	1938	1653	0.54	11.03
			3	7.69	0.86	1799	1538	0.52	5.98
				3.80	0.86	1766	1487	0.09	0.00
				5.70	0.91	1724	1453	0.19	5.34

Table C.3. cont'd

OmpF batch	OmpF/lipid molar ratio	Rep	Smpl	D ($\mu m^2/s$)	1/G0	CPS-ch1	CPS-ch2	Chi-sqr	# AqpZ /ves
1	1/250	2	1	3.73	0.83	7115	6797	0.36	25.82
				4.20	1.10	6979	6504	0.35	18.78
				4.20	1.00	7237	6754	0.31	21.44
			2	5.29	0.79	6847	6397	0.47	25.61
				4.17	1.04	6078	5673	0.23	17.38
				4.31	1.14	6092	5772	0.97	16.01
			3	4.22	0.93	5875	5501	0.38	18.70
				4.81	0.91	6671	6306	0.43	21.98
				4.15	1.07	6533	6174	0.27	18.17
1	1/100	2	1	7.01	3.94	22047	20819	0.27	16.70
				6.76	3.97	21801	20653	0.14	16.42
				6.21	3.96	21632	20576	0.21	16.38
			2	6.79	3.73	21621	20650	0.36	17.38
				6.87	4.14	20999	19972	0.42	15.20
				6.82	4.01	21086	20166	0.25	15.80
			3	6.59	4.27	16945	17536	0.20	12.40
				5.99	4.15	17063	17577	0.19	12.81
				7.18	4.38	16815	17375	0.19	11.99
				7.97	3.60	20747	19970	0.45	17.36
1	1/50	2	1	4.11	3.63	48212	48202	0.17	40.79
				3.68	3.55	47227	47371	0.11	40.88
				4.77	3.72	46506	46766	0.85	38.50
			2	4.13	3.75	45232	45851	0.29	37.32
				4.55	3.98	44728	45678	0.45	34.88
				4.47	3.95	43603	44479	0.20	34.21
			3	4.42	3.57	47701	43966	0.22	39.47
				4.66	3.62	47513	43983	0.14	38.80
				4.67	3.63	45573	42389	0.41	37.20
2	1/3000	1	1	6.84	0.37	2090	1803	1.55	49.16
				5.22	0.39	2040	1773	0.61	44.94
				5.10	0.24	2175	1888	0.63	79.69
			2	8.56	0.36	1809	1495	0.45	42.73
				7.59	0.51	1815	1520	0.79	30.32
				4.35	0.25	1868	1553	1.40	62.34
			3	5.07	0.44	2116	1786	0.33	41.59
				4.50	0.46	1967	1672	1.08	36.49
				5.34	0.30	1970	1630	1.61	55.14

Table C.3. cont'd

OmpF batch	OmpF/lipid molar ratio	Rep	Smpl	D ($\mu m^2/s$)	1/G0	CPS-ch1	CPS-ch2	Chi-sqr	# AqpZ /ves
2	1/1000	1	1	5.93	0.60	4243	3786	0.57	62.02
				5.87	0.45	4182	3747	0.66	82.33
			2	5.84	0.89	3582	3237	0.55	35.40
				5.92	0.62	3633	3319	0.40	52.06
				5.96	0.44	3775	3413	0.91	76.08
			3	5.81	0.91	3582	3237	0.60	34.62
	1/250	1	1	5.58	0.96	13659	12819	0.78	128.11
				4.96	0.53	14399	13510	0.37	242.00
				5.37	0.83	14046	13062	1.92	151.95
			2	6.28	0.77	14999	14035	0.78	175.10
				6.47	0.42	16753	15927	1.24	362.84
			3	5.47	0.28	14776	13483	0.72	476.58
				6.29	0.46	14212	12852	0.87	270.44
				6.54	0.76	14183	13024	0.87	166.65
	1/100	1	1	4.55	5.75	53585	47672	0.14	81.66
				4.38	6.35	53496	47617	0.15	73.81
				4.43	7.02	52861	46918	0.14	65.96
			2	3.37	5.16	52900	46985	0.38	89.86
				5.74	6.06	52683	46656	0.29	76.04
			3	4.31	5.60	52398	46740	0.23	82.13
				5.71	7.80	51691	46003	0.35	58.06
				5.28	6.72	52368	46672	0.17	68.37
	1/50	1	1	2.42	0.99	71859	69621	1.63	665.60
				1.42	0.81	71964	69821	1.01	810.96
				1.33	0.90	76137	74732	1.92	773.67
			2	1.35	0.79	77418	75803	0.89	898.04
				2.26	0.85	71289	69589	1.12	765.55
				2.46	0.84	69553	67385	2.82	752.08
			3	2.52	0.83	69403	68081	1.44	767.24
				1.55	0.75	69699	67456	1.19	845.93
				1.27	0.65	70178	69601	1.40	1003.66

Table C.3. cont'd

OmpF batch	OmpF/lipid molar ratio	Rep	Smpl	D ($\mu m^2/s$)	1/G0	CPS-ch1	CPS-ch2	Chi-sqr	# AqpZ /ves
2	1/25	1	1	3.98	1.50	94231	92791	1.62	579.05
				3.63	1.60	96595	93968	0.83	553.33
				3.87	1.60	96315	93200	3.43	549.40
			2	2.42	1.62	96147	93760	1.09	545.11
				4.04	1.64	99309	96570	2.32	553.57
				2.46	1.77	95586	93193	1.71	494.54
			3	4.53	1.68	99738	97288	2.15	543.96
				2.41	1.68	92902	91116	1.08	509.59
				3.56	1.70	94841	92155	1.85	510.78
2	1/3000	2	1	2.09	0.68	11499	10306	0.43	148.73
				1.95	0.34	12288	10631	0.64	314.91
				2.57	0.33	12374	10868	0.36	328.57
			2	1.68	0.39	13006	11382	0.14	290.32
				1.15	0.52	12151	10580	0.61	201.60
				2.95	0.65	11801	10153	0.49	157.17
			3	2.47	0.37	12080	10481	0.62	282.56
				2.63	0.48	12052	10394	0.59	218.53
				1.73	0.51	12097	10801	0.08	208.87
	1/1000	2	1	8.83	7.35	7565	6545	0.32	8.90
				8.87	8.02	7676	6667	0.33	8.29
				7.74	6.83	7733	6705	0.35	9.80
			2	7.71	7.52	7498	6480	0.22	8.62
				8.30	6.32	7533	6485	0.30	10.30
				8.23	4.85	7450	6427	0.24	13.28
			3	8.16	8.41	7332	6359	0.24	7.56
				9.19	8.30	7310	6297	0.50	7.61
				7.60	6.83	7271	6259	0.18	9.19
	1/250	2	1	3.04	9.12	36649	35540	0.37	36.71
				2.90	9.01	35726	34723	0.39	36.28
				1.30	3.88	36562	35715	0.14	86.32
			2	3.53	7.32	35832	34852	0.46	44.81
				4.13	6.69	32726	31514	0.34	44.53
				2.19	5.63	32614	31499	0.13	52.84
			3	2.68	7.97	33170	33561	0.26	38.82
				1.83	6.65	33794	34231	0.06	47.42
				3.44	9.28	33128	33265	0.39	33.20

Table C.3. cont'd

OmpF batch	OmpF/lipid molar ratio	Rep	Smpl	D ($\mu m^2/s$)	1/G0	CPS-ch1	CPS-ch2	Chi-sqr	# AqpZ /ves
2	1/100	2	1	1.32	1.18	63823	64726	0.04	586.80
			2	1.98	1.30	63430	63290	0.42	527.88
				2.02	1.49	60188	60073	0.40	435.38
				1.88	1.37	62363	61818	0.30	489.45
			3	1.48	1.41	60000	60042	0.20	460.43
				1.59	1.15	63282	63619	0.22	596.86
				1.87	1.31	61009	61231	0.47	503.92
	1/50	2	1	1.51	1.94	103707	104067	0.27	496.10
				1.54	2.17	99615	99285	0.46	425.29
				1.24	1.80	104264	104638	0.08	538.09
			2	1.71	2.10	100861	101190	0.51	447.16
				1.92	1.99	100589	100868	0.32	468.80
				1.65	1.91	99588	99918	0.24	485.59
			3	1.56	1.91	102028	102129	0.08	496.37
				2.10	1.96	97401	98495	0.36	463.61
				1.90	1.96	99532	99525	0.49	471.14
	1/25	2	1	0.63	1.42	201436	207892	0.06	1340.47
				0.87	1.30	190898	196285	0.09	1378.26
				0.65	1.31	187192	191645	0.04	1338.30
			2	0.68	1.33	198994	221596	0.10	1466.32
				0.52	1.08	202539	221479	0.15	1821.53
				1.04	1.36	189150	206017	0.33	1344.99
			3	0.75	1.37	191351	210846	0.16	1359.73
				0.76	1.38	188986	207251	0.04	1329.20
				0.83	1.37	196129	215495	0.15	1389.05

Table C.4. Data for the effect of the amount of protein added on permeability of OmpF/lipid vesicles (Figure 3.6)
Abbreviations are as follows: replicate (rep), exponential fitting parameter (k), permeability (P_f), standard deviation (SD), variance (var).

OmpF batch	Rep	OmpF/lipid molar ratio	[Sucrose] (M)	k (s^{-1})	P_f (μm/s)	SD of k (s^{-1})	Var of P_f $(\mu m/s)^2$
1	1	0	1	8.97	24.35	0.04	7.82E-11
		1/3000	1	7.28	20.18	0.01	6.95E-12
		1/1000	1	10.24	29.13	0.13	8.99E-10
		1/250	1	21.32	44.69	0.27	2.11E-09
		1/100	1	29.43	38.64	1.40	2.21E-08
		1/50	1	26.58	69.05	0.66	1.93E-08
	2	0	1	7.49	20.43	0.04	9.23E-11
		1/3000	1	7.21	14.15	0.07	1.09E-10
		1/1000	1	3.80	9.87	0.03	4.01E-11
		1/250	1	15.45	27.43	0.40	3.32E-09
		1/100	1	45.14	51.07	1.32	1.46E-08
		1/50	1	40.89	81.13	1.50	5.83E-08
2	1	0	1	13.35	31.25	0.43	6.55E-09
		1/3000	1	8.02	26.25	0.11	8.70E-10
		1/1000	1	16.02	45.17	0.32	5.18E-09
		1/250	1	70.98	185.54	10.28	4.74E-06
		1/100	1	353.19	420.27	75.19	5.25E-05
		1/50	1	34.95	112.00	2.11	3.00E-07
		1/25	1	370.20	1151.52	42.35	1.14E-04
	2	0	1	28.05	65.64	0.79476	2.26944E-08
		1/3000	1	41.83	80.15	3.13865	2.37284E-07
		1/1000	1	30.89	38.93	2.44	6.22629E-08
		1/250	1	37.57	65.99	2.97	1.7832E-07
		1/100	1	64.75	176.57	2.95	4.26078E-07
		1/50	1	214.45	611.98	32.78	5.74026E-05
		1/25	1	341.34	1464.80	68.16	0.000561363

Table C.5. Data for the effect of the amount of protein added on insertion in AqpZ/lipid and AqpZ/polymer vesicles (Figure 3.8)
Abbreviations are as follows: membrane (mem), material (mat'l), replicate (rep), sample (smpl), diffusion coefficient (D), number of molecules (1/G0), counts per second (CPS), channel (ch), Chi square (chi-sqr), vesicle (ves).

Mem mat'l	AqpZ batch	AqpZ/mem mat'l molar ratio	Rep	Smpl	D ($\mu m^2/s$)	1/G0	CPS-ch1	CPS-ch2	Chi-sqr	# AqpZ /ves
Polymer	1	1/1000	1	1	1.90266	1.88	26536	21865	0.20	55.26
					1.96132	1.02	13228	11167	0.22	51.22
				2	2.62816	2.25	30016	24247	0.63	51.68
					1.95022	2.72	28248	22712	0.09	40.18
				3	2.68427	2.81	29471	23808	0.93	40.64
		1/500	1	1	1.78	1.02	17115	14333	0.24	66.29
					2.17	1.00	19609	15731	0.10	75.86
					2.37	2.09	33483	26951	0.15	62.01
					2.17	1.88	34834	28107	0.31	71.65
					2.13	1.55	35077	28332	0.19	87.56
				2	1.50	1.32	37321	30204	0.49	109.95
					1.79	1.22	36749	29852	0.31	116.87
					1.61	1.34	37379	30387	0.68	108.63
					1.42	0.76	19719	15975	0.19	100.77
					1.97	1.74	17508	14852	0.17	40.00
		1/250	1	1	2.17	0.45	2034	1687	0.96	17.90
					2.84	0.38	3531	2815	0.12	35.74
				2	2.40	0.48	14757	12334	0.07	120.37
					3.24	0.47	20059	16327	0.18	166.78
					2.78	0.89	21265	17329	0.16	92.68
					1.94	0.39	21787	17770	0.88	218.69
				3	3.06	0.55	9176	7411	0.16	65.13
					2.48	0.24	11409	9320	0.17	183.04
					1.50	0.54	8515	6902	0.18	61.49
					3.23	0.59	9412	7626	0.10	62.08
		1/100	1	1	1.76	0.34	45384	39482	0.53	529.25
				2	1.83	0.47	49917	40982	0.59	412.94
				3	2.50	0.98	99736	81363	0.15	397.75
					1.72	1.02	99333	81228	0.17	380.66
					2.04	0.92	103737	84834	0.44	439.17
		1/50	1	1	0.24	0.26	1571	1385	0.10	24.10
					0.15	0.12	2042	1541	0.35	64.11
				2	0.29	0.78	2228	1745	0.46	10.92
					1.38	0.72	2035	1592	0.23	10.77

Table C.5. cont'd

Mem mat'l	AqpZ batch	AqpZ/mem mat'l molar ratio	Rep	Smpl	D ($\mu m^2/s$)	1/G0	CPS-ch1	CPS-ch2	Chi-sqr	# AqpZ /ves
Polymer	1	1/5000	2	1	1.40	0.71	4744	3628	0.33	25.35
				2	1.24	0.64	4768	3640	0.26	28.01
				3	1.32	0.94	4642	3545	0.33	18.73
		1/1000	2	1	1.80	1.64	22165	16847	0.08	51.17
					2.28	1.53	22007	16736	0.13	54.17
					3.24	2.03	21659	16466	0.76	40.21
				2	2.32	1.59	24149	18414	0.22	57.33
					1.07	1.63	23676	18061	0.50	55.09
					1.77	2.16	23293	17760	0.25	40.73
				3	1.15	0.96	24945	18994	0.12	98.13
					2.00	0.84	26611	20309	0.45	120.27
					1.79	1.86	25006	19014	0.19	50.87
		1/500	2	1	0.89	1.74	25355	19523	0.11	55.21
					2.53	2.31	23646	18110	0.13	38.75
				2	1.94	2.72	25034	19159	0.23	34.91
					2.38	2.07	24140	18443	0.89	44.18
				3	0.76	1.64	25084	19202	0.05	57.86
					2.03	2.58	23519	17915	0.12	34.51
		1/250	2	1	4.42	0.41	2034	1687	0.77	19.63
				2	2.89	0.48	14757	12334	0.08	121.88
		1/100	2	1	2.57	0.46	23186	18044	0.33	191.92
					3.91	0.36	23603	18312	0.49	248.67
				2	2.14	0.52	12149	9250	0.40	87.80
					2.00	0.31	12395	9522	0.46	149.74
				3	3.77	0.26	13647	10315	0.77	198.65
					2.59	0.61	12222	9159	0.15	75.03
		1/50	2	1	1.09	2.12	64052	50757	0.40	116.15
					1.77	3.09	63840	50500	0.38	79.46
				2	1.42	1.99	63257	50035	0.37	122.22
					0.47	2.35	67843	53746	0.04	111.15
				3	1.34	1.21	68107	53962	0.20	215.74
					1.01	0.89	69417	55279	0.22	301.42

Table C.5. cont'd

Mem mat'l	AqpZ batch	AqpZ/mem mat'l molar ratio	Rep	Smpl	D ($\mu m^2/s$)	1/G0	CPS-ch1	CPS-ch2	Chi-sqr	# AqpZ /ves
Polymer	1	1/25	2	1	0.91	0.75	87920	69259	0.08	450.80
					1.47	0.75	83671	65759	0.31	428.08
					0.73	0.85	83029	65226	0.33	374.80
				2	0.72	0.78	79225	61016	0.27	386.36
					0.77	0.55	84344	65220	0.48	584.67
					1.18	1.34	80509	61667	0.36	227.18
					1.35	0.89	86322	66378	0.26	366.58
				3	0.70	0.58	85947	66273	0.10	567.87
					1.35	1.12	82176	63443	0.04	279.24
					0.86	0.62	85617	65800	0.05	525.65
Lipid	2	1/1000	-	-	Not measurable					
		1/100	1	1	0.59	0.19	29210	22232	0.04	281.61
					0.92	0.17	27210	19967	0.10	281.25
					0.91	0.28	32351	26084	0.09	218.99
					0.52	0.15	35783	26210	0.15	421.45
				2	1.00	0.21	33116	25052	0.10	289.63
					1.07	0.24	25182	18871	0.08	192.31
				3	0.95	0.19	29449	21902	0.20	280.97
					1.39	0.17	23293	17234	0.12	248.79
					0.66	0.14	27789	20944	0.14	361.35
		1/50	1	1	3.47	2.45	4921	3549	0.03	3.60
					1.31	0.37	5592	4039	0.10	27.19
					2.06	1.07	5216	3777	0.08	8.71
				2	1.59	1.24	5081	3639	0.17	7.31
					0.71	0.88	5207	3765	0.13	10.59
					3.17	2.81	4823	3478	0.11	3.08
				3	0.49	0.40	5486	3946	0.23	24.31
					1.13	0.64	5158	3704	0.16	14.43
					1.64	0.46	5369	3905	0.16	20.95
		1/25	1	1	2.06	1.07	5216	3777	0.15	8.71
				2	0.00	3.07	15707	11825	0.10	9.34
				3	0.33	1.17	15162	11400	0.04	23.70
					1.52	12.27	15276	11517	0.13	2.27

Table C.5. cont'd

Mem mat'l	AqpZ batch	AqpZ/mem mat'l molar ratio	Rep	Smpl	D ($\mu m^2/s$)	1/G0	CPS-ch1	CPS-ch2	Chi-sqr	# AqpZ /ves
Lipid	2	1/1000	2	1	2.23	0.38	3854	2867	0.21	20.40
					3.48	0.55	3476	2579	0.27	12.74
					3.42	0.28	3899	2884	0.34	27.64
				2	1.58	0.31	3950	2880	0.25	25.40
					2.16	0.49	3457	2521	0.42	13.97
					2.74	0.42	3614	2636	0.10	17.21
				3	1.33	0.23	3189	2351	0.30	27.20
					4.99	0.63	2654	1974	0.22	8.38
					1.60	0.46	2929	2209	0.06	12.94
		1/100	2	1	1.35	0.33	29210	22232	0.08	178.83
					2.27	0.33	6441	4710	0.12	38.38
					1.93	0.23	6839	4936	0.18	59.37
					1.40	0.17	7342	5415	0.20	85.75
				2	1.92	0.22	8403	6280	0.28	74.95
					0.84	0.21	7447	5623	0.09	70.69
					1.31	0.21	7844	5796	0.45	73.28
				3	1.79	0.24	6767	5002	0.18	56.57
					1.71	0.18	7086	5228	0.07	78.31
					1.00	0.20	7654	5823	0.03	77.98
		1/50	2	1	1.34	1.82	5759	4286	0.15	6.33
					1.25	1.56	5798	4304	0.09	7.45
					3.02	1.90	5490	4065	0.17	5.76
				2	2.08	2.59	5509	4079	0.17	4.26
					2.15	2.25	5553	4106	0.10	4.94
					1.59	2.06	5543	4122	0.14	5.39
				3	1.85	2.39	5833	4390	0.43	4.92
					2.02	2.28	5899	4430	0.31	5.21
					2.36	0.98	5973	4483	0.20	12.31
		1/25	2	1	0.62	0.62	33613	24992	0.03	108.86
					1.18	11.95	14976	11343	0.14	2.53
				2	0.36	1.41	42306	33045	0.02	61.50
				3	0.33	1.17	40809	33578	0.04	73.24
					0.31	1.47	43533	33019	0.04	59.80
					0.81	2.48	47148	36514	0.01	38.80

Table C.5. cont'd

Mem mat'l	AqpZ batch	AqpZ/mem mat'l molar ratio	Rep	Smpl	D ($\mu m^2/s$)	1/G0	CPS-ch1	CPS-ch2	Chi-sqr	# AqpZ /ves
Lipid	3	1/1000	1	1	2.44	1.66	7946	6527	0.07	2.29
					1.95	2.87	7416	6045	0.15	1.24
					3.96	3.05	7170	5851	0.12	1.13
				2	1.81	1.82	7885	6473	0.08	2.08
					1.15	1.62	8228	6759	0.04	2.44
				3	1.26	2.17	7676	6389	0.29	1.71
					1.61	2.92	7756	6446	0.79	1.28
					1.84	2.32	7761	6413	0.52	1.61
		1/100	1	1	0.60	0.86	71159	59688	0.23	40.26
					0.33	0.97	71107	59534	0.15	35.48
				2	0.55	1.27	70395	58928	0.10	26.84
					0.62	0.80	72519	60783	0.08	43.88
					0.90	1.35	70980	59161	0.11	25.44
				3	0.46	0.82	80575	68225	0.07	47.91
					0.34	0.72	81007	68383	0.27	54.96
					0.43	1.66	77130	65530	0.13	22.65
		1/50	1	1	0.51	0.77	110430	94919	0.59	70.73
					1.93	1.02	101922	87619	0.11	48.81
				2	1.34	1.09	99579	83576	0.28	44.24
					1.61	0.79	107965	90879	0.08	66.18
				3	1.43	1.02	96573	80615	0.06	45.82
					0.95	0.76	103634	87253	0.09	66.32
					1.21	1.04	94430	79497	0.08	44.23
		1/25	1	1	0.41	0.35	39757	33884	0.20	55.94
					1.90	0.47	30971	26032	0.33	31.75
					0.57	0.36	35998	30281	0.05	48.42
				2	0.78	0.42	32373	26971	0.20	37.47
					0.86	0.43	32216	26896	0.07	36.20
				3	2.05	0.60	30659	25458	0.28	24.58
					1.55	0.46	34517	28601	0.06	36.53
					0.98	0.67	29765	24716	0.17	21.50

Table C.5. cont'd

Mem mat'l	AqpZ batch	AqpZ/mem mat'l molar ratio	Rep	Smpl	D ($\mu m^2/s$)	1/G0	CPS-ch1	CPS-ch2	Chi-sqr	# AqpZ /ves
Lipid	3	1/1000	2	1	2.90	0.34	4743	3805	0.79	122.52
					3.89	0.93	4816	3873	0.63	44.98
					5.48	0.79	4759	3841	0.38	52.58
				2	2.03	0.62	5152	4168	0.18	72.40
					3.24	0.78	5050	4120	0.23	56.35
					3.63	1.03	5267	4313	0.36	44.85
				3	2.94	0.84	4886	4022	0.17	50.81
					3.59	0.57	5104	4389	0.54	80.76
		1/100	2	1	3.39	0.46	8472	7541	0.09	166.84
					3.60	0.31	8908	7949	0.18	263.43
					3.71	0.45	8589	7671	0.38	174.69
					4.39	0.28	9118	7985	0.52	299.40
				2	3.36	0.23	17489	14861	0.36	691.91
					3.24	0.25	16515	13998	0.33	597.41
					2.44	0.24	18312	15396	0.68	673.93
				3	2.13	0.23	11691	9986	0.14	449.96
					3.03	0.22	11163	9620	0.23	457.42
					2.61	0.24	11540	9772	0.16	424.49
		1/50	2	1	2.05	0.21	49606	46624	0.08	2189.23
					1.07	0.27	49428	47495	0.20	1700.06
					1.82	0.20	43090	40903	0.38	2002.47
				2	2.04	0.44	35053	33442	0.68	751.10
					1.44	0.35	45935	39094	0.49	1182.61
					1.63	0.31	48894	41804	0.34	1388.43
				3	1.05	0.19	41158	48512	0.16	2313.62
					2.15	0.27	56024	39828	0.24	1733.74
					3.59	2.65	46116	46116	4.39	167.45
		1/25	2	1	1.52	0.18	43386	36807	0.16	2153.70
					3.69	0.25	31329	26350	0.30	1109.67
					3.06	0.28	33084	28158	0.47	1046.63
				2	2.15	0.21	31230	26278	0.10	1339.87
					2.27	0.22	29469	25207	0.15	1191.71
					1.85	0.20	41158	34265	0.44	1825.39
				3	2.67	0.30	40142	29157	0.28	1120.12
					3.03	0.30	33968	30677	0.23	1036.13

Table C.5. cont'd

Mem mat'l	AqpZ batch	AqpZ/mem mat'l molar ratio	Rep	Smpl	D ($\mu m^2/s$)	1/G0	CPS-ch1	CPS-ch2	Chi-sqr	# AqpZ /ves
Lipid	3	1/100	3	1	1.62	0.46	41913	42591	0.25	889.80
					2.49	0.65	40882	41630	0.11	609.27
					2.04	0.40	47450	48484	0.07	1154.16
				2	1.10	0.52	42428	43417	0.26	791.95
					1.48	0.47	44130	45975	0.11	920.28
					1.47	0.38	44361	46483	0.14	1160.03
				3	2.41	1.18	40557	41295	0.17	335.10
					1.85	0.92	44283	45142	0.21	467.58
					1.77	1.77	59891	59599	0.16	325.39
		1/50	3	1	2.18	0.21	22583	21065	0.09	1013.41
					1.39	0.18	23676	22488	1.11	1260.24
					1.99	0.24	20312	19089	0.28	788.05
				2	1.39	0.30	22402	20974	0.60	695.98
					2.30	0.27	22012	20431	0.12	763.11
					1.82	0.23	23738	22784	0.11	981.34
				3	1.82	0.23	23738	22784	0.11	981.34
					2.93	0.22	22395	22533	0.06	991.43
					1.27	0.24	21323	20546	0.72	832.97
		1/25	3	1	1.97	0.28	21472	20367	0.30	711.73
					2.98	0.26	18859	17716	0.25	665.69
					3.35	0.29	20119	19693	0.14	666.21
				2	1.29	0.25	19546	18829	0.38	738.04
					2.23	0.23	22745	22653	0.16	954.20
					2.07	0.21	22377	22261	0.20	1016.60
				3	2.14	0.22	19723	19470	0.11	871.90
					2.14	0.22	19723	19470	0.11	871.90
					2.32	0.28	19514	19235	0.14	663.45

Table C.5. cont'd

Mem mat'l	AqpZ batch	AqpZ/mem mat'l molar ratio	Rep	Smpl	D ($\mu m^2/s$)	1/G0	CPS-ch1	CPS-ch2	Chi-sqr	# AqpZ /ves
Lipid	4	1/100	1	1	1.10	1.52	1921	1690	0.78	12.60
					1.26	1.08	1888	1671	0.86	17.54
				2	1.38	0.94	1936	1701	0.49	20.60
					1.97	2.39	1852	1632	1.11	7.76
					1.31	2.42	1841	1622	0.72	7.60
				3	0.89	0.97	1913	1823	0.56	20.44
					1.15	1.99	1820	1690	1.41	9.36
		1/25	1	1	0.70	0.11	1467	1351	0.25	132.49
					0.63	0.15	1510	1405	0.81	105.25
					0.43	0.12	1489	1403	0.38	133.57
				2	0.62	0.13	1417	1364	0.90	117.43
					0.52	0.10	1559	1493	0.97	157.52
				3	0.35	0.15	1557	1448	0.71	107.79
Lipid	4	1/100	2	1	6.10	0.16	1210	780	0.06	67.12
					5.04	0.09	1228	868	0.06	124.10
					6.92	0.22	1093	661	0.36	42.65
				2	9.46	0.19	1196	765	0.41	55.75
					7.37	0.12	1301	890	0.08	99.29
					7.56	0.19	1219	774	0.16	55.30
				3	8.94	0.14	1230	806	0.35	77.80
					5.24	0.08	1504	1021	0.10	175.29
					12.87	0.14	1197	779	1.01	75.73
		1/25	2	1	2.02	0.14	5816	5146	0.14	421.28
					3.97	0.16	5587	4967	0.43	356.16
					3.52	0.18	5580	4862	0.33	308.04
				2	4.36	0.17	4951	4260	0.04	287.56
					3.46	0.20	5257	4726	0.30	262.61
					3.69	0.16	5450	4906	0.20	336.86
				3	3.72	0.17	4943	4513	0.11	294.61
					4.06	0.14	5340	4739	0.16	387.01
					3.53	0.16	5652	5045	0.10	360.40

Table C.6. Data for the effect of the amount of protein added on permeability of AqpZ/lipid and AqpZ/polymer vesicles (Figure 3.8)
Abbreviations are as follows: membrane (mem), material (mat'l), exponential fitting parameter (k), permeability (P_f), standard deviation (SD), variance (var).

Mem mat'l	AqpZ batch	AqpZ/mem mat'l molar ratio	[NaCl] (M)	k (s^{-1})	P_f (μm/s)	SD of k (s^{-1})	Var of P_f $(\mu m/s)^2$
Polymer	1	0	1	0.00	0.00	0.00	0.00E+00
		1/1000	1	47.26	95.62	4.66	9.34E-06
		1/500	1	43.23	107.07	5.64	2.05E-05
		1/250	1	57.84	119.28	5.17	1.19E-05
		1/100	1	240.70	375.98	16.01	6.56E-05
		1/50	1	131.49	359.40	24.83	4.83E-04
Polymer	1	0	1	0.00	0.00	0.00	0.00E+00
		1/5000	1	233.89	452.26	12.65	6.28E-05
		1/1000	1	245.71	552.32	26.87	3.83E-04
		1/500	1	233.01	468.89	12.34	6.47E-05
		1/250	1	200.83	508.09	84.00	4.74E-03
		1/100	1	464.71	1026.80	87.47	3.92E-03
		1/50	1	258.60	660.71	132.33	1.20E-02
		1/25	1	473.67	1256.26	123.35	1.12E-02
Lipid	2	0	1	16.71	25.10	0.28	1.85E-08
		1/1000	1	8.38	11.38	0.10	1.97E-09
		1/100	1	317.87	739.75	19.61	2.19E-04
		1/50	1	9.06	16.85	0.15	8.31E-09
		1/25	1	15.22	33.49	0.42	9.02E-08
Lipid	2	0	1	15.32	20.07	0.10	1.7E-09
		1/1000	1	16.46	20.77	0.11	2.1E-09
		1/100	1	48.06	74.85	1.63	6.7E-07
		1/50	1	21.58	27.08	0.29	1.4E-08
		1/25	1	21.58	31.42	0.33	2.4E-08
Lipid	3	0	1	4.26	0.73	0.03	3.0E-10
		1/1000	1	9.36	1.45	0.09	2.1E-09
		1/100	1	51.09	9.56	1.37	6.9E-07
		1/50	1	50.90	10.56	1.06	5.1E-07
		1/25	1	32.88	5.36	0.33	2.9E-08
Lipid	3	0	1	11.30	13.60	0.09	1.2E-09
		1/1000	1	14.87	20.12	0.11	2.4E-09
		1/100	1	13.74	20.46	0.12	3.4E-09
		1/50	1	27.43	51.00	0.41	6.0E-08
		1/25	1	15.00	26.70	0.16	8.2E-09

Table C.6. cont'd

Mem mat'l	AqpZ batch	AqpZ/mem mat'l molar ratio	[NaCl] (M)	k (s^{-1})	P_f (um/s)	SD of k (s^{-1})	Var of P_f $(um/s)^2$
Lipid	3	1/100	1	19.32	31.78	0.12	4.0E-09
		1/50	1	26.20	47.61	0.46	7.3E-08
		1/25	1	20.24	27.46	0.77	1.2E-07
Lipid	4	0	1	13.35	15.84	0.43	2.69E-08
		1/100	1	39.47	56.87	1.25	3.40E-07
		1/25	1	61.64	114.24	7.00	1.77E-05
Lipid	4	0	1	16.13	24.78	0.26	1.65E-08
		1/100	1	19.48	31.40	0.80	1.75E-07
		1/25	1	33.91	71.63	2.67	3.34E-06

Table C.7. Data for effect of AqpZ on permeability of *E. coli* (Figures 5.2, 5.3, 5.4, 5.6)
The reconstructed NCM3306R strains were not used in Figures 5.2, 5.3, 5.4 and 5.6. Abbreviations are as follows: stopped-flow instrument (SF), exponential fitting parameter (k), permeability (P_f), standard deviation (SD), error calculated from the standard deviation of the curve fitting (error).

Date	Strain	SF	pH	[Proline] (M)	k	P_f (µm/s)	SD of fit	error (µm/s)
1/12/2011	NCM3105	1	7.4	1	3.29	83.08		5.35
1/26/2011	NCM3105	1	7.4	1	2.35	59.22		3.03
1/26/2011	NCM3105	1	7.4	1	2.70	68.26		5.61
1/26/2011	NCM3105	1	7.4	1	2.27	57.42		3.81
1/26/2011	NCM3105	1	7.4	1	2.38	60.03		5.61
2/22/1/11	NCM3105	1	7.4	2	3.01	38.02	0.038	0.48
3/1/2011	NCM3105	1	7.4	2	3.49	44.05	0.035	0.44
3/2/2011	NCM3105	1	7.4	2	3.36	42.37	0.039	0.49
3/5/2011	NCM3105	1	7.4	2	3.37	42.60	0.039	0.49
3/8/2011	NCM3105	1	7.4	2	3.28	41.41	0.040	0.50
3/9/2011	NCM3105	1	7.4	2	9.65	121.89	0.191	2.41
6/25/2011	NCM3105	1	7.4	1	2.97	75.06	0.045	1.15
6/25/2011	NCM3105	1	4.0	1	8.06	203.47	0.225	5.69
6/12/2014	NCM3105	2	7.4	1	6.24	157.48	0.173	2.19
6/12/2014	NCM3105	2	7.4	2	9.48	119.73	0.168	1.06
6/12/2014	NCM3105	2	4.0	1	4.01	101.37	0.181	2.29
6/12/2014	NCM3105	2	4.0	2	6.62	83.61	0.286	1.80
7/29/2014	NCM3105	2	7.4	1	22.27	562.43	2.939	37.10
7/29/2014	NCM3105	2	7.4	2	2.62	33.03	0.072	0.45
7/29/2014	NCM3105	2	4.0	1	3.55	89.68	0.152	1.92
7/29/2014	NCM3105	2	4.0	2	2.36	29.81	0.103	0.65
3/1/2011	NCM3306	1	7.4	2	3.50	44.18	0.055	0.70
3/2/2011	NCM3306	1	7.4	2	2.92	36.82	0.033	0.41
3/5/2011	NCM3306	1	7.4	2	2.05	25.83	0.027	0.34
3/8/2011	NCM3306	1	7.4	2	3.28	41.41	0.040	0.50
3/9/2011	NCM3306	1	7.4	2	5.46	68.95	0.066	0.84
6/25/2011	NCM3306	1	7.4	1	2.00	50.53	0.027	0.69
6/25/2011	NCM3306	1	4	1	4.42	111.71	0.133	3.35
6/12/2014	NCM3306	2	7.4	1	6.27	158.42	0.266	3.36
6/12/2014	NCM3306	2	7.4	2	8.05	101.65	0.285	1.80
6/12/2014	NCM3306	2	4.0	1	6.42	162.18	0.217	2.74
6/12/2014	NCM3306	2	4.0	2	5.63	71.14	0.235	1.49
7/29/2014	NCM3306	2	7.4	1	1.70	42.95	0.043	0.55
7/29/2014	NCM3306	2	7.4	2	2.19	27.59	0.214	1.35
7/29/2014	NCM3306	2	4.0	1	3.85	97.20	0.100	1.26
7/29/2014	NCM3306	2	4.0	2	2.44	30.76	0.075	0.48

Table C.7. cont'd

Date	Strain	SF	pH	[Proline] (M)	k	P_f (μm/s)	SD of fit	error (μm/s)
2/22/2011	ME9062	1	7.4	2	2.24	28.29	0.021	0.26
3/1/2011	ME9062	1	7.4	2	4.16	52.49	0.049	0.62
3/2/2011	ME9062	1	7.4	2	3.66	46.22	0.040	0.50
6/12/2014	ME9062	2	7.4	1	6.29	158.92	0.365	4.60
6/12/2014	ME9062	2	7.4	2	7.82	98.75	0.452	2.85
6/12/2014	ME9062	2	4.0	1	4.69	118.43	0.134	1.70
6/12/2014	ME9062	2	4.0	2	8.03	101.42	0.208	1.31
2/22/1/11	JW0859	1	7.4	2	2.18	27.49	0.033	0.42
3/1/2011	JW0859	1	7.4	2	3.10	39.12	0.044	0.56
3/2/2011	JW0859	1	7.4	2	3.35	42.28	0.035	0.45
6/12/2014	JW0859	2	7.4	1	9.60	242.33	0.408	5.15
6/12/2014	JW0859	2	7.4	2	10.41	131.38	0.339	2.14
6/12/2014	JW0859	2	4.0	1	5.22	131.71	0.403	5.09
6/12/2014	JW0859	2	4.0	2	5.76	72.72	0.114	0.72
3/8/2011	JM109 pTrcAqpZ, Ind.	1	7.4	2	48.68	614.61	1.565	19.77
3/9/2011	JM109 pTrcAqpZ, Ind.	1	7.4	2	113.81	1436.95	25.806	325.84
3/5/2011	JM109 pTrc1	1	7.4	2	14.59	184.18	0.683	8.62
3/8/2011	JM109 pTrc1, Ind.	1	7.4	2	15.20	191.89	0.241	3.04
3/9/2011	JM109 pTrc1, Ind.	1	7.4	2	31.03	391.84	0.903	11.40
7/29/2014	NCM3306R1*	2	7.4	1	1.70	42.95	0.043	0.55
7/29/2014	NCM3306R1*	2	7.4	2	2.19	27.59	0.214	1.35
7/29/2014	NCM3306R1*	2	4.0	1	3.85	97.20	0.100	1.26
7/29/2014	NCM3306R1*	2	4.0	2	2.44	30.76	0.075	0.48
7/29/2014	NCM3306R2*	2	7.4	1	2.54	64.26	0.121	1.52
7/29/2014	NCM3306R2*	2	7.4	2	2.71	34.16	0.163	1.03
7/29/2014	NCM3306R2*	2	4.0	1	4.76	120.32	0.150	1.90
7/29/2014	NCM3306R2*	2	4.0	2	3.63	45.82	0.071	0.45

*The NCM3306 strain was reconstructed using recipient strain NCM3105 and donor strain NCM3306 for P1-mediated transduction. The P1 lysate was grown on ME9062. The transduction was performed using the protocol by Thomason et al. (226) and the new strain was designated NCM3306R.

Table C.7. cont'd

Date	Strain	SF	pH	[Proline] (M)	k	P_f (µm/s)	SD of fit	error (µm/s)
6/25/2011	NCM3105	1	7.4	1	2.97	75.06	0.045	1.15
6/12/2014	NCM3105	2	7.4	1	6.24	157.48	0.173	2.19
6/12/2014	NCM3105	2	7.4	2	9.48	119.73	0.168	1.06
7/29/2014	NCM3105	2	7.4	1	22.27	562.43	2.939	37.10
7/29/2014	NCM3105	2	7.4	2	2.62	33.03	0.072	0.45
6/25/2011	NCM3105	1	4	1	8.06	203.47	0.225	5.69
6/12/2014	NCM3105	2	4	1	4.01	101.37	0.181	2.29
6/12/2014	NCM3105	2	4	2	6.62	83.61	0.286	1.80
7/29/2014	NCM3105	2	4	1	3.55	89.68	0.152	1.92
7/29/2014	NCM3105	2	4	2	2.36	29.81	0.103	0.65
6/25/2011	NCM3105 pTrc10His1	1	7.4	1	3.48	87.92	0.056	1.42
6/25/2011	NCM3105 pTrc10His1	1	4	1	6.32	159.57	0.228	5.75
6/25/2011	NCM3105 pTrc10His1, Ind.	1	7.4	1	8.17	206.27	0.241	6.08
6/25/2011	NCM3105 pTrc10His1, Ind.	1	4	1	45.00	1136.38	5.189	131.03
6/25/2011	NCM3105 pTrc10HisAqpZ	1	7.4	1	29.32	740.43	3.100	78.29
6/25/2011	NCM3105 pTrc10HisAqpZ	1	4	1	34.72	876.65	5.329	134.58
6/25/2011	NCM3105 pTrc10HisAqpZ, Ind.	1	7.4	1	35.85	905.18	3.168	79.99
6/25/2011	NCM3105 pTrc10HisAqpZ, Ind.	1	4	1	25.69	648.81	3.688	93.13
6/12/2014	NCM3306	2	7.4	1	6.27	158.42	0.266	3.36
6/13/2014	NCM3306	2	7.4	2	8.05	101.65	0.285	1.80
6/14/2014	NCM3306	2	4	1	6.42	162.18	0.217	2.74
6/15/2014	NCM3306	2	4	2	5.63	71.14	0.235	1.49
6/25/2011	NCM3306	1	7.4	1	2.00	50.53	0.027	0.69
6/25/2011	NCM3306	1	4	1	4.42	111.71	0.133	3.35
6/25/2011	NCM3306 pTrc10His1	1	7.4	1	3.02	76.23	0.066	1.66
6/25/2011	NCM3306 pTrc10His1	1	4	1	25.92	654.59	2.432	61.40
6/25/2011	NCM3306 pTrc10His1, Ind.	1	7.4	1	23.84	601.96	0.960	24.23
6/25/2011	NCM3306 pTrc10His1, Ind.	1	4	1	39.76	1003.93	2.612	65.97
6/25/2011	NCM3306 pTrc10HisAqpZ	1	7.4	1	32.15	811.98	4.153	104.88
6/25/2011	NCM3306 pTrc10HisAqpZ	1	4	1	36.62	924.74	4.038	101.98

Table C.7. cont'd

Date	Strain	SF	pH	[Proline] (M)	k	P_f (µm/s)	SD of fit	error (µm/s)
2/22/2011	ME9062	1	7.4	2	2.24	28.29	0.021	0.26
3/1/2011	ME9062	1	7.4	2	4.16	52.49	0.049	0.62
3/2/2011	ME9062	1	7.4	2	3.66	46.22	0.040	0.50
6/12/2014	ME9062	2	7.4	1	6.29	158.92	0.365	4.60
6/12/2014	ME9062	2	7.4	2	7.82	98.75	0.452	2.85
6/12/2014	ME9062	2	4	1	4.69	118.43	0.134	1.70
6/12/2014	ME9062	2	4	2	8.03	101.42	0.208	1.31
2/22/2011	JW0859	1	7.4	2	2.18	27.49	0.033	0.42
3/1/2011	JW0859	1	7.4	2	3.10	39.12	0.044	0.56
3/2/2011	JW0859	1	7.4	2	3.35	42.28	0.035	0.45
6/12/2014	JW0859	2	7.4	1	9.60	242.33	0.408	5.15
6/12/2014	JW0859	2	7.4	2	10.41	131.38	0.339	2.14
6/12/2014	JW0859	2	4	1	9.60	242.33	0.408	5.15
6/12/2014	JW0859	2	4	2	10.41	131.38	0.339	2.14

Table C.8. Data for percent survival of *E. coli* under shock conditions (Figures 5.5, 5.6)
Red text denotes plate counts < 25 and blue text denotes plate counts > 250. Blue shading denotes plate counts used for acid shock, light yellow shading denotes plate counts used for osmotic shock, and green shading denotes plate counts used for combined shock. Bright yellow shading with bold text denotes plate counts between 20-25 used because they allowed use of an additional biological replicate. Only 2011 data was used in Figures 5.5 and 5.6. For data from 2014, replicate plates of the same biological replicate were averaged before further use.

NCM3105 (parent)

7/9/2011	Condition	Plate (10^x)	Count	% Survival	Plate (10^x)	Count	% Survival
	Control	8	40	100	7	230	100
	Acid	7	21	5.25	6	144	6.26
	Osmotic	8	68	170.00	7	508	220.87
	Both	6	18	0.45	5	193	0.84
7/11/2011	Condition	Plate (10^x)	Count	% Survival	Plate (10^x)	Count	% Survival
	Control	8	80	100	7	563	100
	Acid	8	14	17.50	7	162	28.77
	Osmotic	8	72	90.00	7	582	103.37
	Both	7	16	2.00	6	254	4.51
7/13/2011	Condition	Plate (10^x)	Count	% Survival	Plate (10^x)	Count	% Survival
	Control	8	79	100	7	568	100
	Acid	7	38	4.81	6	400	7.04
	Osmotic	8	65	82.28	7	556	97.89
	Both	6	29	0.37	5	273	0.48
7/27/2011	Condition	Plate (10^x)	Count	% Survival	Plate (10^x)	Count	% Survival
	Control	8	45	100	7	434	100
	Acid	7	24	5.33	6	252	5.81
	Osmotic	8	101	224.44	7	946	217.97
	Both	5	65	0.14	4	660	0.15

Table C.8. cont'd

NCM3306 (null mutant)

7/9/2011	Condition	Plate (10^x)	Count	% Survival	Plate (10^x)	Count	% Survival
	Control	8	65	100	7	570	100
	Acid	7	58	8.92	6	680	10.46
	Osmotic	8	77	118.46	7	722	111.08
	Both	7	148	22.77			
7/11/2011	Condition	Plate (10^x)	Count	% Survival	Plate (10^x)	Count	% Survival
	Control	8	76	100	7	684	100
	Acid	7	128	16.84			
	Osmotic	7	1060	139.47			
	Both	8	9	11.84	7	85	11.18
7/13/2011	Condition	Plate (10^x)	Count	% Survival	Plate (10^x)	Count	% Survival
	Control	8	50	100			
	Acid	8	10	20.00	7	137	27.40
	Osmotic	8	28	56.00			
	Both	6	40	0.80	5	408	0.82
7/27/2011	Condition	Plate (10^x)	Count	% Survival	Plate (10^x)	Count	% Survival
	Control	8	46	100	7	394	100
	Acid				7	738	160.43
	Osmotic	8	39	84.78	7	488	106.09
	Both	8	24	52.17	7	180	39.13

Table C.8. cont'd

NCM3105 pTrc10HisAqpZ, uninduced

7/11/2011	Condition	Plate (10^x)	Count	% Survival	Plate (10^x)	Count	% Survival
	Control	8	75	100			
	Acid	6	262	3.49			
	Osmotic	8	68	90.67	7	712	94.93
	Both	6	5	0.07	5	63	0.08
7/13/2011	Condition	Plate (10^x)	Count	% Survival	Plate (10^x)	Count	% Survival
	Control	8	37	100	7	418	100.00
	Acid	6	13	0.35	5	129	0.35
	Osmotic	8	51	137.84	7	564	152.43
	Both	4	19	0.01	3	348	0.01
7/27/2011	Condition	Plate (10^x)	Count	% Survival	Plate (10^x)	Count	% Survival
	Control	8	40	100	7	440	100.00
	Acid	6	10	0.25	5	119	0.30
	Osmotic	8	70	175.00	7	494	123.50
	Both	5	37	0.09	4	648	0.16
7/29/2011	Condition	Plate (10^x)	Count	% Survival	Plate (10^x)	Count	% Survival
	Control	8	1364	100			
	Acid	5	26	0.07	4	337	0.00
	Osmotic	8	3212	8030.00			
	Both	4	108	0.03	3	1248	0.00
8/9/2011	Condition	Plate (10^x)	Count	% Survival	Plate (10^x)	Count	% Survival
	Control	8	35	100	7	272	100
	Acid	5	11	0.03	4	92	0.03
	Osmotic	8	68	194.29	7	538	153.71
	Both	4	20	0.01	3	173	0.00

Table C.8. cont'd

NCM3105 pTrc10His1, uninduced

7/27/2011	Condition	Plate (10^x)	Count	% Survival	Plate (10^x)	Count	% Survival
	Control	8	13	100	7	160	100
	Acid	4	16	0.01	3	188	0.01
	Osmotic				7	100	62.50
	Both	4	50	0.03	3	476	0.03
7/29/2011	Condition	Plate (10^x)	Count	% Survival	Plate (10^x)	Count	% Survival
	Control	8	1748	100			
	Acid	4	11	0.01	3	169	0.00
	Osmotic	8	2628	16425.00			
	Both	4	5	0.00	3	73	0.00
8/9/2011	Condition	Plate (10^x)	Count	% Survival	Plate (10^x)	Count	% Survival
	Control	8	23	100	7	191	100
	Acid	4	42	0.02	3	376	0.02
	Osmotic	8	15	78.53	7	279	146.07
	Both	4	10	0.01	3	89	0.00

Table C.8. cont'd

NCM3105 pTrc10HisAqpZ, induced

7/29/2011	Condition	Plate (10^x)	Count	% Survival	Plate (10^x)	Count	% Survival
	Control	8	5304	100			
	Acid	5	38	0.49	4	268	0.00
	Osmotic	6	32	4.16	5	327	0.01
	Both	4	99	0.15	3	964	0.00
8/9/2011	Condition	Plate (10^x)	Count	% Survival	Plate (10^x)	Count	% Survival
	Control	7	13	100			
	Acid	5	30	0.39	4	269	2.07
	Osmotic	7	6	7.79	6	50	38.46
	Both	4	5	0.01	3	1200	0.92
8/21/2011	Condition	Plate (10^x)	Count	% Survival	Plate (10^x)	Count	% Survival
1	Control	8	9	100	7	77	100
	Acid	6	11	1.43	5	123	1.60
	Osmotic	7	20	25.97	6	203	26.36
	Both	4	38	0.05	3	356	0.05
8/21/2011	Shock	Plate (10^x)	Count	% Survival	Plate (10^x)	Count	% Survival
2	Control	7	56	100	6	438	100
	Acid	7	11	19.64	6	99	22.60
	Osmotic	7	13	23.21	6	124	28.31
	Both	5	48	0.86	4	374	0.85

Table C.8. cont'd

NCM3105 pTrc10His1, induced

7/29/2011	Condition	Plate (10^x)	Count	% Survival	Plate (10^x)	Count	% Survival
	Control	8	1520	100			
	Acid	7	223	43.73			
	Osmotic	8	98	192.16			
	Both	7	49	9.61	6	668	0.44
8/9/2011	Condition	Plate (10^x)	Count	% Survival	Plate (10^x)	Count	% Survival
	Control	9	10	100	8	51	100
	Acid	8	48	94.12	7	423	82.94
	Osmotic				7		
	Both	3	15	0.00	2	200	0.00
8/21/2011	Condition	Plate (10^x)	Count	% Survival	Plate (10^x)	Count	% Survival
1	Control	8	108	100	7	794	100
	Acid	8	24	22.22	7	143	13.24
	Osmotic	8	71	65.74	7	540	50.00
	Both	5	24	0.02	4	192	0.02
8/21/2011	Condition	Plate (10^x)	Count	% Survival	Plate (10^x)	Count	% Survival
2	Control	8	54	100	7	430	100
	Acid	8	62	114.81	7	612	113.33
	Osmotic	8	83	153.70	7	920	170.37
	Both	7	189	35.00			

Table C.8. cont'd

NCM3105 (parent)

7/10/2014	Condition	Plate (10^x)	Count	Plate (10^x)	Count	% Survival	Plate (10^x)	Count	% Survival
	Control	6	>250	7	200		8	27	100
			>250	7	193		8	<25	
			>250	7	168		8	<25	
	Acid	6	>250	7	37	19.8	8	<25	
			>250	7	36	19.3	8	<25	
			>250	7	29	15.5	8	<25	
	Osmotic	6	>250	7	240	128.3	8	<25	
			>250	7	151	80.7	8	<25	
			>250	7	180	96.3	8	<25	
	Both	6	>250	7	213	113.9	8	<25	
			>250	7	192	102.7	8	<25	
			>250	7	234	125.1	8	<25	
7/14/2014	Condition	Plate (10^x)	Count	Plate (10^x)	Count	% Survival	Plate (10^x)	Count	% Survival
	Control	6	>250	7	73		8	<24	
			>250	7	71		8	<25	
			>250	7	81		8	<25	
	Acid	6	>250	7	48	64.0	8	<25	
			>250	7	55	73.3	8	<25	
			>250	7	61	81.3	8	<25	
	Osmotic	6	>250	7	45	60.0	8	<25	
			>250	7	49	65.3	8	<25	
			>250	7	65	86.7	8	<25	
	Both	6	>250	7	>250		8	26	346.7
			>250	7	>250		8	35	466.7
			>250	7	>250		8	31	413.3

Table C.8. cont'd

NCM3105 (parent)

7/15/2014	Condition	Plate (10^x)	Count	Plate (10^x)	Count	% Survival	Plate (10^x)	Count	% Survival
	Control	6	>250	7	119		8	<25	
			>250	7	139		8	<25	
			>250	7	120		8	<25	
	Acid	6	>250	7	102	81.0	8	<25	
			>250	7	112	88.9	8	<25	
			>250	7	108	85.7	8	<25	
	Osmotic	6	>250	7	74	58.7	8	<25	
			>250	7	93	73.8	8	<25	
			>250	7	69	54.8	8	<25	
	Both	6	>250	7	>250		8	37	293.7
			>250	7	>250		8	22	174.6
			>250	7	>250		8	32	254.0
7/29/2014	Condition	Plate (10^x)	Count	Plate (10^x)	Count	% Survival	Plate (10^x)	Count	% Survival
	Control	6	>250	7	219		8	19	
			>250	7	196		8	17	
			>250	7	249		8	26	
	Acid	6	>250	7	91	41.1	8	5	
			>250	7	67	30.3	8	7	
			>250	7	94	42.5	8	5	
	Osmotic	6	>250	7	68	30.7	8	4	
			>250	7	56	25.3	8	8	
			>250	7	66	52.4	8	6	
	Both	6	>250	7	>250		8	79	382.3
			>250	7	>250		8	61	295.2
			>250	7	>250		8	57	275.8

Table C.8. cont'd

ME9062 (parent)

7/10/2014	Condition	Plate (10^x)	Count	Plate (10^x)	Count	% Survival	Plate (10^x)	Count	% Survival
	Control	6	>250	7	106		8	32	
			>250	7	90		8	<25	
			>250	7	131		8	<25	
	Acid	6	>250	7	29	27.4	8	<25	
			>250	7	41	38.7	8	<25	
			>250	7	38	35.8	8	<25	
	Osmotic	6	>250	7	89	84.0	8	<25	
			>250	7	83	78.3	8	<25	
			>250	7	100	94.3	8	<25	
	Both	6	>250	7	36	34.0	8	<25	
			>250	7	40	37.7	8	<25	
			>250	7	45	42.5	8	<25	
7/14/2014	Condition	Plate (10^x)	Count	Plate (10^x)	Count	% Survival	Plate (10^x)	Count	% Survival
	Control	6	>250	7	163		8	18	
			>250	7	215		8	20	
			>250	7	209		8	30	
	Acid	6	>250	7	60	30.7	8	<25	
			>250	7	52	26.6	8	<25	
			>250	7	92	47.0	8	<25	
	Osmotic	6	>250	7	37	18.9	8	<25	
			>250	7	32	16.4	8	<25	
			>250	7	25	12.8	8	<25	
	Both	6	>250	7	144	73.6	8	12	
			>250	7	151	77.2	8	10	
			>250	7	103	52.6	8	15	

Table C.8. cont'd

ME9062 (parent)

7/15/2014	Condition	Plate (10^x)	Count	Plate (10^x)	Count	% Survival	Plate (10^x)	Count	% Survival
	Control	6	>250	7	45		8	<24	
			>250	7	74		8	<25	
			>250	7	68		8	<25	
	Acid	6	>250	7	93	149.2	8	<25	
			>250	7	73	117.1	8	<25	
			>250	7	84	134.8	8	<25	
	Osmotic	6	>250	7	64	102.7	8	<25	
			>250	7	53	85.0	8	<25	
			>250	7	73	117.1	8	<25	
	Both	6	>250	7	>250		8	29	465.2
			>250	7	>250		8	46	738.0
			>250	7	>250		8	34	545.5
				7			8	36.333	582.9

7/29/2014	Condition	Plate (10^x)	Count	Plate (10^x)	Count	% Survival	Plate (10^x)	Count	% Survival
	Control	6	>250	7	261		8	**23**	100.0
			>250	7	280		8	18	
			>250	7	253		8	20	
				7	264.67	100	8	20.333	100
	Acid	6	>250	7	71	34.9	8	7	
			>250	7	64	31.5	8	3	
				7	67.5	36.1			
	Osmotic	6	>250	7	51	25.1	8	3	
			>250	7	53	26.1	8	6	
				7	52	27.8			
	Both	6	>250	7	>250		8	42	206.6
			>250	7	>250		8	44	216.4
			>250	7	>250		8	44	216.4
				7			8	43.333	695.2

Table C.8. cont'd

NCM3306R1 (null mutant, reconstructed #1)*

7/29/2014	Condition	Plate (10^x)	Count	Plate (10^x)	Count	% Survival	Plate (10^x)	Count	% Survival
	Control	6	>250	7	122		8	8	
			>250	7	96		8	14	
			>250	7	98		8	6	
	Acid	6	>250	7	251	238.3	8	26	246.8
			>250	7	255	242.1	8	19	
			>250	7	268	254.4	8	17	
	Osmotic	6	>250	7	150	142.4	8	15	
			>250	7	183	173.7	8	24	227.8
			>250	7	218	207.0	8	15	
	Both	6	>250	7	>250		8	126	1196.2
			>250	7	>250		8	113	1072.8
			>250	7	>250		8	125	1186.7
7/30/2014	Condition	Plate (10^x)	Count	Plate (10^x)	Count	% Survival	Plate (10^x)	Count	% Survival
(Wet plates)	Control	6	>250	7	67		8	10	
			>250	7	60		8	4	
			>250	7	288		8	16	
	Acid	6	>250	7	38	27.5	8	0	
			>250	7	48	34.7	8	2	
			>250	7	74	53.5	8	11	
	Osmotic	6	>250	7	30	21.7	8	3	
			>250	7	28	20.2	8	3	
			>250	7	13	9.4	8	6	
	Both	6	>250	7	>250		8	127	918.1
			>250	7	>250		8	102	737.3
			>250	7	>250		8	120	867.5

*The NCM3306 strain was reconstructed using recipient strain NCM3105 and donor strain NCM3306 for P1-mediated transduction. The P1 lysate was grown on ME9062. The transduction was performed using the protocol by Thomason et al. (226) and the new strain was designated NCM3306R.

Table C.8. cont'd

NCM3306R2 (null mutant, reconstructed #2)*

7/29/2014	Condition	Plate (10^x)	Count	Plate (10^x)	Count	% Survival	Plate (10^x)	Count	% Survival
	Control	6	>250	7	190		8	27	
			>250	7	149		8	19	
			>250	7	178		8	23	
	Acid	6	>250	7	126	73.1	8	7	
			>250	7	102	59.2	8	4	
			>250	7	106	61.5	8	9	
	Osmotic	6	>250	7	98	56.9	8	12	
			>250	7	103	59.8	8	8	
			>250	7	93	54.0	8	16	
	Both	6	>250	7	>250		8	71	308.7
			>250	7	>250		8	105	456.5
			>250	7	>250		8	73	317.4
7/30/2014	Condition	Plate (10^x)	Count	Plate (10^x)	Count	% Survival	Plate (10^x)	Count	% Survival
(Wet plates)	Control	6	>250	7	54		8	5	
			>250	7	52		8	5	
			>250	7	48		8	7	
	Acid	6	>250	7	122	237.7	8	4	
			>250	7	112	218.2	8	10	
			>250	7	100	194.8	8	15	
	Osmotic	6	>250	7	9	17.5	8	1	
			>250	7	17	33.1	8	2	
			>250	7	36	70.1	8	6	
	Both	6	>250	7	>250		8	72	1402.6
			>250	7	>250		8	54	1052.0
			>250	7	>250		8	79	1539.0

*The NCM3306 strain was reconstructed using recipient strain NCM3105 and donor strain NCM3306 for P1-mediated transduction. The P1 lysate was grown on ME9062. The transduction was performed using the protocol by Thomason et al. (226) and the new strain was designated NCM3306R.